Doctoral Thesis

Modular Engineering and Redesign of the Bimolecular Group I Ribozyme to form RNA Nano-assemblies and their Applications in RNA Evolution

Md. Motiar Rahman

Graduate School of Innovative Life Science,

University of Toyama, Japan

2019

Abstract

Two types of bimolecular derivatives of the *Tetrahymena* (TetRz) group I ribozyme were used to construct unit RNAs, which act as the structural platforms, to design assembled RNA with various shapes. Firstly, the author modified and expanded the interfaces between P5abc RNA and ΔP5 RNA, which form the P5abc/ΔP5 bimolecular ribozymes by replacing parental tertiary interactions with artificial alternatives. Then, this bimolecular system was employed to construct two-dimensional (2D) triangle and square, and one-dimensional (1D) array. Secondly, two-way junction of P4-6 RNA of the TetRz was replaced with a three-way junction motif in the P4-6 domain of the *Pneumonia carinii* type group I ribozyme. The resulting chimeric P4-6 RNA formed its folded structure like the parental P4-6 RNA and activated the substrate cleavage reaction in combination with P3-7 RNA to form the P4-6/P3-7 bimolecular ribozyme. The new P4-6 RNA variant contains a free helical region at the three-way junction, which has been connected to the P8 position of the P3-7 element to design unit RNA for the fabrication of 1D array. Biochemical analysis shows that 1D oligomerization through the self-assembly of P4-6 RNA and P3-7 RNA rescued the structural defects of the P4-6/P3-7 bimolecular ribozyme which were weakly active or completely inactive. Finally, the author analyzed the effects of PEG molecular crowders on the ribozyme systems and found that PEG exceptionally overcame some types of structural defects in those ribozymes which could not activate substrate cleavage reaction in presence of reaction buffer alone.

List of contents

Chapter 1. General introduction

1.1. RNA (Ribonucleic acid)

Ribonucleic acids (RNAs) are promising biopolymers that play indispensable roles in the cell including gene regulations [1, 2], chemical transformations (substrate cleavage or ligation reaction) [3-5], molecular recognitions [6, 7] and RNA modifications [8, 9]. Cell entities use mRNA, called messenger RNA, to carry genetic information and direct the synthesis of proteins into the ribosome. During the process of protein synthesis, tRNA encodes the amino acids to the ribosome, which consists of 2~4 distinct rRNAs that connect the amino acid unit to form protein through the formation of a peptide bond [10]. Several viruses also use single-stranded RNA molecules as the carrier of their genetic information [11].

RNAs are nucleotides polymers like DNA (deoxyribonucleic acids) biomolecules; however, it possesses ribose sugar moiety with phosphate backbone rather than deoxyribose sugar (**Figure 1-1**). RNAs polymers are composed of four repeated nucleotides as monomer units, consists of four types of nitrogenous bases (Adenine or A, Guanine or G, Cytosine or C, and Uracil or U), which are bound to ribose sugar via β-N-glycosidic bond (**Figure 1-1A**) and bound to phosphate group via ester bond (**Figure 1-1C)**. Among the four bases present in RNA, adenine and guanine are called purine, and cytosine and uracil are called pyrimidine. In standard Watson-Crick base pairing, adenine pairs with uracil by two hydrogen bonds and guanine pairs with cytosine by three hydrogen bonds. Like RNA, DNA biomolecules are also composed of four repeated nucleobases; however; they contain thymine or T instead of uracil or U. DNA forms double helical structures through the formation of canonical based pairing and forms the

B-conformation under physiological conditions. On the other hand, RNA possesses a hydroxyl group at 2′ position of sugar group. The presence of the 2′-OH group in the sugar moiety of RNA makes them unstable and leads to the formation of particular sugar conformation, such as A-form helix [10, 12, 13].

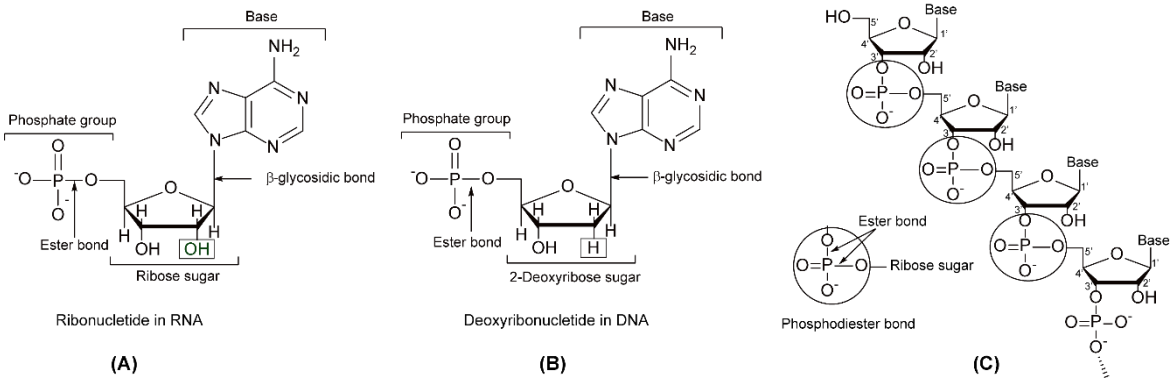

Figure 1-1. Structural variation in DNA and RNA nucleotides. (A) Ribose sugar in RNA, (B) deoxy ribose in DNA and (C) the phosphodiester bond in nucleic acid polymers.

RNAs hold three different types of structural organizations such as primary, secondary and tertiary structures (**Figure 1-2**). The primary structure of RNA is rather simple and consists of repetitive nucleotide chain interconnected through the phosphodiester bond (**Figure 1-1C**). The secondary structure of RNA consists of several double helices and loops, i.e. hairpin loop, internal loop, and bulge. Tertiary structure of RNA molecules are found as folded onto itself or intertwist within RNA molecules through multiple interactions, such as kissing loop interaction, base stacking, loop-receptor interaction, pseudoknot interaction, and T-loop/D-loop interaction [14-16]. The complex structure of RNA molecules is mediated by the presence of canonical Watson-Crick (A–U, C–G) bases pairing, non-Watson-Crick base pairing or stacking interaction, base triples including A-minor motif and ribose zipper (**Figure 1-2B, C**) [14, 17]. Like

the protein molecules, the non-coding functional RNAs frequently need to form intricate three-dimensional (3D) network for their functions [18]. Scaffolds for these 3D network are brought by several secondary structural motifs, which are usually governed by hydrogen bonds within the RNA molecules. RNAs are negatively charged molecules and metal ions (K^+, Na^+, Mg^{2+} and Mn^{2+}) are necessary to neutralize the negatively charged surrounding RNA backbones and stabilize their global tertiary structure (**Figure 1-2C**) [19].

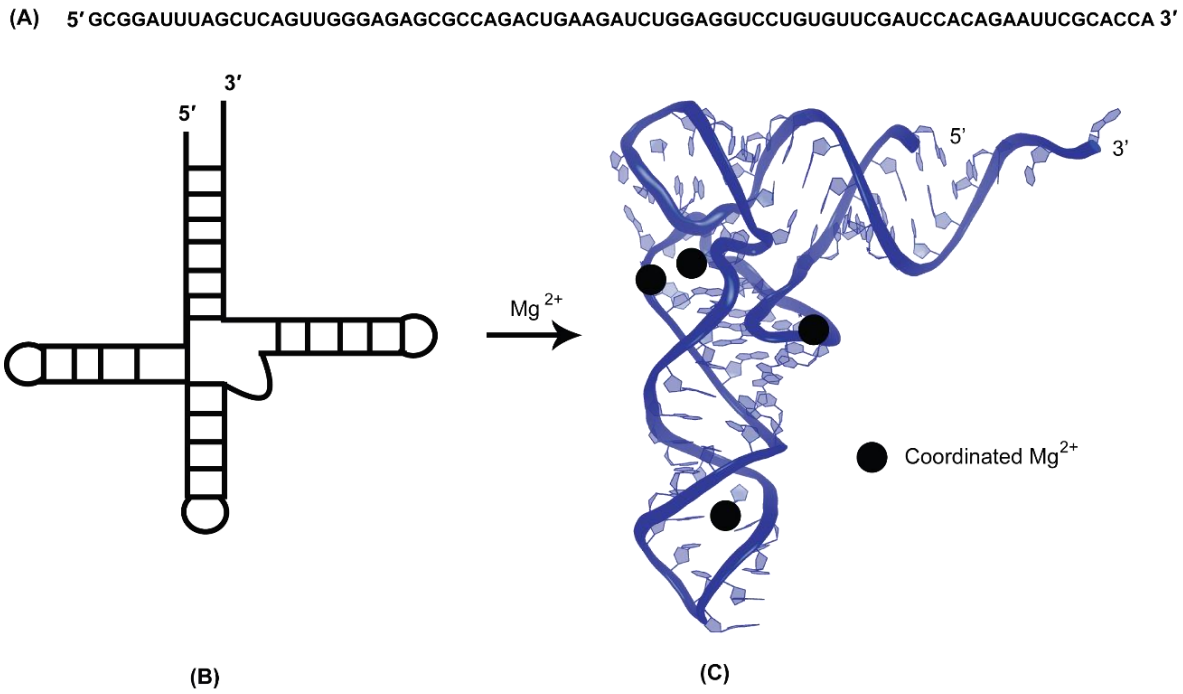

Figure 1-2. Various stages of structures of RNA biomolecule. (A) Primary structure (B) secondary structure and (C) tertiary structure coordinated with magnesium ion, (adapted with the permission from [20]).

1.2. RNA building blocks or motifs

RNA biomolecules consist of ‘directed and ordered stacked array of the non-Watson-Crick bases that form specific folding of the phosphodiester backbone of the interacting RNA strands are called motifs [21]. In other words, RNA motif is defined as the distinct short sequence or group of base juxtapositions generally found in naturally occurring functional RNAs [22].

In order to function, some classes of non-coding RNA molecules must fold into intricate three-dimensional (3D) structure, which is stabilized by multiple interactions within several RNA secondary structural motifs, the local three-dimensional (3D) structure of sheets, helices, or other forms adopted by RNA chain by electrostatic attraction between neighboring residues [14]. In some instance, the interaction can be found between RNA and protein (RNase P RNA) [23], RNA and ligand (Aptamer) [24] and RNA and metal ions [25, 26]. Tertiary structure of RNA demonstrates an inclusive three-dimensional (3D) shape of a single molecule that has been determined by several methods such as, crystallography, NMR or computational molecular modeling methods. Here, the author summarized some of the structural motifs that are commonly found in RNA molecules.

1.3. RNA structural motifs

1.3.1. RNA helices

RNA primarily consists of double helical Watson-Crick base and forms the basis of RNA secondary structure. In order to form a helix, the complementary elements within the RNA biomolecules should be antiparallel. Double helices are generally formed

between either A−U or G−C through multiple hydrogen bonds. In some helices, G−U, A−C wobble base pair(s) could be found (**Figure 1-3**) [14, 27].

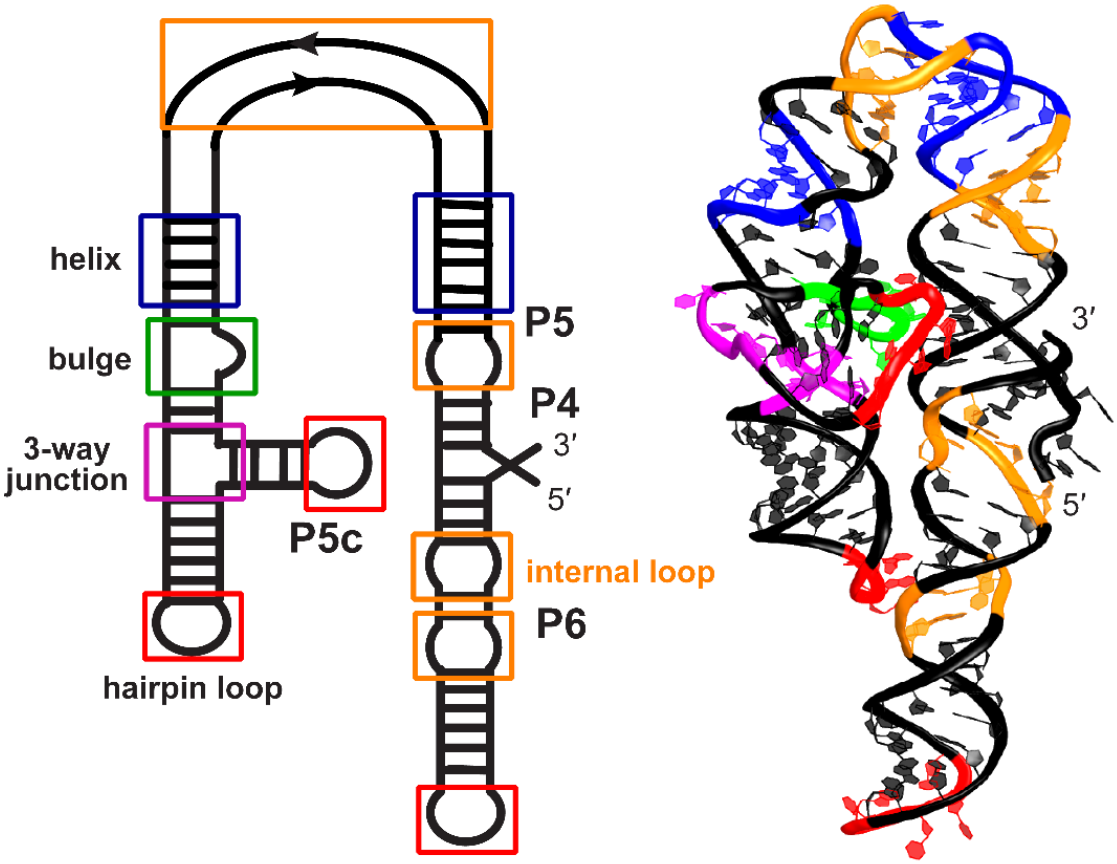

Figure 1-3: Structure of P4-P6 RNA of the *Tetrahymena* group I ribozyme indicating several motifs (L) secondary structure and (R) 3-dimensional structure. (Orange box indicates internal loops, red hairpin loops, blue helices, green asymmetric internal loop or bulge, pink 3-way junction).

1.3.2. Loop motifs

Loops are characterized as single-stranded regions within the RNA helices which are generally formed through the linkage of the 3′ and 5′ ends of double helical structures. The loops are crucial for functional RNA acting as bending sites and allow the helix to

form. According to the SCOR (The Structural Classification of RNA) databases [21], the hairpin or external loop must be close with Watson-Crick pairing, and the length might vary between 2~14 nucleotides. Depending on the position of the loop within a RNA module, loop motifs are of several types: hairpin loop (end of double helices: such as, GNRA and UNCG tetraloop motifs, T-loop and D-loop motifs), internal loops (separate double helices into two fragments: such as, C-loop, tetraloop receptors and kink-turn motif). Internal loop sometimes composed of an unequal number of nucleotides bases in RNA strands, called bulges (**Figure 1-3**) [21, 27].

1.3.3. Junction motifs

Junction motifs are the intersection of multiple double helices (three or more). These double helices are separated by single-strand sequences of zero or more residues. There are N linker (joining) sequences for N helices in a junction loop motif, however; some of the linker sequences may be of zero length. Although multi-helical junction loops have not been as systematically or extensively studied as the simpler hairpin and internal loops, some generalizations have been made for the comparatively common three-way and four-way junctions. The examples of three-way junction motif are the hammerhead ribozymes and P5abc subdomain in the P4-P6 RNA of the *Tetrahymena* group I ribozyme (**Figure 1-3**) [14, 21].

1.3.4. Binding motifs

RNAs are negatively charged biomolecules. So, it is very significant for RNA molecules to bind with the positively charged ligands for either their structural stability or for their function. Ligand binding is vital for ribozymes, riboswitches and spliceosomal

splicing reaction, and in facilitating RNA-protein interactions and mediating intermolecular RNA tertiary interactions. RNA ligand-binding is generally used as a parameter to reveal high selectivity and specificity, even though the presence of several motifs capable of controlled binding of a particular ligand [21].

1.3.4.1. Metal ion binding

Metal ions (mostly magnesium and potassium) play crucial roles in the formation of globular RNA structures through association with the major groove of RNA molecules [26]. Until now, several classes of metal ion complexation with RNA biomolecules have been demonstrated [21]. Herein, the author mentions three metal ion-RNA interactions. The first class is the diffuse ion association which is governed through electrostatic interaction between negatively charged RNA and positively charged metal ion. Consequently, the negatively charged ion, surrounding the phosphate oxygens of RNA, would be neutralized.

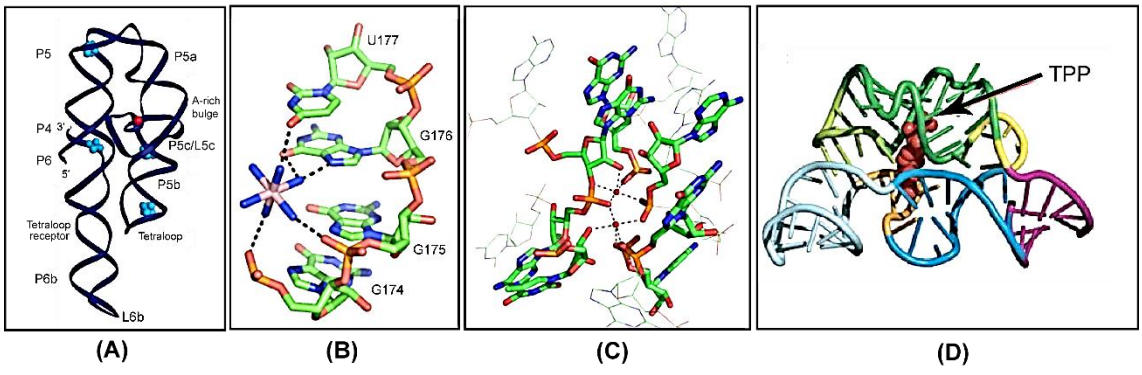

Figure 1-4. Metal ion coordination with RNA molecules. (A) Metal ions binding site in the crystal structure of the P4-P6 RNA (adapted with the permission from [26]). (B) Outer sphere coordination of metal ion in the P5c element of the *Tetrahymena* group I ribozyme (adapted with the permission from [28]). (C) Inner sphere coordination. The red balls designate metal ions and dashes line coming from the ions specify coordination with the particular groups on nucleotides (adapted with the permission from [29]) (D) TPP binding motif in TPP riboswitch (adapted with the permission from [30]).

The second class is outer sphere coordination which is formed between the charged metal ion and a precise location of RNA (**Figure 1-4**). The crystallography and cobalt (II) hexamine or osmium hexamine analysis of the P4-6 domain of the *Tetrahymena* group I ribozyme showed that G–U tandems (a conserved pair in rRNA) generally coordinates with a magnesium ion through the outer-sphere mechanism. These G–U tandems were identified in the several positions of the P4-P6 RNA including P5b and P5c, and lower extend P5 regions bearing high electron density. The outer sphere magnesium coordination is usually maintained by hydrogen bond acceptor including N7 and O6 of guanosine, O4 of uridine and neighboring phosphate oxygens [26]. The third class is inner sphere coordination which is essential for the catalytic reaction. Three magnesium ions are necessary for catalyzing substrate cleavage reaction by the group I ribozymes.

1.3.4.2. Ligand binding

Three classes of RNA molecules have been well-known which bind to small ligands: in vitro evolved (SELEX) aptamers, riboswitches, and specific functional RNAs such as the group I introns that bind GTP cofactor. GTP binding at the P7 position of the group I ribozymes have been shown to govern by base triple sandwich (stacking) motif [21]. TPP riboswitch of *E.coli* thiM mRNA specifically binds with TPP ligand (**Figure 1-4D**) [30].

1.3.5. Long range tertiary interacting motifs

Some classes of functional RNA molecules hold well-organized shape critical for their biological functions. Diverse metabolic processes such as mRNA splicing, tRNA processing and the peptide bond formation in protein synthesis, are maintained by RNA

molecules with intricate tertiary structures that are governed by repeated tertiary motifs interconnected through several interactions. In this section, the author demonstrated several tertiary interacting motifs that support RNA to form globular shape through multiple interactions.

1.3.5.1. Base triples, ribose zipper and A-minor motif

Base triples are very common in RNA tertiary structures, which are defined as the repeated cluster of three nucleotides that interact edge-to-edge through hydrogen bonds. Although several base triples occur in the shallow/minor groove (called A-minor motif), base triples can also be found in the major groove of RNA helices. Base triples which involve a third strand within the major groove often use the Hoogsteen face of the purine nucleotides. In some cases, the hydrogen bonding occurs between the free 2′–OH groups of a ribose sugar of double helical bases and a neighboring RNA strands through non-Watson-Crick base pairing are called ribose zipper (**Figure 1-5, 0-II**) [14, 31].

On the other hand, the insertion of adenosines into the minor/shallow groove of neighboring double helical base pairs through base triples is called A-minor motif (**Figure 1-5, 0-III**) [32-34]. A-minor motif usually an essential type of tertiary interacting motif which stabilizes interactions between RNA helices, interactions between junctions and tight turns and contraction between loops and helices. A-minor motif is a dominant motif among the tertiary interacting motifs present in RNA molecules accounted for 37% followed by coaxial stacking (32%) and ribose zipper (20%). There are mainly four types of A-minor motif namely type 0, type I, type II and type III. Among the four kinds of A-minor motifs, 52% are of the type I followed by 31% type II, 10% type 0 and 7% type III [35].

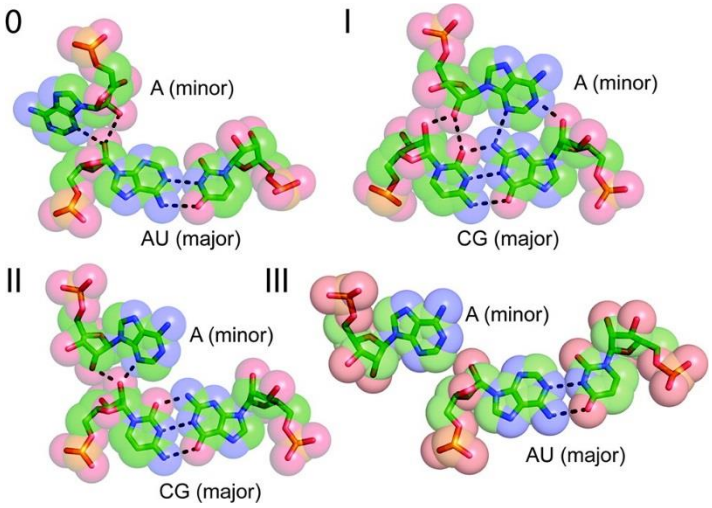

Figure 1-5: Base triples showing ribose zipper (0-II) and A-minor motif (0-IV) tertiary interactions (adapted with the permission from) [14].

1.3.5.2. Coaxial stacking

Base stacking is one of the most crucial driving forces during the development of RNA tertiary structures. Nucleotide bases of two distinct helices stack to each other and form more stable helical structure, are called coaxial stacking [21, 36, 37]. The loop-receptor interaction between P5b and P6a motifs of the *Tetrahymena* group I ribozyme is mediated by coaxial stacking (**Figure 1-6A**) through base triples.

1.3.5.3. Loop-receptor interacting motif

Loop-receptor interaction is among the most common interactions in the large ribozymes. This interaction is generally formed between a terminal hairpin loop and its corresponding receptor through base-triple interaction [31]. For example, the interaction between GAAA tetraloop (GNRA tetraloop) and 11 nucleotide receptor motif which has

been reported as a stable interaction in the RNA tertiary structure. Experimental studies have shown that loop-receptor interaction has been used extensively in the fabrication of complex RNA nanostructures. 3D structure of tetraloop/receptor interaction was first revealed in the three-dimensional (3D) contacts during the structural study of a hammerhead ribozyme. Similar interactions were also reported within the group I ribozymes, RNase P ribozymes and so on [14]. In the *Tetrahymena* group I ribozyme, the interaction form through base triples within A151-U224-A248 (**Figure 1-6A**) [31].

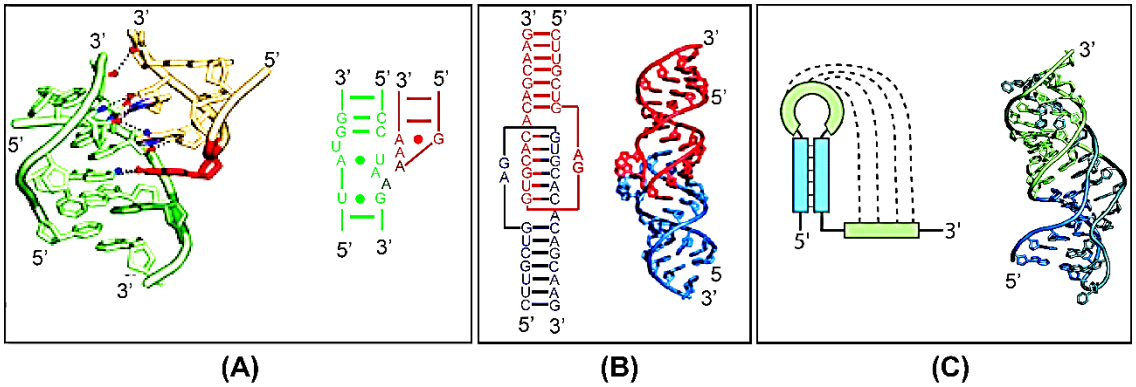

Figure 1-6: Long range tertiary interactions in RNA molecules. (A) GAAA tetraloop-receptor interaction from the *Tetrahymena* group I ribozyme, PDB ID 1HR2. (Left) Green indicates receptor and tan indicates tetraloop, stacking interaction occurs between an A-platform (dark green) and the second adenine of GAAA tetraloop (dark red); (right) consensus sequence. (B) The HIV-1 dimerization initiation complex (kissing loop), PDB ID 1K9W. Red and blue color indicates hairpin loop in both (left) secondary and (right) tertiary structures. (C) Hairpin structure with long-range pseudoknot interaction (left). The crystal structure of telomerase pseudoknot, PDB ID 2K96. (Figure A, B and C were adapted with the permission from [14])

1.3.5.4. Kissing loop interaction

Kissing-loop interaction is formed between two unpaired hairpin loops through complementary canonical (Watson-Crick) base pair. The base pair in kissing loop interaction may occur within two to several complementary bases. The human immunodeficiency virus-1 (HID-1) dimerization initiation site is the best example of kissing loop interaction which has six continuous coaxially stacked base pairs (**Figure 1-6B**) [38]. In the *Tetrahymena* group I ribozyme, P13 (P9.1-P2.1) and P14 (P5c-P2) kissing loop interaction has been shown to occur within four continuous nucleotide bases [39].

1.3.5.5. Pseudoknot interaction

Pseudoknot forms between an unpaired hairpin loop and a single stranded complementary sequence (**Figure 1-6C**). This interaction sometimes contains coaxial helices and form a stable RNA. One particular example of this type of interaction is human telomerase RNA [40].

1.4. Ribozymes and its history

Ribozymes, which are also called RNA enzymes, have been nomenclatured from the combination of shortening form of ribonucleic acids and enzyme. Ribozymes are well-studied functional RNAs. Before the discovery of ribozymes, protein enzymes were considered as only the biological molecules responsible for catalytic activity. In 1982, Thomas Cech at the University of Colorado discovered the first catalytic RNA molecule (*Tetrahymena* group I ribozyme) [41, 42].

In 1967, Francis Crick et al. suggested that RNA materials could also have catalytic activity. This notion formed the basis upon the discovery that ribonucleic acid (RNA) could organize complex secondary structures [43]. Later in the 1980s, Thomas Cech, a Chemist at the University of Colorado, was studying the self-splicing activity of ribosomal RNA intron in *Tetrahymena thermophila*. When he was trying to purify the biological enzyme liable for this cleavage activity, he eventually observed that the intron could be spliced out without adding any cell extract. After a long cherish efforts, Cech proposed the intron could involve in the breakdown and reform the phosphodiester bond [44, 45]. The term ribozyme was first coined by Kelly Kruger group in 1982 in an article published in Cell [46].

In the meantime (1983), Sidney Altman from Yale University, who had been studying the way of tRNA processing in the cell using an enzyme, called ribonuclease P (RNP) or RNase P consisting of RNA and protein components, responsible for the maturation of tRNA. He found that RNA component of RNase P was catalytic part of the enzyme. Later, Altman exposed that RNA could act as a biological catalyst by presenting that the ribonuclease P RNA subunit can mediate the hydrolysis and catalysis of pre-

tRNA into mature tRNA even in the absence of protein molecule. In 1989, Thomas Cech and Sidney Altman were awarded the Nobel Prize in chemistry for their outstanding contribution in the discovery of catalytic RNA [45]. After the discovery of the *Tetrahymena* group I ribozyme and RNase P ribozyme by Cech and Altman, respectively, several researchers have unveiled various examples of catalytic RNAs involved in the self-cleaving activity. In the following section, the author discussed various types of ribozymes that have been discovered until now.

1.5. Classification of ribozymes

Until now, several classes of ribozymes can be found that could be differentiated according to their nature, sources, biochemical structures, and reaction mechanisms. The author grouped the ribozymes into two classes based on their sources namely natural ribozyme and artificial ribozymes (**Flowchart**). Naturally occurring ribozymes can further be divided into small (<200 nt) ribozymes and large (>200 nt) ribozymes. The small ribozymes excise itself through transesterification and also called ribonucleolytic ribozymes. Hammerhead, hairpin, Hepatitis delta virus (HDV)-like, *glm*S, Varkud satellite, twister, twister sister, pistol, hatchet [47], CoTC (co-transcriptional cleavage) [48], *CPEB3* [49] are the examples of small ribozymes (**Figure 1-7**). The large ribozymes, including group I and group II ribozymes, catalyze self-cleavage reaction using GTP cofactor. These ribozymes follow the transesterification to remove its intron and rejoin the mRNA exons. On the other hand, RNase P ribozymes, a large ribozyme, involve in the processing of immature tRNA to the mature tRNA through hydrolysis of 5′-ladder sequence [44]. The ribosome, consists of rRNAs and several proteins, acts as catalytic

machinery, which involves in the catalysis of the peptide bond formation during protein synthesis (**Figure 1-8)** [50].

The author also listed some of the artificial ribozymes (Class I RNA ligase, R3C ligase, L1 ligase, self-aminoacylating ribozyme, aminoacyl tranferase ribozyme, sulfer alkylating ribozyme, self-nitrogen alkylating ribozyme, Mg^{2+} self-cleaving ribozyme, bridged biphenyl isomerase ribozyme, mesoporphyrin metalating ribozyme, leadzyme) which have been discovered through various strategies (**Flowchart**) [182].

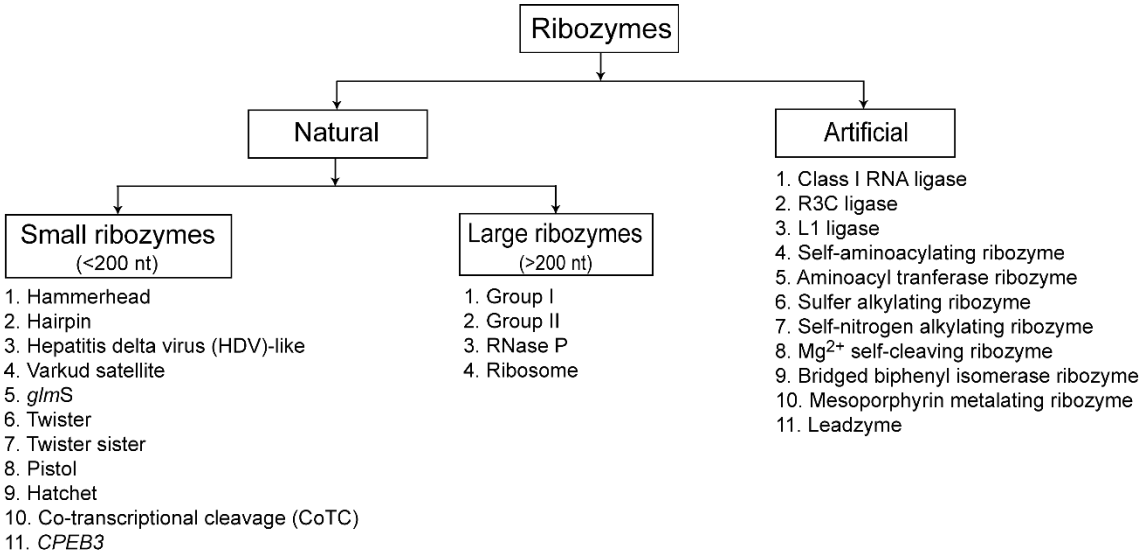

Flowchart: Various types of ribozymes

1.5.1. Small ribozymes

The author listed eleven small naturally occurring ribozymes. These ribozymes catalyze site-specific cleavage in the absence of protein enzymes, and usually follow internal phosphoester transfer using general acid/bases and metal ions chemistry. Small ribozymes including, hammerhead, hepatitis delta virus-like and twister are ubiquitous in

nature, i.e. can be found all species of life. The *glm*S ribozymes are widely distributed in bacteria, existing in around 50 UTR of genes essential for the production of glucosamine-6-phosphate. Recently, Breaker and co-workers discovered four novel classes of ribozymes namely, twister, twister sister, pistol and hatchet with the help of advanced bioinformatics pipeline [47].

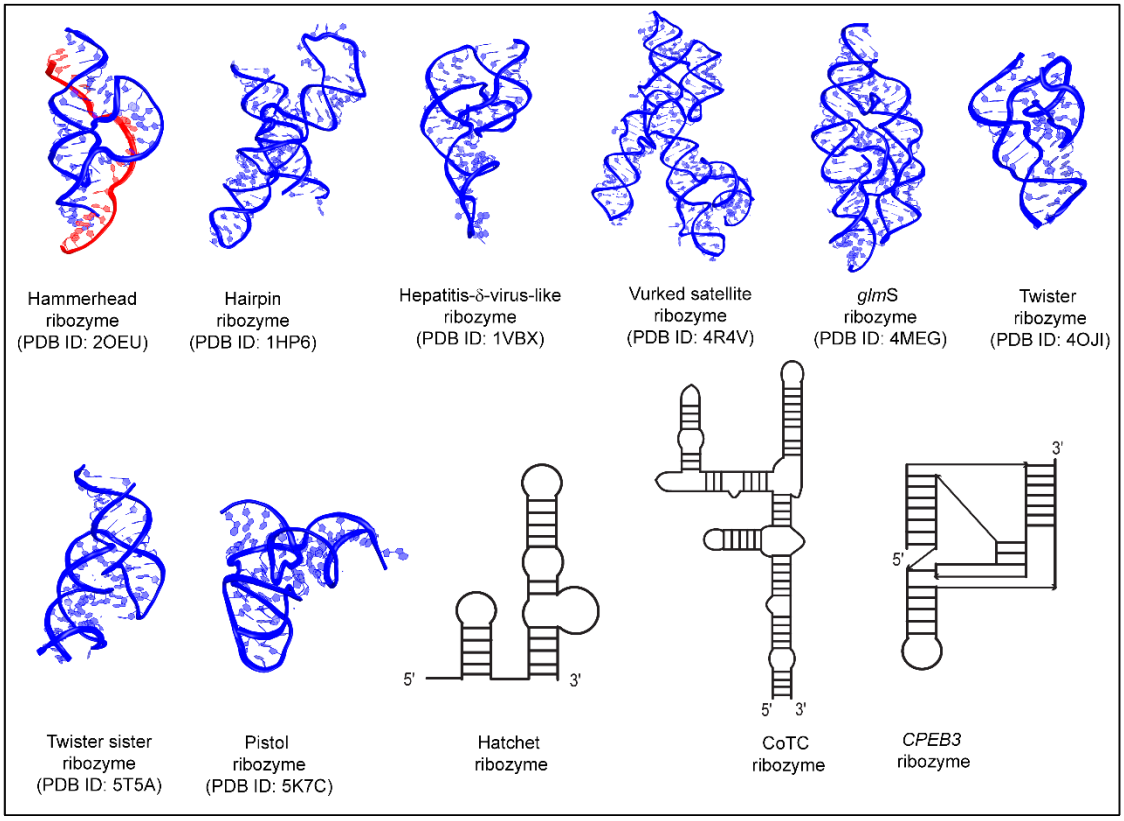

Figure 1-7: Structure of naturally occurring small ribozymes.

1.5.2. Large ribozymes

Large ribozymes are those which consist of several hundreds to 300 nucleotides or more and were first discovered ribozymes. Large ribozymes perform very essential functions in the cell, for example, peptide bond formation during protein synthesis, tRNA maturation and mRNA splicing. The author listed four large ribozymes, such as group I,

group II, RNase P and ribosome. Among them, group I and group II ribozymes are involved with splicing reaction using metal ions. These ribozymes catalyze the reaction via two step transesterification reaction. Bacterial RNase P ribozymes are ribonucleoprotein, consists of around 375-nucleotides and a small protein. The RNA of RNase P consists of S-domain and C-domain. S-domain recognize the tRNA precursor and C-domain cleave 5'-ladder of tRNA for its maturation [51]. The protein synthesis from the amino acids utilizing an mRNA template is a fundamental reaction in the cell, which occurs in an RNA-protein complexes called ribosome. Amino acids units are added to the growing peptides through the formation of peptide bond. The catalysis of peptide bond formation occurs in ribosome, the catalytic core of which has been found to be made entirely of RNA (rRNA) [50].

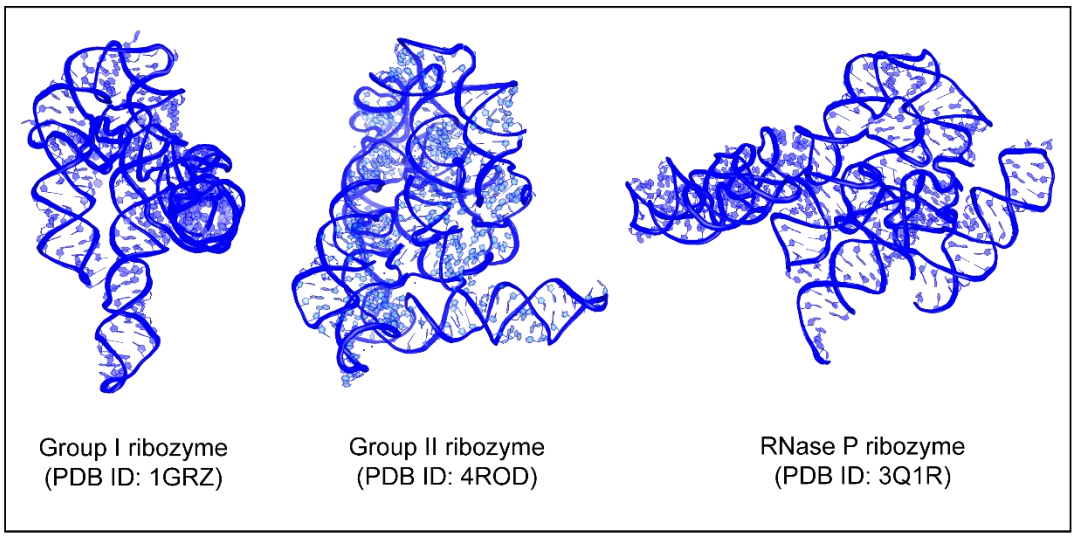

Figure 1-8: Structure of naturally occurring large ribozymes

1.6. Structures of group I ribozymes from *Tetrahymena thermophila* and *Pneumocystis carinii*

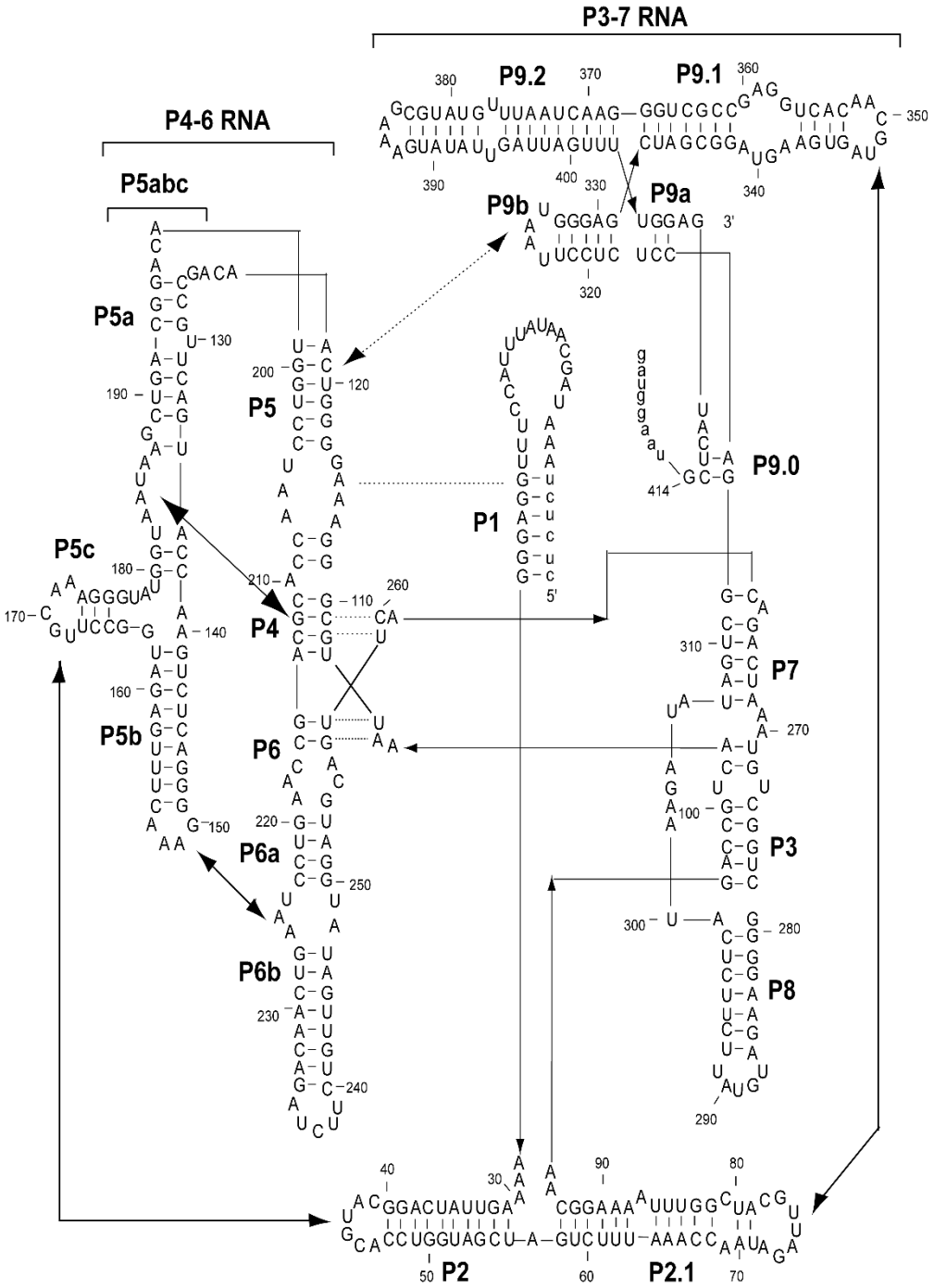

Figure 1-9: Secondary structure of a group I ribozyme from *Tetrahymena thermophila.* Solid line with two arrowhead indicated long-range tertiary interaction. Dot line with two arrowheads indicate tertiary interaction essential for organizing the binding pocket of the guanosine cofactor. Small letters in both 3′ and 5′ sites indicate the exon nucleotides.

Group I introns are an important class of ribozymes which catalyze their own excision through two sequential transesterification reaction using GTP as a cofactor. The secondary structures of group I ribozymes share similar structural framework consisting of nine (P1-P9) regions organized into three elements P1-3, P4-6, and P3–7 [52]. The conserved catalytic core is positioned at the intersection of P4-6 and P3-7 modules. In the *Tetrahymena* group I ribozyme, P5abc element provides additional stability of the active structure through P5b–P6b and P5c–P2 (P14) interactions. Although a group I ribozyme from the *Pneumocystis carinii* contains P5b–P6b (loop/receptor) interaction but does not have the P5c–P2 (P14) interaction (**Figure 1-9, 1-10**).

The P9 module of the *Tetrahymena* ribozyme consists of several helical stems and loops. Two of these loops are involved in the long-range tertiary interactions including P5–P9b and P2.1–P9.1 (P13) interactions. The loop involves in P5–P9b interaction consists of UAAU at P9b element. The P4-6 domain of the *Tetrahymena* ribozyme consists of two-way junction motif which acts as a sharp bending site between two (P5-4-6 and P5abc) modules of P4-6 RNA (**Figure 1-9**).

On the other hand, the P9 module of the *Pneumocystis carinii* type group I ribozyme is rather short and consists of only a GAAA tetraloop with a short helix which is involved in the long-range P5–P9 interaction (**Figure 1-10**). The P4-6 domain of *Pneumocystis carinii* ribozyme consists of three-way junction (3-WJ) motif. This 3-way junction motif has been placed instead of the two-way junction in the P4-6 RNA of the *Tetrahymena* ribozyme type to design RNA nanoassemblies in my study (**Figure 3-1B, 3-3**). The P5–P9b interaction of the *Tetrahymena* group I ribozyme plays an essential role in fine-tuning of the active tertiary structure to organize the binding pocket of the GTP

cofactor [52].

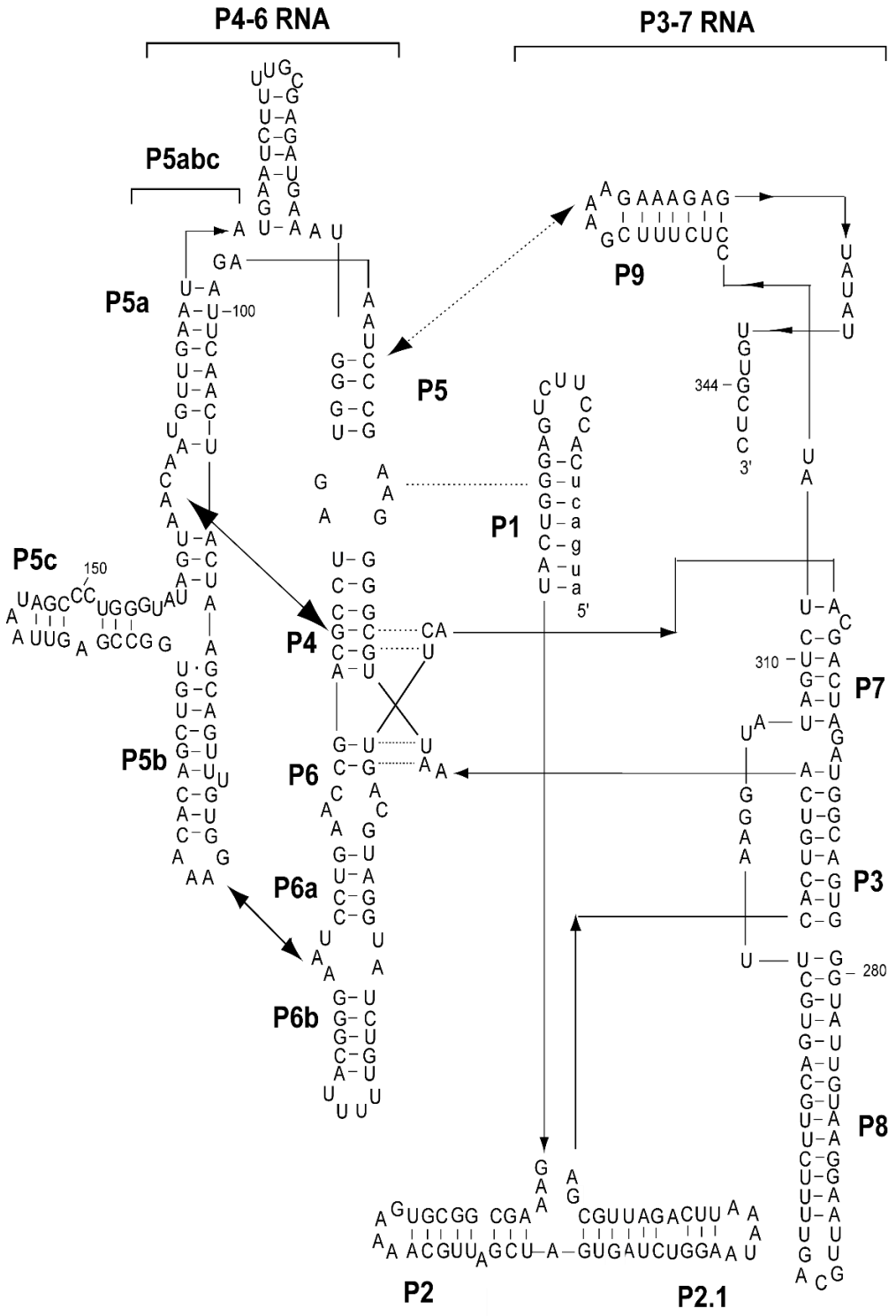

Figure 1-10: Secondary structure of a group I ribozyme from *Pneumocystis carinii.* Solid line with two arrowhead indicated long-range tertiary interaction. Dot line with two arrowheads indicate tertiary interaction essential for organizing the binding pocket of the guanosine cofactor.

Group I introns form complex three-dimensional shapes for their functions through multiple long range tertiary interactions and binding with metal ions (usually Mg^{2+}). Generally, metal ions have three types of interaction with group I ribozymes, namely diffusion, outer sphere coordination and inner sphere coordination. Group I introns contain some conserved nucleotides. Three of them are G-U tandem at P1 helix, G-C at P7 helix and ωG at 3′ splice site. P1 helix acts as binding site for substrate oligonucleotide. On the other hand, G-C tandem at P7 region recognize with GTP or ωG at 3′ site through base triple during the activation of the substrate cleavage reaction.

1.7. Application of RNA biopolymers

1.7.1. Role of RNA in Nanotechnology

Nanotechnology is a rapidly growing field that includes the formation and application of nanoscale-sized materials through the bottom-up assembly. In biology, a wide variety of ordered structures and shapes made up of biopolymers are considered as the attractive materials in the field of nanobioscience. Nucleic acids and proteins are promising molecules sharing similar intrinsic properties at the nanoscale level and hence, can serve as the scaffold for the construction of nanostructures and nanodevices in a bottom-up manner [53].

In the nucleic acid nanotechnology, Seeman pioneered the nanostructures design utilizing the DNA materials before more than 30 years [53]. In 1998, Seeman demonstrated 2D crystalline DNA shape that assembled from double-crossover of DNA molecules through sticky ends association following the complementary Watson-Crick crick base-pairing [54]. In 2006, Ruthemund established the DNA origami technique to design 2D nanomaterials of various shapes (square, rectangle, star, disc with three holes, triangles etc.) using single-stranded DNA (>700 nt) of the M13mp18 virus [55]. With the development of established algorithm, a wide variety of large and arbitrary 2D and 3D-shaped DNA nanostructures and assemblies have been constructed by several researchers [56, 57]. Proteins have large structural diversity than DNA and perform various functions. Since the comprehensive structural and functional properties are known for a wide diversity of peptides and proteins, it has also been attractive to use them as the building blocks for self-assembly with 3D structures and evolutionary fine-tuned function. For example, many peptides can be designed to assume well-ordered helical or β–sheet

structure that could be exploited as the building block of various structural topologies [58-62].

Nucleic acids biomolecules with their controlled assemblies are promising biomaterials for emerging field of nanobioscience including nanobiotechnology and nanomedicines. RNAs are among the most attractive biomaterials for nanotechnology purposes. RNA nanotechnology is rapidly growing field following the invention of DNA origami technique reported in 2006, with which various 2D and 3D assemblies have been constructed using single-stranded DNA molecules. Since RNA also single-stranded molecules and shares common structural properties like DNA, origami technique could be applied to single-stranded RNA with little modification to construct a variety of 2D and 3D RNA nanostructures [63, 64]. Geary et al. [65] co-transcriptionally constructed RNA tiles (150~660 nt bases) using single-stranded RNA origami. They introduced a crossover pattern called "dovetail seam" for the development of the ordered array of coaxially stacked helices. Very recently, Jaeger et al. developed nano-heart of RNA assemblies utilizing multiples RNA motifs following various bending and stacking strategies [66]. Polyhedral and polygonal RNA nanostructures have also constructed to use as molecular cargo to transport siRNA [67].

Until now, researchers constructed a variety of nanoscale-sized RNA following various strategies, however; most of the nanostructure (squares, jigsaw puzzle, octagonal, nanoring shape) were fabricated using short structural motifs and suitable linkers, such as, right angle motif (RA) [63, 68], UA-handle [63], 5-way junction (5-WJ) of tRNA [63, 66] and IIa corner motif of Seneca Valley virus (SVV) genome [69]. Although RNA motifs play an essential role in the development of various nanostructure, these construct

could not activate the biochemical function.

Another strategy of the RNA nanostructures development from naturally occurring ribozymes through modular engineering. In this case, RNA polymers could be constructed via self-assemblies of structural unit or within the variants. Guo, pioneer of RNA nanotechnology, used artificial phi29 RNA to construct dimer, trimer, hexamer and oligomers [70-72]. In addition, 1D and 2D RNA catalytic triangles and squares have also been reported through the modular engineering of the functional *Tetrahymena* group I ribozyme [73, 74]. Jaeger et al. [63] constructed 3D polyhedron from tRNA with precisely controlled over composition and stoichiometry. Such constructs have been suggested to provide the path towards RNA-based therapeutic delivery for nanomedicine.

1.7.2. RNA in modular engineering

In RNA biochemistry, modular engineering is an approach that subdivided a molecule into smaller independent modules and used them in various systems. Since the natural ribozymes are developed through molecular evolution, the emergence principle and methodology for modular engineering of RNA strongly rely on the hierarchical organization of naturally occurring RNA structures and their hierarchical folding. Over the few decades, tremendous advances in RNA structural biochemistry have enriched our knowledge of the structures and folding of self-folding natural RNA, including tRNAs, ribozymes, riboswitches, and ribosomes. The insight regarding the modularity of RNA design further influences us to exploit a number of small RNA modules for the fabrication of artificial building blocks [18, 75]. For example, the modular structure of the

Tetrahymena group I ribozyme has been studied extensively and has been used in various ways to construct one-dimensional array, two-dimensional triangles and squares [73, 74].

Small modular and scaffolding structures are also promising connectors in the development of RNA nanostructures, particularly if they are repeatedly recognized in naturally occurring RNA molecules. To design RNA nanoparticles, RNA duplex which acts as basal bricks, loop-loop interaction and the connector play a vital role in the RNA assembly process into 2D and 3D architectures [18, 76]. To obtain artificial architecture, it is necessary to design the scaffold by various motifs through 3D molecular software. Several natural motifs, such as junction motifs (tRNA), right angle motif (RA motif), and corner motifs have been used to fabricate various shape including, polyhedron [63], squares [64] and nanotriangles [69] through modular engineering.

1.7.3. Molecular evolution

RNAs are nucleotides polymers in which a series of nucleotides combine intermolecularly to form a long chain. RNA consists of nitrogenous bases attached to sugar-phosphate composite. RNA made of the long sequence of specific nucleotides and their nucleotide bases carry genetic information. According to the RNA world hypothesis, there were existing free-floating nucleotides in the prebiotic broth. These nucleotides continuously formed the linkage with one another, which often diffused away because of low free energy changes. However, some of the sequences accidentally had the catalytic abilities that reduced the energy of their sequence being created, facilitating them to hold together for a long time. Since the chain elongated, it had engaged comparatively matching nucleotides faster, insisting chain to form faster they were diffusing away. These

RNA chains had been hypothesized as the primitive form of life [77]. In the hypothetical RNA world, RNA biomolecules carried genetic information and catalyzed biological functions [78]. Such functional RNAs have been increased by their own replications. In some instances, their own-replications were mistakenly copied, mutated and evolved new functional RNAs and generated in the RNA world [79].

The artificial and fastest method of RNA evolution would be triggered by the molecular competition of enzyme mixtures or *in vitro evolution,* also referred as "SELEX" (**S**ystemic **E**volution of **L**igands by **E**xponential **E**nrichment). Through repeated cycles of selection, amplification, and mutagenesis, *in vitro* evolution gives us the opportunity to distinguish molecules of desired characteristics and functions from the large pool of random libraries with as many as 10^{10}–10^{16} individual species. In the pioneering works of *in vitro evolution* in 1990, Szostak et al. [80] and Gold et al. [81] separately demonstrated the selection procedures by which subpopulations of RNA molecules had been generated from the large pool of sequences that efficiently recognized organic dyes and T4 ligase, respectively. Joyce et al. [82] reported a selection strategy in which the *Tetrahymena* group I ribozyme cleaved the single-stranded DNA. In 1993, Szostak et al. [83] isolated novel classes of catalytic RNA from the large pool of RNA library, which can ligate two RNA molecules. Ulrich et al. [183] evolved an efficient aptamer that binds to a vascular endothelial growth factor (VEGF), which has been approved FDA as a therapeutic for age related muscular degeneration (AMD). Recently, Joyce et al. [184] developed L-RNA aptamer that specifically recognizes L-barnase, which breakdown the RNA molecules, thereby inhibit the function of the enzyme.

Although *in vitro selection* method has allowed us to identify particular RNA with

desired functional properties, this technique has some practical drawbacks. Since initial libraries do not possess structural constrains, prediction of secondary and tertiary structures of the identified RNAs is usually time consuming and laborious compared to that RNAs identified from living organism. Rational design of RNA structures and functions is a promising alternative that allow us to avoid or decrease the laborious structures analysis involved in *in vitro* strategy but this technique is still a difficult task. To avoid such difficulties, a new strategy termed "design and selection" has been employed to synthesize several artificial ligase ribozymes, such as, class-hc ligase [185], P4-P6 ligase [186], DSL (Design and Selected Ligase) [187] and class-YFL ligase [188], through the modular engineering of the *Tetrahymena* group I ribozyme.

The *Tetrahymena* group I ribozyme consists of a peripheral module (P5abc RNA) and a core module (ΔP5 RNA). Peripheral element is not directly involved in the substrate cleavage reaction, but, it helps core ribozyme to form a stable catalytic structure suitable for transesterification reaction. However, the absence of peripheral element markedly decreased the ribozyme function at low Mg^{2+} ion concentration. The addition of protein (CYT-18) [189] and polyamines [175], in absence of P5abc activator, recover the ribozyme activity and contribute in the molecular evolution. On the other hand, the addition of P5abc activator in *trans* also recovered the ribozyme activity which is comparable to that of parental ribozyme. Since the wild type *Tetrahymena* ribozyme can be dissected into P5abc element and ΔP5 element, and their interfaces assembly recovered the catalytic ability, this bimolecular ribozyme has been used to construct one-dimensional array [156], two-dimensional triangle and square [73].

Rahman et al. [169] reported that oligomerization of mutated P4-6/P3-7

bimolecular assemblies rescued the structural defects, which are completely inactive in bimolecular system. They also reported that oligomerization activate the bimolecular ribozymes through molecular crowding effects and cellular compartmentalization. Several investigators analyzed the effects of molecular crowders, such as, polyethylene glycol (PEG), on ribozymes activity and demonstrated that the crowders significantly increased the RNA-mediated catalysis [158, 159]. They demonstrated that PEG enhanced the rate of ribozymes-induced catalytic reactions through the destabilization of Watson-Crick bases, changing the water structure and altering conformational equilibria. Holliger et al. [127] proposed eutectic ice as a protocellular medium, which promotes the activity of RNA polymerase enzyme and protects it from the hydrolytic cleavage, allowing the synthesis of long replication products. Apart from these, various media, such as clay, micelles, vesicles, aerosol droplets, have been shown to provide propitious environment for self-replication of RNA and evolution [127].

Recently, Nozawa et al. [190] dissected, engineered and characterized bimolecular RNase P ribozyme from two different sources (E. coli and T. thermophiles). RNase P ribozyme is a class of enzymes involved in the maturation of precursor tRNAs by removal of their 5'-leader sequences. The Ribonuclease P enzyme consists of two self-folded domains (S-domain and C-domain). Such modular domain seems an attractive in the viewpoint of RNA nanotechnology and consequently, may contribute in the molecular evolution.

1.8. Motivation and purpose of study

RNA molecules are promising biopolymers that play pivotal roles in wide varieties of cellular processes, including, chemical transformation (catalysis and ligation), gene regulation, editing and molecular recognition (ligand binding). In order to perform these function, RNA molecules must hold complex and well-defined 3D structures through multiple tertiary interactions within various structural motifs. Such multiple interactions within various modules of naturally occurring RNA are also attractive from the viewpoint of RNA nanotechnology because the bottom-up fabrication of RNA nanoassemblies and nanostructures could be constructed from biological molecules. Some classes of functional RNAs biomolecules possess modular structures bearing several long-range tertiary interactions by which secondary structural domains are held together to form various shapes, including 1D (one-dimensional) assemblies, 2D (two-dimensional) and 3D (3-dimensional) architectures. For example, Guo et al. [70] constructed a variety of shapes from the engineering and redesigning of RNA component of DNA packaging motors of bacteriophage phi29 which has the application in nanomedicine and synthetic biology. Jaeger et al. reported various types of RNA shapes including, tectosquares [64], jigsaw puzzle [68], octagonal [63], nanorings [84, 85] and love [66] of RNA, using various short structural motifs (bending motif, kissing loop motifs and double helical linker). Geary et al. constructed RNA tiles assembling the RNA with total nucleotide size (150~660 nt) [65]. However, until now most of the nanostructures that have been designed used only short structural motifs and linkers. Researchers rarely handled and constructed nanostructures with large nucleotides bearing more than 600 nucleotides [65]. Besides, these nanomaterials have no functional activity at all. In this research, the author used the *Tetrahymena* group I ribozyme (414 nt) as a unit RNA to build up RNA one-dimensional

assembly, triangles and squares using various strategies.

The *Tetrahymena* group I ribozyme consists of a conserved domain (ΔP5) and non-conserved P5abc domain interconnected through multiple long-range tertiary interactions which include loop/receptor interaction, P14 (P5c-P2) kissing loop interaction and a bulge-helix interaction (**Figure 2-1**). The removal of P5abc domain drastically reduced the catalytic activity of the ribozyme at lower Mg^{2+} (3 mM) ion concentration. However, the addition of the peripheral domain (P5abc) in *trans* markedly recovered the ribozyme activity which can be comparable to the parental unimolecular system. This recovery of activity is governed by the stable complex formation between core ribozyme and activator module. Since the unimolecular ribozyme can be dissected into two pieces and its assembly retains the catalytic ability, it might be used as a structural platform to design assembled RNA nanostructures with various shape bearing functional properties.

In Chapter 2, a programmable formation of RNA one-dimensional (1D) array, closed triangles and squares was demonstrated through the modular engineering of P5c-P2 and loop/receptor motifs. To expand the repertoire of molecular recognition in the bimolecular system, the P5c-P2 and P5b-P6b (loop/receptor) motifs were modified with the alternative and orthogonal interfaces that could assemble a P5abc module and a ΔP5 module applicable to the fabrication of a variety of RNA nanostructures with large nucleotide size (>1600 nt).

The *Tetrahymena* group I ribozyme can be dissected into P4-6 self-folding domain and catalytic P3-7 domain (**Figure 3-1**). The P3-7 core cannot activate substrate cleavage reaction alone. The addition of the P4-6 RNA in *trans* govern the complex formation and activate the substrate cleavage reaction at high metal ion (50 mM Mg^{2+}) concentration.

The P4-6 RNA consists of a P5abc and a coreP5-4-6 element joined by a sharp bending (2-way junction) motif at the P5a-J5/5a-P5 module, which possesses a receptor motif for UAAU tetraloop at P9b of P3-7.

In Chapter 3, the two-way junction motif of the P4-6 domain was replaced with a three-way junction motif from a group I ribozyme (*Pneumonia carinii* type*)* which possesses receptor motif for GAAA tetraloop at the P5a-J5/5a-P5 module. Consequently, the new variant possesses a three-way junction, which has shown to form its folded structure as stable as the parent P4-6 RNA and governs the ribozyme activity. The newly constructed variant possesses a free helical region at the three-way junction which has been transplanted to the P8 position of the P3-7 element to design unit RNA for the construction of 1D array (**Figure 3-3**). Several disrupted mutations were installed at P2 and P9 elements of P3-7 RNA. The bimolecular combination of new P4-6 RNA /mutated P3-7 RNA could not activate the ribozyme catalysis. However, the oligomerization of bimolecular ribozymes rescue the structural defect to some extent through the activation of substrate cleavage reaction. Molecular assembly of P4-6/P3-7 ribozymes has been proposed to have the role in the molecular evolution through the effects of molecular crowding and cellular compartmentalization.

The condition within the cell is vastly different and ten to hundreds of times concentrated (due to the presence of macromolecules) than the reaction conditions used merely in most biological studies. Such crowding can alter the conformational equilibria, changes the reaction rates, and changes the water structures and activity. **In Chapter 4,** PEGs (polyethylene glycols) were used as the artificial cellular-like condition, although could not completely mimic, to see the effects to rescue the destabilizing mutation *in vitro*.

Experimental analysis showed that PEG exceptionally overcame the structural defects of those ribozymes systems which could not activate the substrate cleavage reaction in the presence of reaction buffer alone.

Chapter 2. Artificial RNA motifs expand programmable assembly between RNA modules of a bimolecular ribozyme led to application to RNA nanostructure design

2.1. Abstract

A bimolecular ribozyme consisting of a core ribozyme (ΔP5 RNA) and an activator module (P5abc RNA) has been used as a platform to design assembled RNA nanostructures. The tight and specific assembly between the P5abc and ΔP5 modules depends on two sets of intermodule interactions. The interface between P5abc and ΔP5 must be controlled when designing RNA nanostructures. To expand the repertoire of molecular recognition in the P5abc/ΔP5 interface, the interface was modified by replacing the parent tertiary interactions in the interface with artificial interactions. The engineered P5abc/ΔP5 interfaces were characterized biochemically to identify those suitable for nanostructure design. The new interfaces were used to construct 2D-square and 1D-array RNA nanostructures.

2.2. Introduction

Nanometer-sized biomolecules and their assemblies with precisely controlled shapes are attractive materials for the expanding field of nanobioscience, which includes nanomedicine and nanobiotechnology. Nucleic acids (DNA, RNA, and their derivatives) are among the most promising biomaterials for nanobioscience purposes [57, 86-89]. Nucleic acid nanotechnology is a rapidly developing research field as a result of the introduction of the DNA origami technique, first reported in 2006 [55], with which a

variety of 2D- and 3D-shaped DNA structures and assemblies can be constructed according to the established algorithm for structure design [55, 57, 86, 90]. As single-stranded DNAs are used as components for the DNA origami technique, this technique can be applied to RNA with minimal methodology modifications [91-94]. Polygonal and polyhedral RNA nanostructures, which may be used as molecular cargos to deliver siRNAs, have also been constructed using several design strategies [68, 85, 95-96, 67].

RNA is synthesized enzymatically in single-stranded form in the cellular environment, and several classes of RNAs, such as ribozymes and riboswitches, exhibit their functions after folding into defined 3D structures. These properties suggest that artificial RNA nanostructures designed by RNA origami (a methodology analogous to DNA origami) could be constructed *in vivo* [97, 98]. To expand the methodologies of RNA nanostructure construction beyond RNA origami, our group have recently reported the engineering of naturally occurring RNA structures [73]. This methodology allows us to install the biological functions of naturally occurring ribozymes and riboswitches into assembled RNA nanostructures, in which the biological functions can be expressed depending on the assembly of unit-RNA molecules. As a model system for this methodology, a bimolecular group I ribozyme was employed that was derived from the unimolecular *Tetrahymena* group I ribozyme and served as a structural platform.

The bimolecular group I ribozyme consists of a core ribozyme module (ΔP5 RNA) and an activator RNA unit (P5abc RNA), which form a complex expressing the full catalytic activity of the ΔP5 core ribozyme [99]. P5abc RNA binds tightly to ΔP5 RNA and stabilizes the catalytically active conformation of the ΔP5 core ribozyme [99, 100]. Through a rational strategy, P5abc RNA was connected with ΔP5 RNA to design a unit

RNA that can exhibit self-oligomerization. In the unit RNA, the two modules were joined by a connector element to allow the resulting unit to form closed oligomers with polygonal shapes, such as triangular trimers and square tetramers [73]. Self-oligomerization of the unit RNA yielded a mixture of assembled structures containing both triangular trimers and square tetramers. The selective formation of the desired structure was achieved by designing orthogonal interfaces between P5abc and ΔP5 modules [73, 101]. In the orthogonal interfaces, a non-natural RNA-RNA interacting motif, i.e., GGAA/R(GGAA), was employed which belongs to the same RNA motif family (GNRA/receptor motif family) as the natural counterpart GAAA/R(GAAA) [31, 34].

To increase the structural variety of the assembled RNA nanostructures, the repertoire of RNA-RNA interacting motifs is important because it governs the scope of RNA nanostructure design and assembly. In this study, RNA-RNA interacting motifs were exploited that can be used for RNA nanostructure assembly. The author examined artificial RNA-RNA interacting motifs structurally unrelated to the GNRA/receptor family but that act as modular parts to functionally substitute for GNRA/receptor motifs in unimolecular ribozymes.

2.3. Results and Discussion

2.3.1. Assembly of Bimolecular Group I Ribozymes through Artificial RNA–RNA Interacting Motifs

To determine the structural and functional modularity of artificial RNA-RNA interacting motifs that were generated through in *vitro* selection experiments, I investigated their abilities to act as modular parts for the assembly of the bimolecular P5abc/ΔP5 ribozyme derived from the Tetrahymena group I intron. For biochemical characterization of the bimolecular P5abc/ΔP5 ribozyme, simple methods have been established that allow to estimate the physical assembly between the two module RNAs, as well as the catalytic ability of the resulting complex [101, 102]. It was shown that three RNA-RNA interacting motifs could functionally substitute for the naturally occurring GNRA/receptor interacting motifs in unimolecular ribozymes [18, 103, 104]. Three artificial motifs were examined as alternative motifs to substitute the GNRA/receptor interacting motif supporting the intermolecular assembly of P5abc RNA and ΔP5 RNA to conduct catalysis.

Three sets of P5abc/ΔP5 pairs were constructed: the variant P5abc RNAs possessed the C-loop motif, the GAAC loop motif, or the GGAA loop motif in P5b region, substituting for the parent GAAA loop (**Figure 2-1A**); the variant ΔP5 RNAs possessed the R(C-loop) motif, the R(GAAC) motif, or the R(GGAA) motif in the P6 region, substituting for the parent R(GAAA) motif (**Figure 2-1B**). Among the three sets of interacting motifs, only the GGAA/R(GGAA) pair belonged to the GNRA/receptor family [31, 34]. The relative binding affinity between P5abc RNA and ΔP5 RNA was evaluated by electrophoretic mobility shift assay (EMSA) through the analysis of the

Mg^{2+} concentration-dependence of their complex formation. Mg^{2+} is known to act as a general stabilizer of RNA-RNA interactions [105, 106]. Weaker (or mismatched) RNA-RNA interactions require higher Mg^{2+} ion concentrations to establish a P5abc/ΔP5 complex that appears as a retarded band [101, 107]. Nine pairs of P5abc RNA and ΔP5 RNA were examined, among which three pairs were matched P5b/P6 pairs (**Figure 2-2A, lanes 3, 5, and 9**), and the remaining six were mismatched P5b/P6 pairs. EMSA with 10 mM Mg^{2+} showed complex formation in three P5abc/ΔP5 pairs with matched P5b-P6 interactions (**Figure 2-2A, lanes 3, 5, and 9**). The remaining six pairs with mismatched P5b-P6 interactions showed no retarded band, indicating that the disruption of the P5b-P6 interaction made the P5abc/ΔP5 complex unstable in the presence 10 mM Mg^{2+}. The importance of the P5b-P6 interaction in P5abc/ΔP5 complex formation was confirmed by the observation that no mismatched complex was stably formed even with 15 mM Mg^{2+}, although a very weak band was detectable in the mismatched P5b-GAAC/P6-R(GGAA) pair (**Figure 2-3A**). Then, the relative order of physical affinity was investigated among the three artificial RNA-RNA interacting motifs by reducing the Mg^{2+} ion concentration to 5 mM (**Figure 2-3B**). In EMSA with 5 mM Mg^{2+}, the P5b-GGAA/P6-R(GGAA) pair formed a bimolecular complex. However, neither the P5b-GAAC/P6-R(GAAC) pair nor the P5b-C-loop/P6-R(C-loop) pair showed a retarded band (**Figure 2-3B**), indicating that the physical affinities of these two matched pairs were not sufficiently high to stably form the P5abc/ΔP5 ribozyme complex in the presence of 5 mM Mg^{2+}. These observations indicated that the three artificial interacting motifs are orthogonal to each other. On the other hand, in the structural context of the P5abc/ΔP5 complex, the binding affinities of the two non-GNRA/receptor interactions were lower than that of the GGAA/R(1) interaction belonging to the GNRA/receptor family.

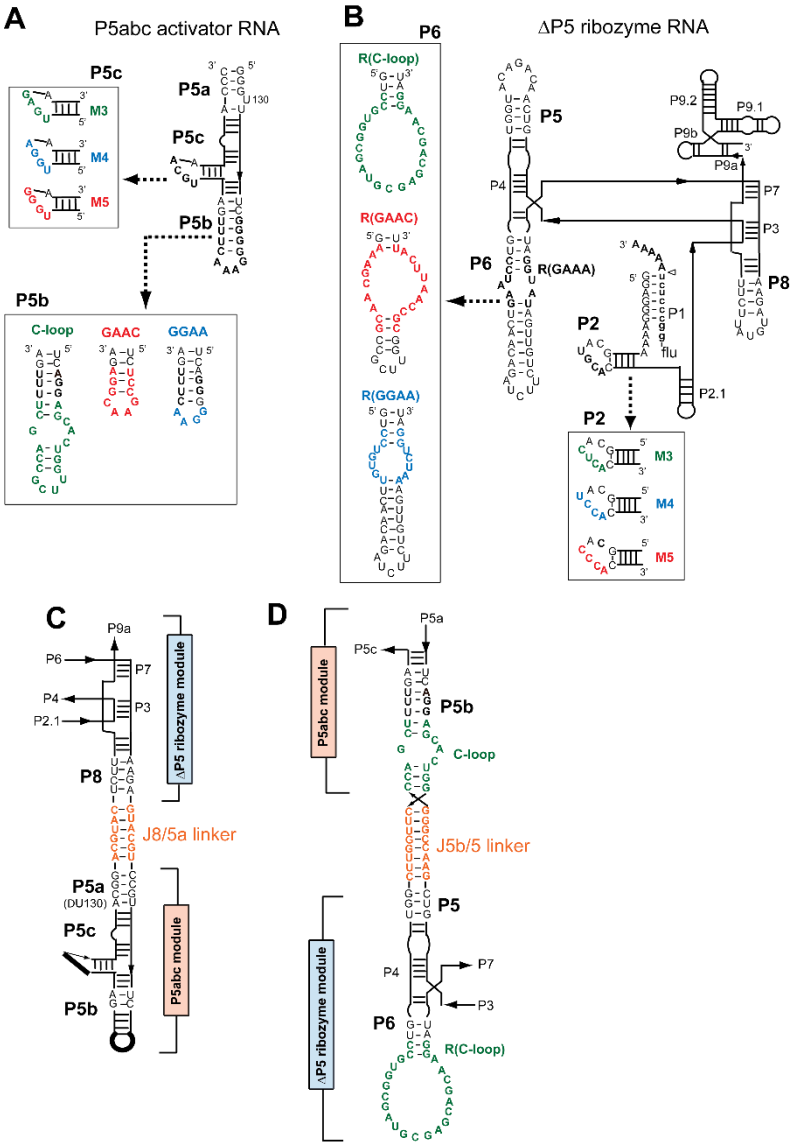

Figure 2-1. The activator RNA unit (P5abc RNA) and the core ribozyme module (ΔP5 RNA) were used to form a bimolecular group I ribozyme and engineered group I ribozymes for the assembly of RNA nanostructures. (**A**) Secondary structures of P5abc RNA and its variants used in this study. (**B**) ΔP5 RNA corresponding to the core structure of the *Tetrahymena* group I ribozyme. (**C**) Partial structure of Lα RNA and Lβ RNA showing the modular organization of the ΔP5 module and P5abc module, which are connected at P8 and P5a via a duplex linker. (**D**) Partial structure of F RNA showing the modular organization of the ΔP5 module that presents the R(C-loop) motif and the P5abc module with the C-loop motif. The two modules are connected at P5 and P5b via a duplex linker. In F RNA, the original 5′and 3′ends of the C-loop P5abc RNA (see **Figure 2-1A**) were capped with a stable 5′-UUCG-3 tetraloop.

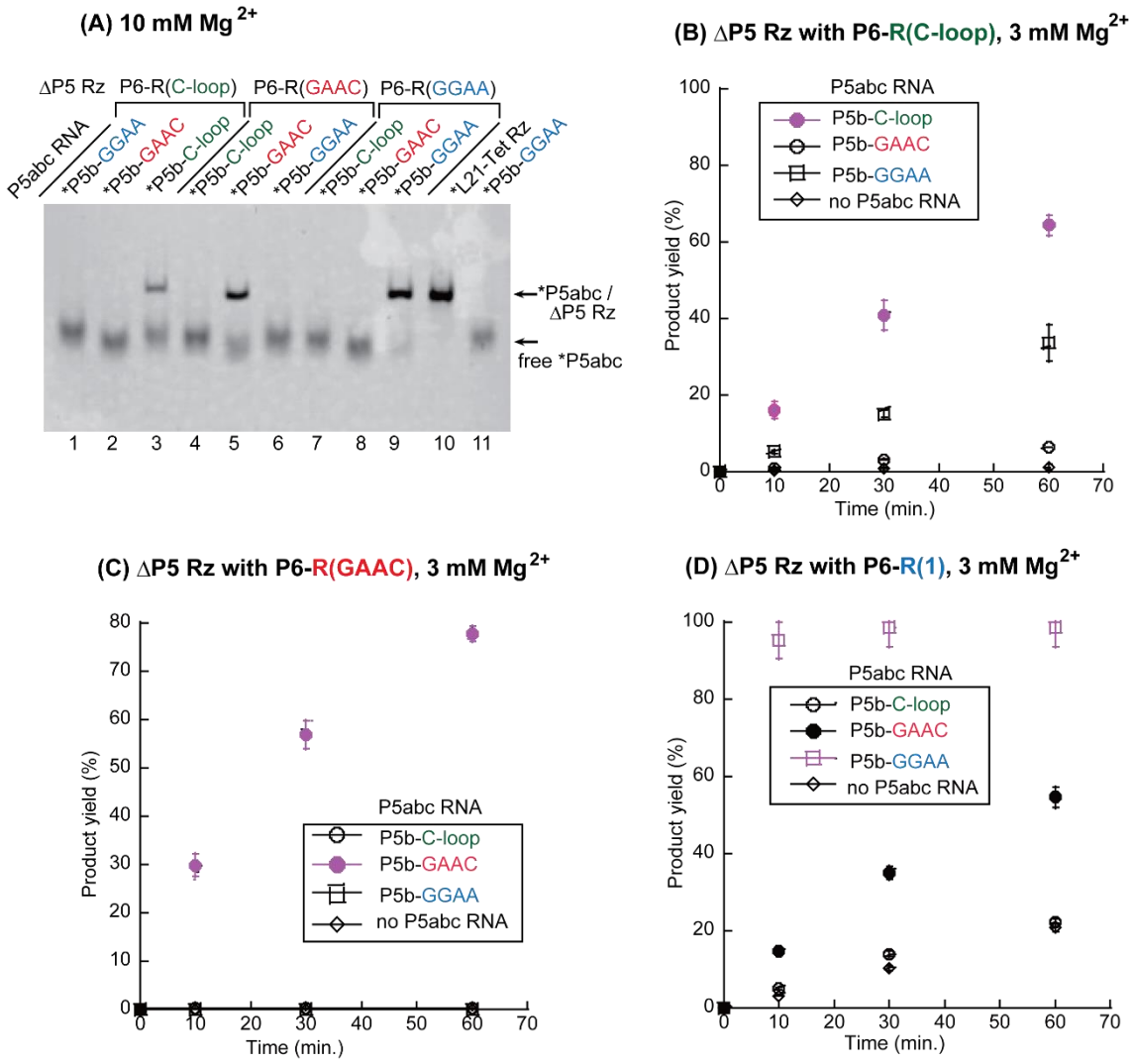

Figure 2-2. Biochemical analyses of RNA-RNA interacting motifs that alternatively support the P5b-P6 interaction in the P5abc/ΔP5 bimolecular ribozyme. (**A**) Electrophoretic mobility shift assay (EMSA) of the P5abc/ΔP5 complexes in the presence of 10 mM Mg^{2+}. L21-Tet Rz RNA (the parental unimolecular ribozyme from which the P5abc/ΔP5 complex was derived) and P5b-GGAA RNA were used as size markers for the complex and free-P5abc RNA, respectively. The asterisks indicate RNAs labeled with the BODIPY fluorophore. (**B-D**) Time courses of substrate-cleavage reactions catalyzed by the P5abc/ΔP5 bimolecular ribozymes in the presence of 3 mM Mg^{2+}. Some error bars are small enough to be hidden by the symbols.

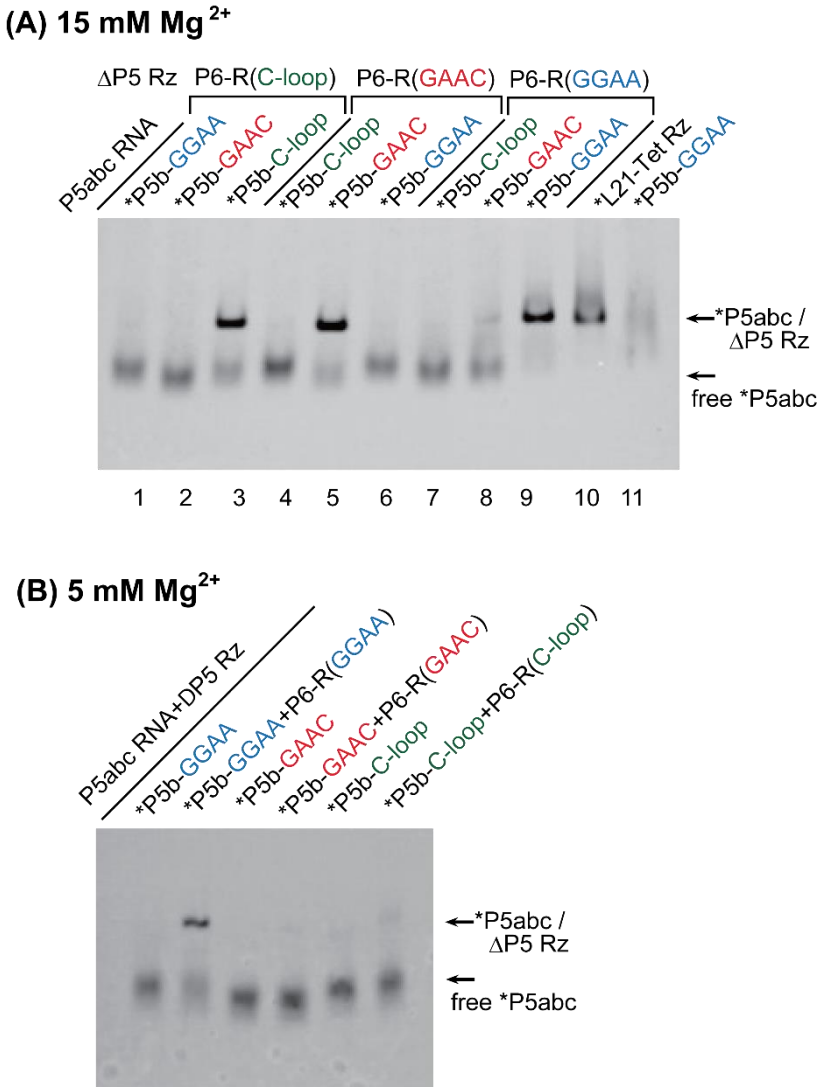

Figure 2-3. Electrophoretic mobility shift assay of P5abc/ΔP5 complexes in the presence of 15 mM Mg^{2+} (A) and 5 mM Mg^{2+} (B). L21-Tet Rz RNA (the parental unimolecular ribozyme from which the P5abc/ΔP5 complex was derived) and P5b-GGAA RNA were used as size markers for the complex and free-P5abc RNA, respectively. Asterisks indicate RNAs labeled with the BODIPY fluorophore.

To determine whether the P5abc/ΔP5 complexes supported by artificial motifs were catalytically active, their abilities to promote substrate-cleavage reactions were examined. A 1.5-fold excess molar amount of P5abc RNA (0.75 μM) was added to activate the ΔP5 core ribozyme in the presence of equimolar amounts of the substrate RNA (0.5 μM) and the ΔP5 RNA (0.5 μM). In the presence of 3 mM Mg^{2+}, three biomolecular ribozymes possessing matched P5b-P6 interactions exhibited higher catalytic activity than the remaining six pairs possessing mismatched P5b-P6 interactions (**Table 2-1**). On the other hand, the activity of the ribozyme with the matched C-loop/R(C-loop) pair (k_{obs} = 0.02 min^{-1}, **Figure 2-2B**) was the same as that with a mismatched GAAC/R(GGAA) pair (k_{obs} = 0.02 min^{-1}, **Figure 2-2D**). The comparison of nine bimolecular ribozymes indicated that a ΔP5 RNA variant with an R(GAAC) motif showed the highest specificity to its cognate partner P5abc with a GAAC loop (k_{obs} = 0.04 min^{-1}), since the remaining two P5abc RNAs could not activate the core ribozyme (**Figure 2-2C**). A ΔP5 RNA variant with an R(GGAA) motif exhibited the highest catalytic activity in the presence of its cognate partner (k_{obs} = 0.34 min^{-1}), among the three matched complexes. On the other hand, the P6-R(GGAA) variant was also moderately activated by a mismatched P5abc with a GAAC loop (**Figure 2-2D**). This was consistent with the results of EMSA in the presence of 15 mM Mg^{2+}, in which the mismatched GAAC/R(GGAA) pair weakly supported the P5abc/ΔP5 complex (**Figure 2-3A, lane 8**). The C-loop/R(C-loop) pair was the least active pair among the three matched pairs in terms of both the binding specificity of P5abc and ΔP5 RNA and the catalytic activity of the matched P5abc/ΔP5 complex.

Table 2-1: Effects of P5b-P6 interactions on observed rate constants of the bimolecular ribozymes.

P6 in ΔP5 ribozyme	P5b in P5abc RNA	k_{obs} (min^{-1})
R(C-loop)	C-loop	0.02
R(GAAC)	GAAC	0.04
R(GGAA)	GGAA	0.34
R(GGAA)	GAAC	0.02

2.3.2. Artificial Kissing Loop Interactions to Assemble Bimolecular Group I Ribozymes

It has been reported that complex formation of P5abc RNA and ΔP5 RNA is supported not only by the RNA-RNA interaction between P5b and P6, but also by four Watson-Crick base pairs between P5c in P5abc RNA and P2 in ΔP5 RNA [39, 101]. The P5c-P2 interaction has been shown to govern P5abc/ΔP5 complex formation cooperatively with, and dominantly over the P5b-P6 interaction [107]. To engineer the binding specificity between P5abc RNA and ΔP5 RNA, an artificial P5c/P2 base pair termed M3 (**Figure 2-1A**) were generated [101]. The M3 pair was orthogonal to the parent P5c/P2 pairs, but the P5abc/ΔP5 complex supported by M3 was less stable than the parent P5abc/ΔP5 complex [101]. Employing the new P5c/P2 base pairs in combination with three P5b-P6 interactions, the repertoire of P5abc/ΔP5 interfaces can be expanded, and some of the interfaces would be orthogonal to each other.

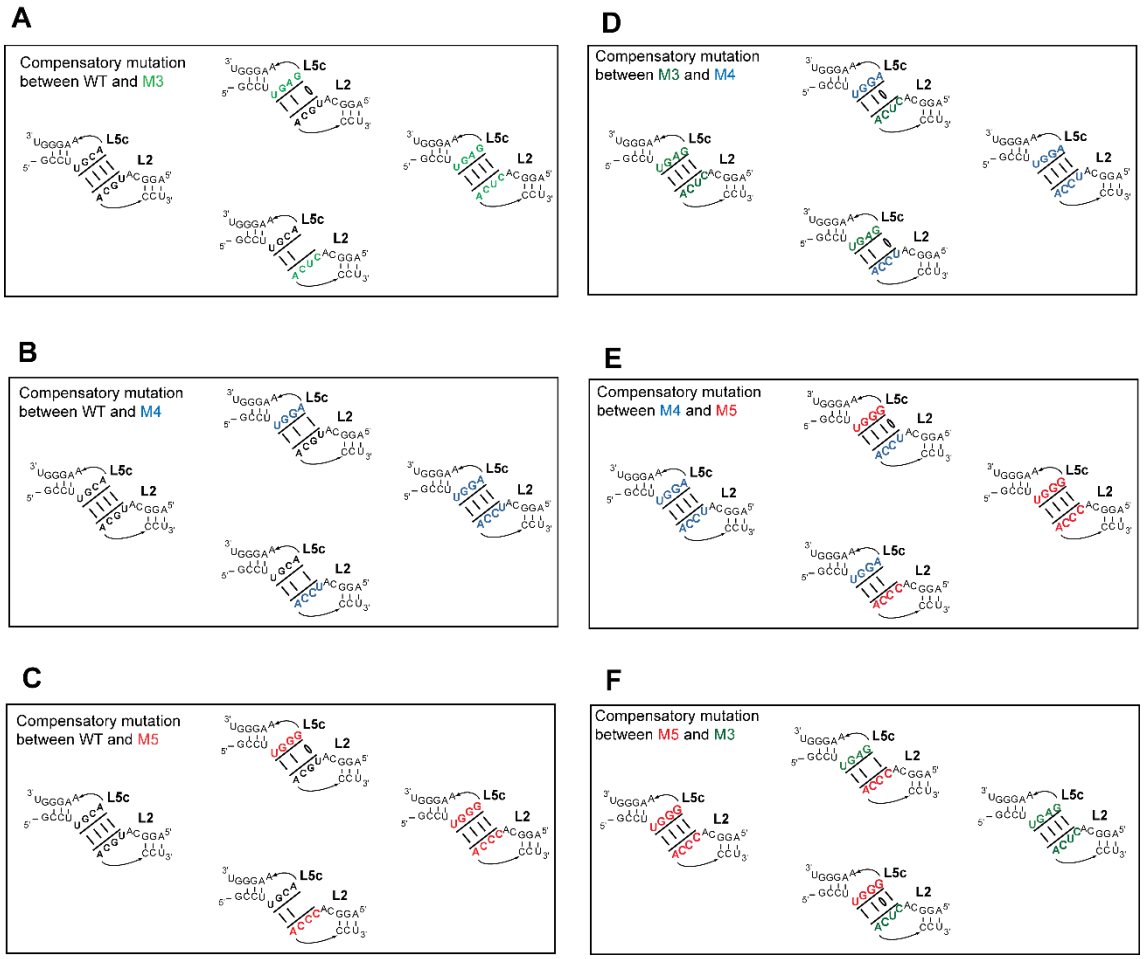

Figure 2-4. Possible base pairs between matched and mismatched combinations of P5c and P2. L5c and L2 indicate the loop regions of P5c and P2 elements, respectively.

In this study, two new P5c/P2 base pairs (M4 pair and M5 pair, see **Figure 2-1A**) were designed and compared their properties with the previously characterized M3 pair and with the parental, wild-type (WT) pair, by EMSA and a catalytic activity assay of the P5abc/ΔP5 complex (**Figure 2-5**). Although the design of M4 and M5 pairs was primarily focused on the orthogonality to the WT pair, I also examined all the 16 possible combinations of P5c/P2 base pairs (**Figure 2-4**) by EMSA and the activity assay.

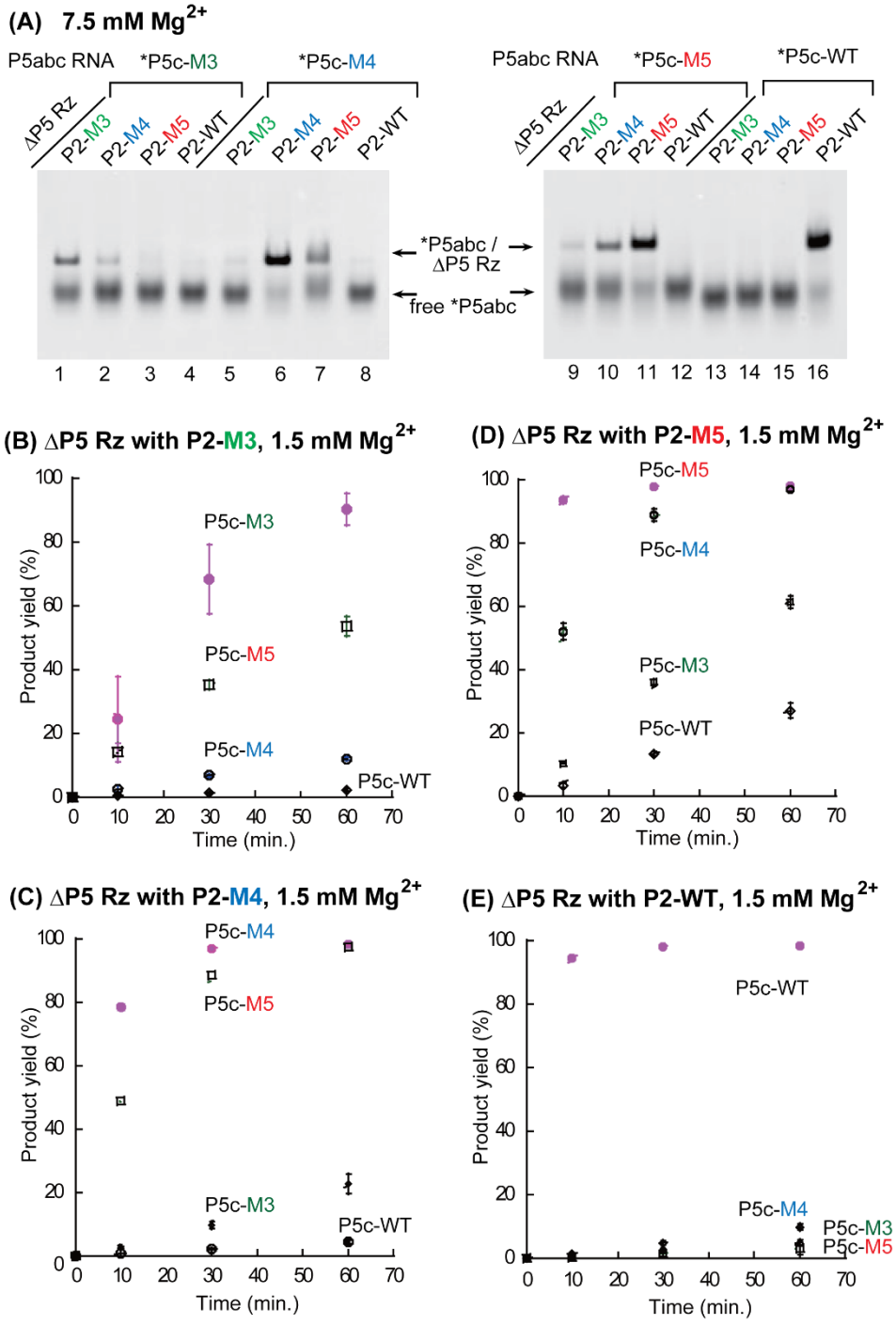

Figure 2-5. Biochemical analyses of the base pairs that can substitute the parental P5c-P2 base-pair interaction in the P5abc/ΔP5 bimolecular ribozyme. (**A**) EMSA of the P5abc/ΔP5 complexes in the presence of 7.5 mM Mg^{2+}. The asterisks indicate RNAs labeled with the BODIPY fluorophore. (**B**-**E**)Time courses of substrate-cleavage reactions catalyzed by the P5abc/ΔP5 bimolecular ribozymes in the presence of 1.5 mM Mg^{2+}. Some error bars are small enough to be hidden by the symbols.

In the presence of 5 mM Mg^{2+} (**Figure 2-6**) and 7.5 mM Mg^{2+} (**Figure 2-5A**), two matched P5c/P2 base pairs (WT and M5) stably supported the P5abc/ΔP5 complex (**Figure 2-5A and Figure 2-6, lanes 11 and 16**). At 5 mM Mg^{2+}, the M4 pair also formed the complex, but free P5abc RNA remained (**Figure 2-6, lane 6**). On the other hand, the M3 pair poorly supported the complex in the presence of 5 mM Mg^{2+} (**Figure 2-6, lane 1**), confirming the previous observation that the M3 pair interacted less strongly than the parental pair.

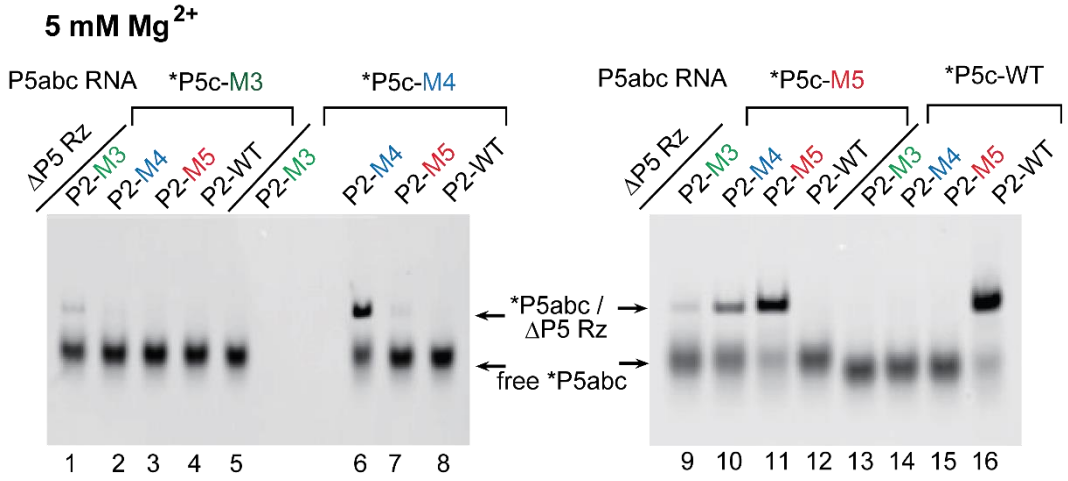

Figure 2-6. Electrophoretic mobility shift assay of P5abc/ΔP5 complexes in the presence of 5 mM Mg^{2+}. Asterisks indicate RNAs labeled with the BODIPY fluorophore.

While the M5 pair supported the complex more efficiently than both the M4 pair and the M3 pair (**Figure 2-6**), P5abc RNA with P5c-M5 (P5abc-M5) recognized its cognate ΔP5 RNA less selectively, because P5abc-M5 also formed complexes with mismatched ΔP5 RNAs containing P2-M3 and P2-M4 (**Figure 2-5A, lanes 9 and 10**). This property was expected, since, as shown in **Figure 2-4**, P5c-M5 forms four base pairs containing single G-U with P2-M3 and P2-M4. The formation of similar base pairs was

also predicted between P5c-M5 and P2-M4, and the pair formed the corresponding complex at a modest degree (**Figure 2-5A, lane 7**).

I then investigated whether the binding affinity and the specificity of base pairs, which were predicted in **Figure 2-4** and examined by EMSA (**Figure 2-5A**), correlated with the catalytic activity of P5abc/ΔP5 bimolecular ribozymes. In the presence of 1.5 mM Mg^{2+}, each of the four ΔP5 RNAs exhibited its highest activity with its cognate partner P5abc (**Table 2-2**). The parent WT bimolecular ribozyme (k_{obs} = 0.32 min^{-1}) and its M5 variant (k_{obs} = 0.31 min^{-1}) showed closely similar activity, and were 2-fold more active than the M4 variant (k_{obs} = 0.16 min^{-1}). The M3 variant (k_{obs} = 0.03 min^{-1}) was distinctly less active than the three complexes. The rate constant of the M3 variant (0.03 min^{-1}) was even smaller than those of two mismatched complexes having the P5c-M5/P2-M4 mismatched pair (**Figure 2-5C**, k_{obs} = 0.069 min^{-1}) and the P5c-M4/P2-M5 pair (**Figure 2-5D**, k_{obs} = 0.076 min^{-1}). These observations are qualitatively consistent with those from structure prediction and EMSA.

Table 2-2: Effects of P5c-P2 interactions on observed rate constants of the bimolecular ribozymes.

P2 in ΔP5 ribozyme	P5c in P5abc RNA	k_{obs} (min^{-1})
WT	Wt	0.32
M5	M5	0.31
M4	M4	0.16
M3	M3	0.03
M4	M5	0.069
M5	M4	0.076

2.3.3. Formation of RNA Squares through Selective Assembly of Engineered Group I ribozymes

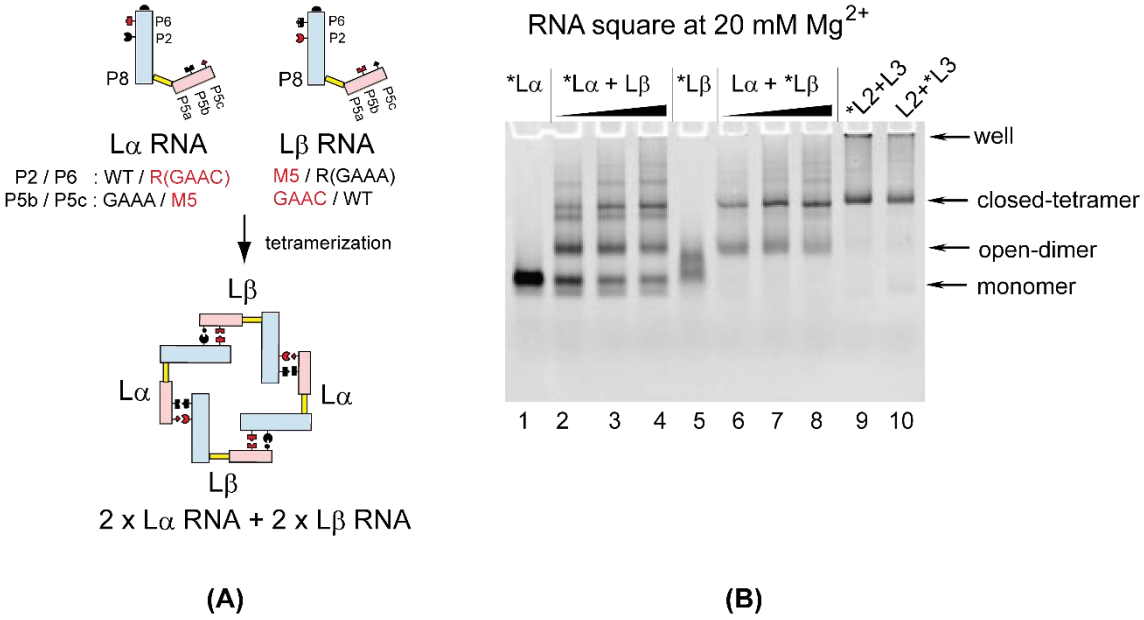

Figure 2-7. Formation of RNA squares whose assembly was mediated by the association between the P5abc module and the ΔP5 module. (**A**) Selective formation of closed tetramers by Lα RNA and Lβ RNA. (**B**) EMSA of Lα RNA + Lβ RNA in the presence of 20 mM Mg^{2+}. The asterisks indicate monomer RNAs labeled with the BODIPY fluorophore. In lanes 1 and 5, the concentrations of Lα and Lβ were 0.5 μM. The concentrations of Lα + Lβ were 0.5 + 0.5 μM in lanes 2 and 6, 1.0 + 1.0 μM in lanes 3 and 7, and 2.0 + 2.0 μM in lanes 4 and 8. The concentrations of L2 + L3 were 0.5 + 0.5 μM in lanes 9 and 10.

To design artificial RNA nanostructures with new P5b/P6 and P5c/P2 interacting pairs through modular engineering of the group I ribozyme, the GAAC-R(GAAC) pair and the M5 pair were chosen as new modular parts for a closed RNA tetramer with square shape. Monomer units of this square tetramer are engineered variants of the group I ribozyme (**Figure 2-7A**) that was described previously [73]. In the monomer units, the P5a region of the P5abc module and the P8 region of the ΔP5 module were covalently bonded with a duplex serving as a rigid spacer (**Figure 2-1C**). The resulting unit RNAs,

containing both P5abc and ΔP5 modules in a single RNA molecule, assembled intermolecularly to form oligomers of modular ribozymes [73]. Two engineered ribozymes were designed to alternately oligomerize, thus preferentially forming a closed tetramer.

Our group has previously characterized the closed tetramer consisting of L2 RNA and L3 RNA. L2 RNA possesses P2-M3, P6-R(GAAA), P5c-WT, and P5b-GGAA, whereas L3 RNA possesses P2-WT, P6-R(GGAA), P5c-M3, and P5b-GAAA (**see lanes 9 and 10 in Figure 2-7B**). In this study, the M3 pair and the GGAA/R(GGAA) pair in L2 and L3 RNAs were replaced with the M5 pair and the GAAC/R(GAAC) pair, respectively. The resulting unit RNAs were designated as Lα RNA and Lβ RNA. Lα RNA possessed P2-WT, P6-R(GAAC), P5c-M5, and P5b-GAAA, while Lβ RNA possessed P2-M5, P6-R(GAAA), P5c-WT, and P5b-GAAC (**Figure 2-7A**). In the presence of 20 mM Mg^{2+}, L2 and L3 RNAs were shown to efficiently and selectively form a closed tetramer through the formation of an L2 + L3 heterodimer. The assembly behavior of L2 and L3 RNAs allowed me to employ them as a size marker for closed tetramers (**Figure 2-7B, lanes 9 and 10**). In the presence of 20 mM Mg^{2+}, a major band was clearly seen in samples containing equimolar amounts of Lα RNA and Lβ RNA. The mobility of this major band was similar to that in L2 + L3 samples, suggesting that the band corresponds to a closed tetramer consisting of 2 x Lα RNA + 2 x Lβ RNA. The alternate oligomerization of Lα and Lβ was also supported by the mobility of Lα RNA and Lβ RNA in the absence of partner RNA. Lα RNA migrated as a single band (**Figure 2-7B lane 1**) corresponding to its monomeric form, whereas Lβ RNA showed a broad band (**Figure 2-7B, lane 5**), suggesting that Lβ RNA may have structural polymorphism

in its monomeric state possibly because of misfolding. This possible structural polymorphism was dissolved upon assembly with Lα RNA to form an open heterodimer that was further converted to the closed tetramer (**Figure 2-7B, lanes 2-4, 6–8**). The Lα + Lβ closed tetramer migrated slightly faster than the L2 + L3 closed tetramer, probably because the total number of nucleotides in the Lα + Lβ tetramer was 18 nucleotides smaller than that in the L2 + L3 tetramer.

2.3.4. Formation of RNA Triangles through Selective Assembly of Engineered Group I ribozymes

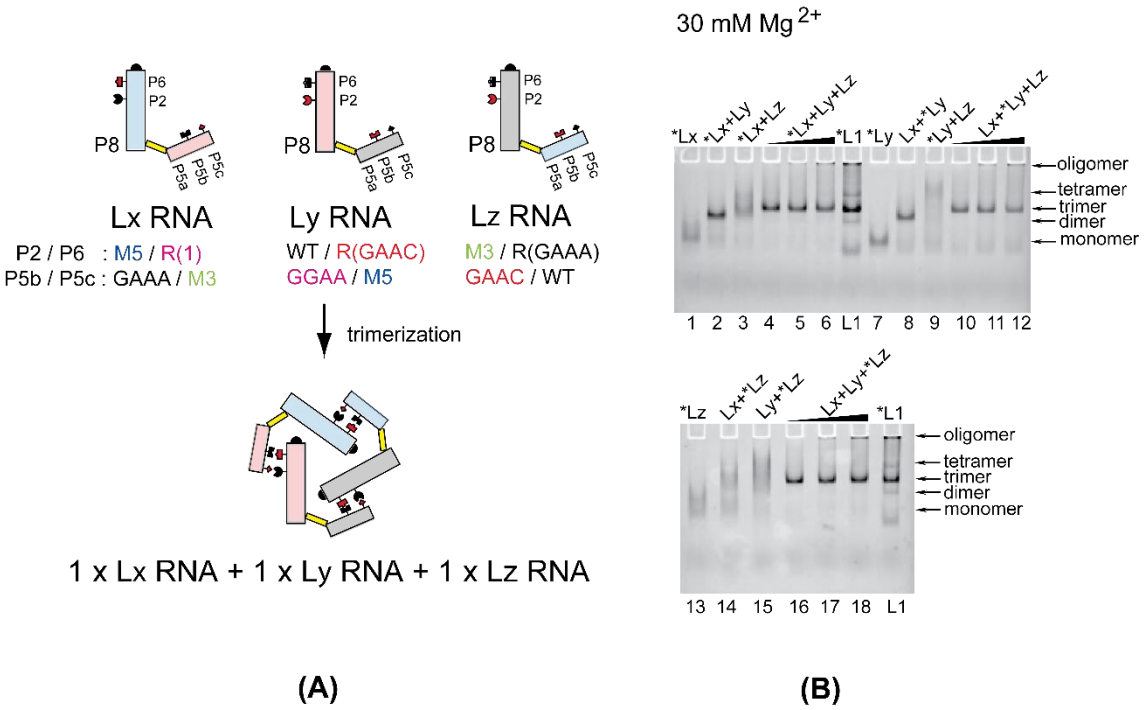

Figure 2-8. Formation of RNA triangles whose assembly was mediated by the association between the P5abc module and the ΔP5 module. (**A**) Selective formation of closed hetero-triangles by Lx RNA, Ly RNA and Lz RNA. (**B**) EMSA of Lx RNA + Ly RNA + Lz RNA in the presence of 30 mM Mg^{2+}. The asterisks indicate monomer RNAs labeled with the BODIPY fluorophore. In lanes 1, 7 and 13, the concentrations of Lx RNA, Ly RNA and Lz RNA were 0.5 μM. The concentrations of Lx + Ly, Ly + Lz and Lz + Lx were 0.5 + 0.5 μM in lanes 2, 3, 7, 8, 14 and 15. The concentrations of Lx + Ly + Lz were 0.5 + 0.5 + 0.5 μM in lanes 4, 10 and 16, were 1.0 + 1.0 + 1.0 μM in lanes 5, 11 and 17, and were 2.0 + 2.0 + 2.0 μM in lanes 6, 12 and 18.

To selective formation of artificial RNA closed triangles with novel P5b/P6 and P5c/P2 interacting pairs through modular engineering of the group I ribozyme, the GAAC-R(GAAC), GGAA-R(GGAA) and GAAA-R(GAAA) pairs, and the WT, M3 and M5 pairs were selected as modular parts for a closed RNA trimer with triangular shape (**Figure 2-8A**). Monomer unit of this triangular trimer were engineered variants of the group I ribozyme (**Figure 2-8A**) [73]. In the unit RNAs, the P5a region of the P5abc module and the P8 region of the ΔP5 module were covalently bonded with the help of a flexible linker (**Figure 2-1C**). The resulting unit molecules, possessing both P5abc and ΔP5 modules in a single RNA, assembled in an intermolecular manner to form oligomer [73]. Three distinct unit RANs were engineered to alternately assemble and preferentially form a closed triangle. Our group has also characterized the closed trimer consisting of three molecules of L1 RNAs which possess P2-WT, P6-R(GAAA), P5c-WT, and P5b-GAAA (**see lanes L1 in Figure 2-8B**). In this study, three sets of loop-receptor and P5c-P2 (P14) pairs were selected to construct a closed triangle using Lx, Ly and Lz RNAs (**Figure 2-8A**). Lx RNA possessed P2-M5, P6-R(1), P5c-M3, and P5b-GAAA, Ly RNA possessed P2-WT, P6-R(GAAC), P5c-M5, and P5b-GGAA and Lz possessed P2-M3, P6-R(GAAA), P5c-WT, and P5b-GAAC (**Figure 2-8A**). In the presence of 30 mM Mg^{2+}, Lx, Ly and Lz RNAs were shown to selectively form a closed trimer through intermolecular assembly of Lx + Ly + Lz (**Figure 2-8B, lanes 4, 5 and 6, lanes 10, 11 and 12, lanes 16, 17 and 18**) and L1 RNA was used as a size marker for closed trimer.

In the presence of 30 mM Mg^{2+}, the major bands were clearly seen in samples containing equimolar amounts of Lx RNA, Ly RNA and Lz RNA. The mobility of these major bands was similar to that in L1 samples, indicating that the band corresponds to the

closed trimers consisting of 3 x L1 RNAs. In the absence of partner RNAs, Lx RNA, Ly RNA and Lz RNA migrated as single bands in the gel matrices (**Figure 2-8B, lanes 1, 7 and 13**) corresponding to its monomeric form. Lx RNA + Ly RNA, Ly RNA + Lz RNA and Lx RNA + Lz RNA combinations showed bands migrated slower than its monomeric units indicating dimeric forms, but the presence of Lz RNA unit in the monomeric and dimeric systems led to smear bands suggesting that Lz may possess structural polymorphism (**Figure 2-8B, lanes 3, 9, 14 and 15**). These structural polymorphisms were removed upon the assembly of Lx + Ly + Lz RNAs, leading to the closed trimers (**Figure 2-8B**).

2.3.5. Formation of Novel RNA 1D Array through Selective Oligomerization

Biochemical characterization of the C-loop-R(C-loop) interaction in the context of the bimolecular ribozyme demonstrated that this interacting motif, which can be used as a possible alternative to the naturally occurring GNRA-receptor interactions [103], showed no advantage over the parent motif and two other artificial motifs, in terms of binding affinity or specificity between P5abc and ΔP5 modules (**Figure 2-2**). The secondary structures of the C-loop motif (internal loop, **Figure 2-1A**) and the R(C-loop) motif (terminal hairpin loop, **Figure 2-1B**) are the opposite of those of GNRA loops (terminal hairpin loops, **Figure 2-1A**) and their receptors (internal loops, **Figure 2-1B**) [103]. The unique structure of the C-loop/R(C-loop) interacting pair, however, enabled me to connect the P5abc module and ΔP5 RNA in a manner that would otherwise have been impossible (**Figure 2-1D**). The original 5′ and 3′ ends of the C-loop P5abc RNA with a stable 5′-UUCG-3′ tetraloop were capped and removed the UUCG loop in the C-loop motif (**Figure 2-1A**). This modified C-loop P5abc RNA was then connected to the

P5 region of the ΔP5 RNA with the R(C-loop) in P6. The resulting unit RNA (designated as F RNA) was expected to self-oligomerize to form 1D open oligomers (**Figure 2-9A**). Similar design of 1D open oligomers has been reported by using tecto-RNA as a unit RNA [108]. In the presence of 50 mM Mg^{2+}, the mobility of F-RNA was retarded gradually in an RNA concentration-dependent manner (**Figure 2-9B, lanes 1-4**). This type of mobility changes is usually caused by a dynamic equilibrium between monomeric and oligomeric states [109]. In addition, possible higher-order oligomers of F RNA, which could not enter the gel matrix, were also observed in an RNA concentration-dependent manner (**Figure 2-9B, lanes 1-4**). To test whether the retarded bands in lanes 1-4 resulted from self-oligomerization of F RNA, two mutant F RNAs (Fx and Fy) were prepared, which had a UUCG loop in P2 and the M5 loop (**Figure 2-1A**) in P5c, respectively. Each RNA existed in the monomeric state because no retarded bands were formed in the absence of their partner RNAs (**Figure 2-9B, lanes 5 and 6**). In each sample lane containing both Fx RNA and Fy RNA, a single retarded band was observed (**Figure 2-9B, lanes 7 and 8**), which would correspond to the Fx + Fy heterodimer. Consistent with the molecular design, on the basis of which Fx and Fy RNAs can form only heterodimers, no oligomers larger than dimers were observed in lanes 7 and 8. The resulting 1D open oligomers of F RNA may be insufficiently stable because of the limited recognition ability of the C-loop-R(C-loop) interaction (**Figure 2-2**). The molecular design of F RNA may be potentially attractive to expand the nanostructure design based on large modular ribozyme.

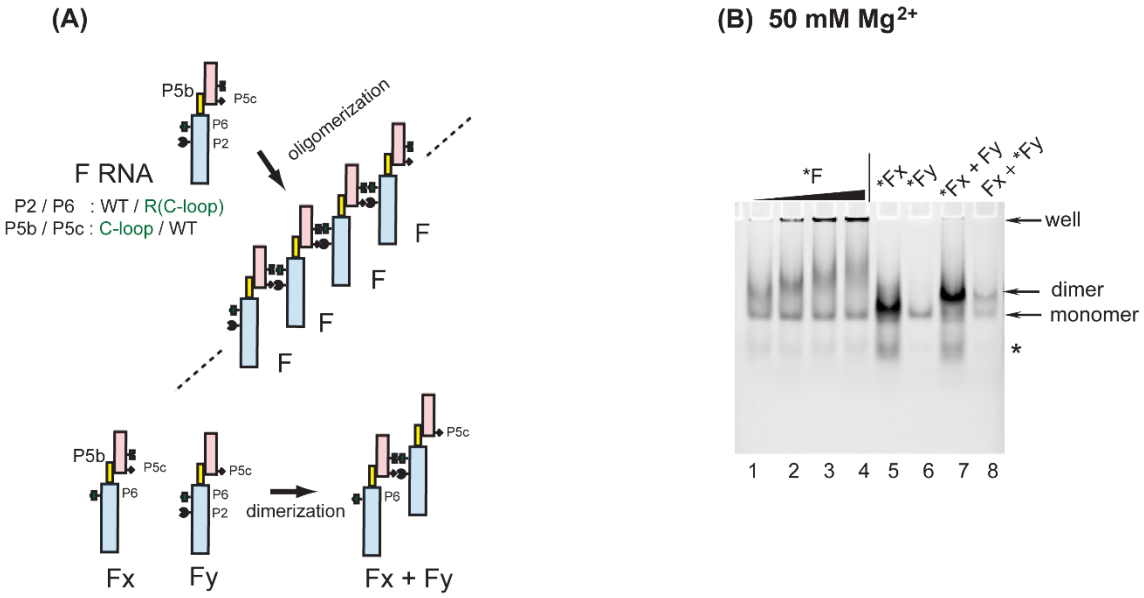

Figure 2-9. Oligomeric RNA nanostructures whose assembly was mediated by the association between the P5abc module and the ΔP5 module. (**A)** One-dimensional open oligomers of F, Fa, Fb and Fc RNAs and selective dimerization of its mutants. **(B)** EMSA of F RNA and its mutants in the presence of 50 mM Mg^{2+}. The asterisks indicate monomer RNAs labeled with the BODIPY fluorophore. The concentrations of F RNA were 0.25 μM, 0.5 μM, 1.0 μM, and 2.0 μM in lanes 1, 2, 3, and 4, respectively. The concentrations of Fx RNA and Fy RNA were 0.5 μM in lanes 5 and 6. The concentrations of Fx RNA + Fy RNA were 0.5 + 0.5 μM in lanes 7 and 8.

2-4. Conclusions

In this chapter, artificial RNA-RNA interactions were characterized to determine their abilities to support the assembly of the two module RNAs in the P5abc/DP5 bimolecular ribozyme. Some of the new RNA-RNA interactions characterized in this study were used as alternative modular parts to produce new P5abc/DP5 interfaces. These new interfaces can be applied to design ribozyme-based RNA nanostructures.

Chapter 3. Oligomerization of a bimolecular ribozyme modestly rescues its structural defects that disturb interdomain assembly to form the catalytic site

3.1. Abstract

The emergence of cellular compartmentalization was a crucial step in the hypothetical RNA world and its evolution because it would not only prevent the extinction of RNA self-replication systems due to dispersion/diffusion of their components but also facilitate ribozyme reactions by molecular crowding effects. Here, I proposed and examined self-assembly of RNA components as a primitive cellular-like environment, which may have the ability to mimic cellular compartmentalization and crowding effects. A bimolecular group I ribozyme was engineered to form a one-dimensional (1D)-ribozyme assembly. In the 1D assembly form, severe mutations that inactivated the parent bimolecular ribozyme were modestly rescued resulting in weak catalytic ability.

3.2. Introduction

In the hypothetical RNA world, RNA molecules catalyzed chemical reactions necessary for RNA self-replication [78, 110, 111]. The minimal unit of RNA self-replication may consist only of one (or a few) RNA sequence(s) that can serve as both catalyst molecule to synthesize its RNA sequence and also as information molecule to be

copied [112, 113]. Such minimal self-replication systems likely then evolved and diverged to produce cross-replication systems and more complex RNA-based reaction networks, through which the variety of molecules synthesized by RNA catalysts would have expanded [114-116]. Such evolutionary expansion in the RNA world would have been triggered by mutations occurring in the primitive systems with limited replication fidelity.

The concentrations of self-replicating RNAs and their building blocks in the reaction medium are crucial issues for sustaining a stable RNA self-replication system [117-119]. If their concentrations become too low, the systems would undergo extinction through dispersion–dilution and/ or hydrolytic degradation of the catalyst/template RNAs and their building blocks. Therefore, sustainable RNA self-replication and evolution would have required suitable conditions, where the components in these systems would be maintained at sufficiently high concentrations to overwhelm the risks of their dispersion-dilution and/or hydrolytic degradation.

Montmorillonite clay minerals have been proposed to provide local environments where RNA and its components can be enriched through adsorption on the clay surface [120-125]. More recently, the eutectic ice phase microenvironment has been proposed as a promising aqueous liquid space where RNA molecules, their building blocks, and other components necessary for self-replication systems could be enriched [126-129]. Eutectic ice phases can also provide molecular crowding effects, which are recognized as important factors to understand intracellular enzyme actions [130-134]. These environmental conditions, which can be regarded as protocellular conditions to compartmentalize (i.e., enrich and isolate) self-replication systems, are thought not only

to play passive roles in preventing dispersion of materials but also to contribute to the acceleration of enzymatic and nonenzymatic reactions [124, 127]. Furthermore, protocellular compartmentalization can facilitate the evolution of these systems [127, 134-136]. Compartmentalization can prevent the extinction of rare molecules bearing promising mutations. In a non-compartmentalized environment, rarely occurring mutants would hardly survive due to their low abundance, which would make it difficult to meet their suitable partner variants to form improved systems. The requirement of protocellular compartmentalization environments may have diminished gradually with the emergence of cellular-like assembly structures as improved compartmentalization systems [117, 137]. Fatty acid vesicles have been analyzed as prototypical cellular-like compartments that can perform spontaneous growth and division [138-140]. Moreover, these processes can be synchronized with RNA-replication systems compartmentalized in the vesicles [141, 142]. In the stepwise evolutionary process of the RNA world to establish protocellular compartment structures, an alternative scenario may be presented by proposing an early evolutionary stage. In this newly proposed stage, functional RNAs may provide microcompartments and/or related microenvironment without the help of either external components, such as clay or lipid vehicles, or external conditions, such as eutectic ice phases.

Self-assembly is an important property in modern cellular biological systems and synthetic molecular systems [143, 144]. Self-assembly of molecules enables them to form large and complex structures that would be impossible to achieve with isolated molecules. In addition to lipid molecules, polypeptides also form various types of assembly structures (quaternary structures), some of which organize shell-like structures that serve as 3D compartments (virus capsids) to encapsulate DNA or RNA as genetic materials

[145, 146]. Regardless of three-dimensional (3D) formation of cellar or shell-like structures, formation of one-dimensional (1D) or two-dimensional (2D) assemblies, which form linear and polygonal structures, respectively, may also be effective to increase local concentrations of their monomer components to prevent their dispersion-dilution. Self-assembly of RNA catalysts may represent a simple but promising approach for molecular evolution to increase the local concentrations of RNA components of self-replication systems. Although self-assembling nanostructures of naturally occurring RNA molecules are limited, phage phi29 pRNA forms polygonal structures through its self-assembly [147, 148]. RNA nanotechnology has also developed several types of self-assembling RNA nanostructures, which involve 1D arrays, 2D polygons, and 3D polyhedrons [18, 87, 65]. These artificial RNA nanostructures suggest the ability of RNA to increase their local concentration through self-assembly. In this study, an RNA-assembly system was constructed in which a bimolecular form of the *Tetrahymena thermophila* (Tth) group I ribozyme was redesigned to construct a 1D assembly structure composed of the Tth ribozyme (**Figure 3-1**). The author used the bimolecular Tth ribozyme composed of P4-6 RNA and P3-7 RNA (**Figure 3-2A**), each of which contains catalytically critical elements to organize the catalytic core structure [149, 150]. Each module RNA showed no catalytic ability without its partner. The catalytic activity was a direct indicator of P4-6/P3-7 bimolecular complex formation. Formation of the 1D assembly of the bimolecular Tth ribozyme structure coincided with the formation of its bimolecular catalytic core unit (**Figure 3-1**). This system, therefore, enables comparison of the catalytic abilities of the bimolecular Tth ribozyme in an isolated state and as a unit module of a 1D assembly ribozyme nanostructure.

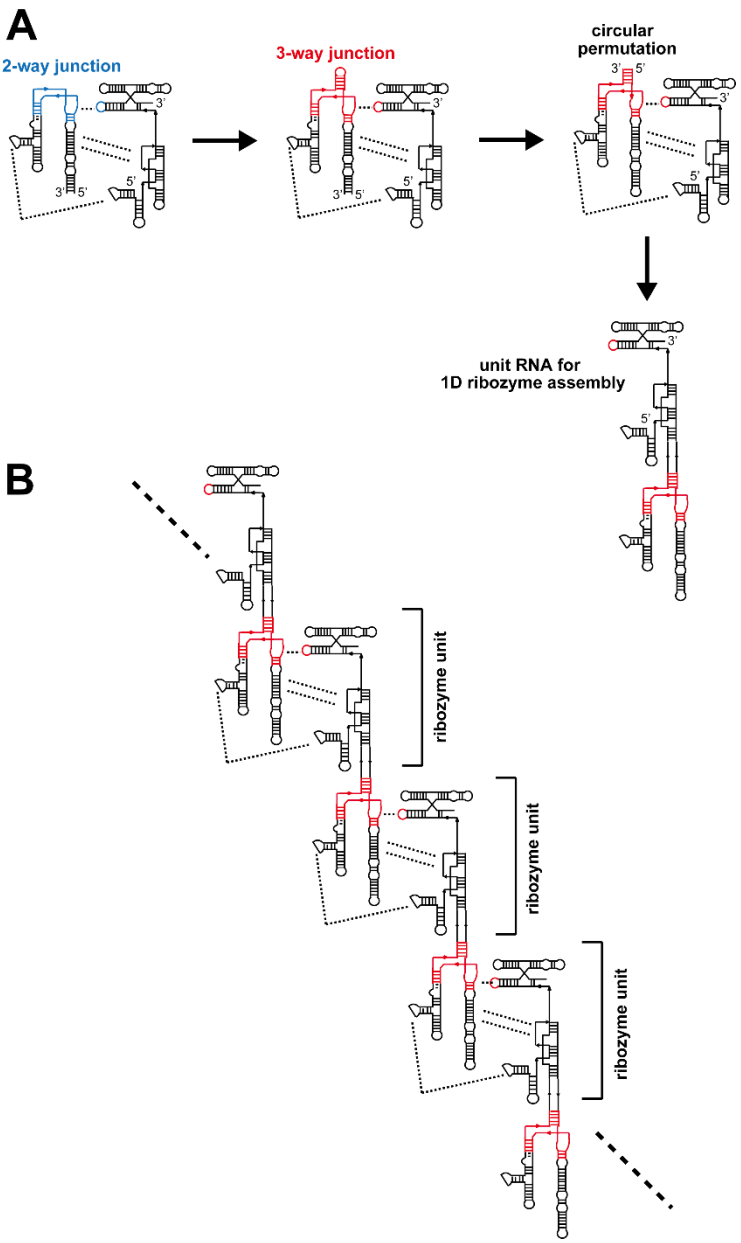

Figure 3-1. A conceptual scheme to redesign a bimolecular ribozyme to form 1D ribozyme assembly. A) Redesign of a bimolecular ribozyme, whose catalytic core is formed by the assembly of two modular RNAs, to generate a unit RNA for 1D ribozyme assembly. Broken lines are interdomain interactions involved in assembly of the two modular RNAs. B) Oligomer formation of the unit RNA through interdomain interactions between the two modular RNAs of the parent parent bimolecular ribozyme.

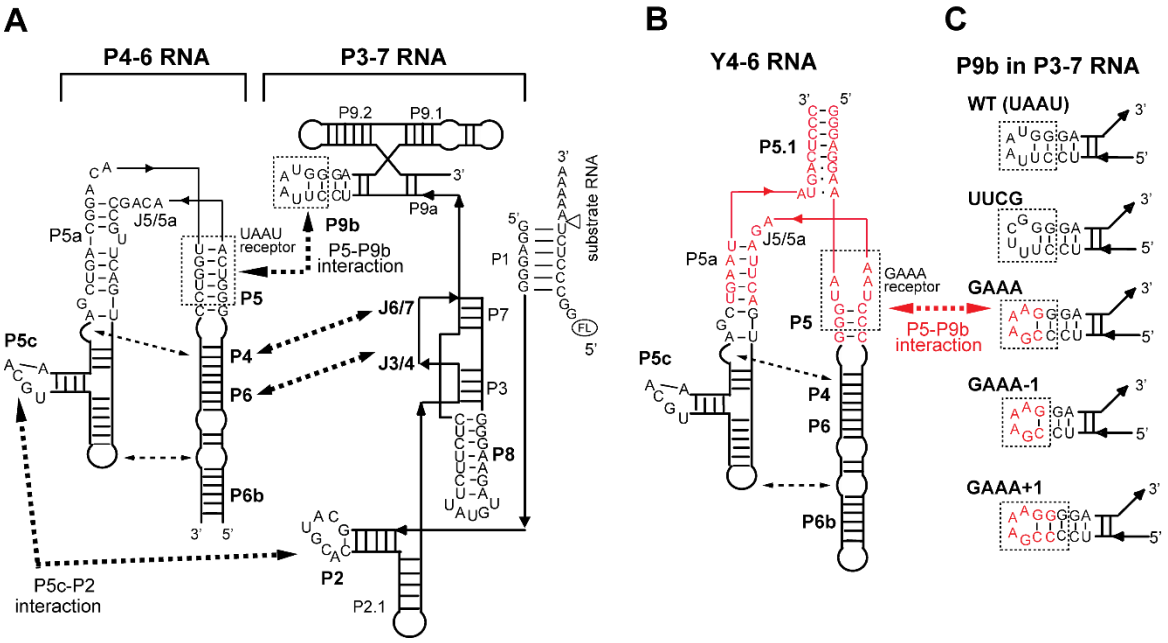

Figure 3-2. Bimolecular P4-6/P3-7 Tth ribozyme and its variants. (A) Secondary structure of P4-6 RNA and P3-7 RNA to form a bimolecular Tth ribozyme. The nucleotide sequences of the structural elements discussed in this study are shown. Broken lines with two arrowheads indicate tertiary interactions. Thin broken lines in P4-6 RNA are intradomain interactions contributing to the hairpin-shaped tertiary structure. Thick broken lines are interdomain interactions involved in assembly of P4-6 and P3-7 domains. (B) Secondary structure of Y4-6 RNA with three-way type J5/5a element to extend the P5.1 stem. (C) The wild-type and variant P9b elements in P3-7 RNA. For the P5 element in P4-6 RNA, P9b-UAAU is the cognate partner loop. For the P5 element in Y4-6 RNA, P9b-GAAA is the cognate partner loop with optimized P9b stem.

3.3. Results

3.3.1. Modular Redesign of the P4‑6/P3‑7 Bimolecular Tth Ribozyme

To use the bimolecular Tth group I ribozyme as a modular unit of a ribozyme 1D assembly (**Figure 3-1**), the P4-6 RNA was redesigned with the addition of a stem element (P5.1) to the P5a-J5/5a-P5 hinge module. For this purpose, the P4-6 variant was employed possessing a three-way junction type (Pc-type) P5a-J5/5a- P5 module found in the *Pneumocystis carinii* (Pc) group I ribozyme [151]. This variant RNA has been shown to form its folded structure as stably as the parent P4-6 RNA possessing a two-way junction type (Tth-type) P5a-J5/5a-P5 module. As the P4-6 RNA variant reported previously had its 5′ and 3′ termini at the junction of P4 and P6 elements, respectively, a variant was engineered to produce two circular permutation mutants [152]. In two of the designed mutants, the 5′ and 3′ termini were present at the P6b element (Y4-6a RNA, see **Figure 3-3A**) or P5.1 element (Y4-6 RNA, see **Figure 3-2B**). Y4-6a RNA shares the structural organization with the P4-6 RNA except the identity of the P5a-J5/5a-P5 module, (**Figure 3-3A**).

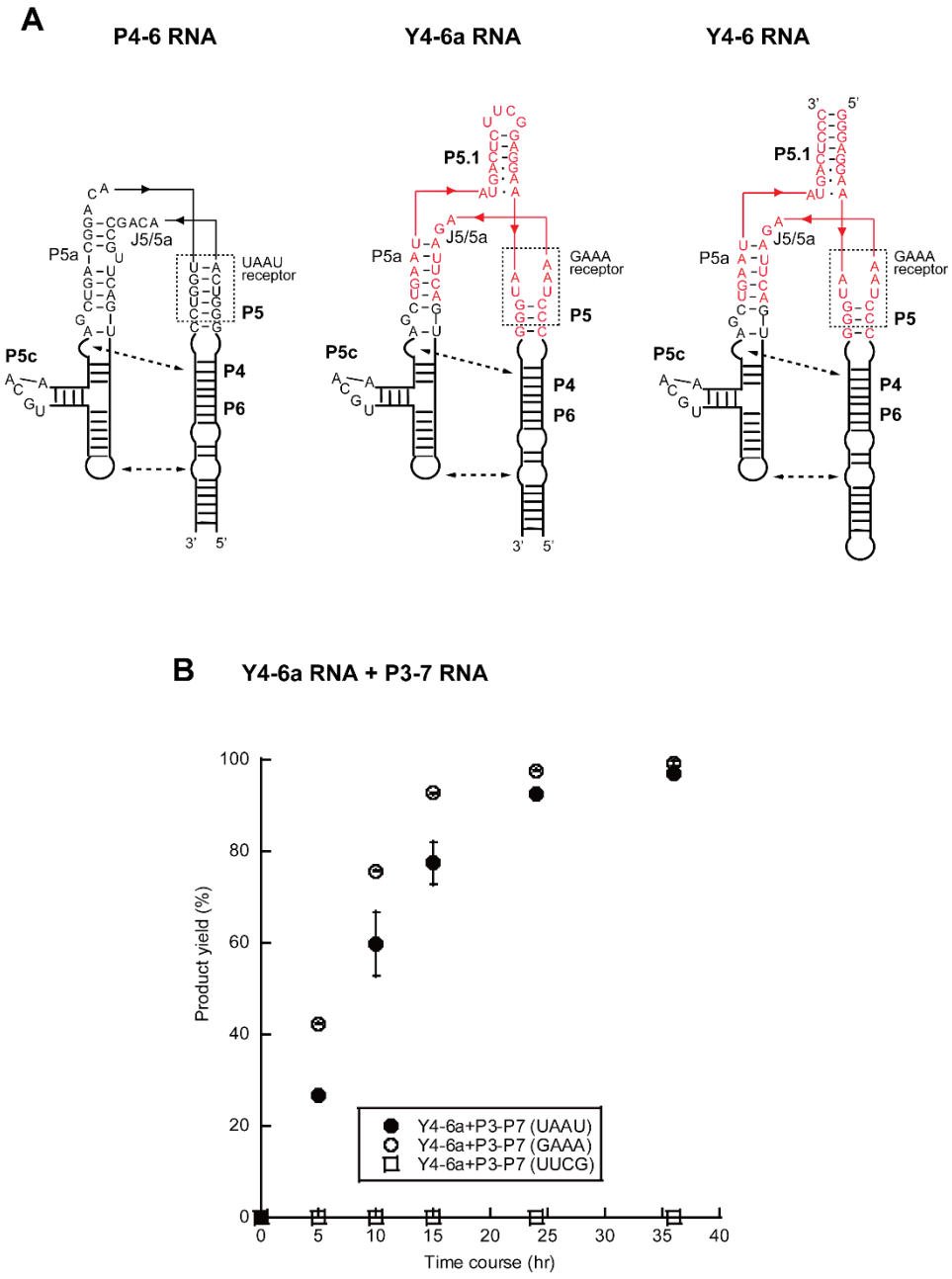

Figure 3-3. Characterization of an Y4-6a/P3-7 bimolecular ribozyme. A) Secondary structures of P4-6, Y4-6a and Y4-6 RNAs. B) Time courses of substrate cleavage reactions catalyzed by the Y4-6a/P3-7 ribozymes in the presence of 50 mM Mg^{2+}. Reactions were performed at 37°C.

In the resulting Y4-6a and Y4-6 RNAs, the Pc-type P5a- J5/5a-P5 module has a functional feature distinct from that of the Tth-type P5a-J5/5a-P5 module. In modular assembly of the P4-6 domain and P3-7 domain to form the active core structure of the Tth group I ribozyme, the P5 element in the P5a-J5/5a-P5 module serves as a receptor motif to accept a UAAU tetraloop in the P9b element of P3-7 RNA [153]. This tertiary interaction (P5-P9b interaction) contributes to the formation and maintenance of the active core structure, with which the Tth group I ribozyme exhibits its full catalytic performance. While the P5-P9b interaction is present in the Pc group I ribozyme, its P9b tetraloop has a GAAA tetraloop and its P5 element serves as a specific receptor motif for a GAAA loop [151, 154]. To optimize the P5–P9b interaction in a complex containing Y4-6 RNA, P3-7 RNA was modified to have a GAAA loop in P9b as a cognate partner loop for the Pc-type P5a-J5/5a-P5 module. To evaluate the importance of tertiary interactions contributing to the assembly between P4-6 domain and P3-7 domain, two mutant P3-7 RNAs were also prepared that could not form the P5–P9b interaction or P5c-P2 interaction due to an interaction-inert UUCG loop in P9b or P2, respectively.

Bimolecular complex formation between three P4-6 RNA units and four P3-7 RNA units was evaluated by electrophoretic mobility shift assay (EMSA). In the presence of 15 mM Mg^{2+}, P4-6 RNA formed complexes with the parent P3-7 (P9b-UAAU) RNA and also less efficiently with P3-7 (P9b-GAAA) RNA (**Figure 3-4A, lanes 2 and 3**). Y4-6a RNA (**Figure 3-4A, lanes 6 and 7**) and Y4-6 RNA (**Figure 3-4A, lanes 10 and 11**) showed no apparent preference between the parent P3-7 (P9b-UAAU) RNA and P3-7 (P9b-GAAA) RNA as a partner RNA. Three P4-6 domain RNAs formed no complex with mutant P3-7 RNAs with a defective P2 element (**Figure 3-4A, lanes 5, 8, and 12**). This observation indicated the importance of the P5c–P2 interaction in stable formation of the

bimolecular P4-6/P3-7 complex. In contrast, P3-7(P9b-UUCG) RNA formed a complex with P4-6 RNA, suggesting that the P5-P9b interaction is less important for bimolecular complex formation (**Figure 3-4A, lanes 13-15**).

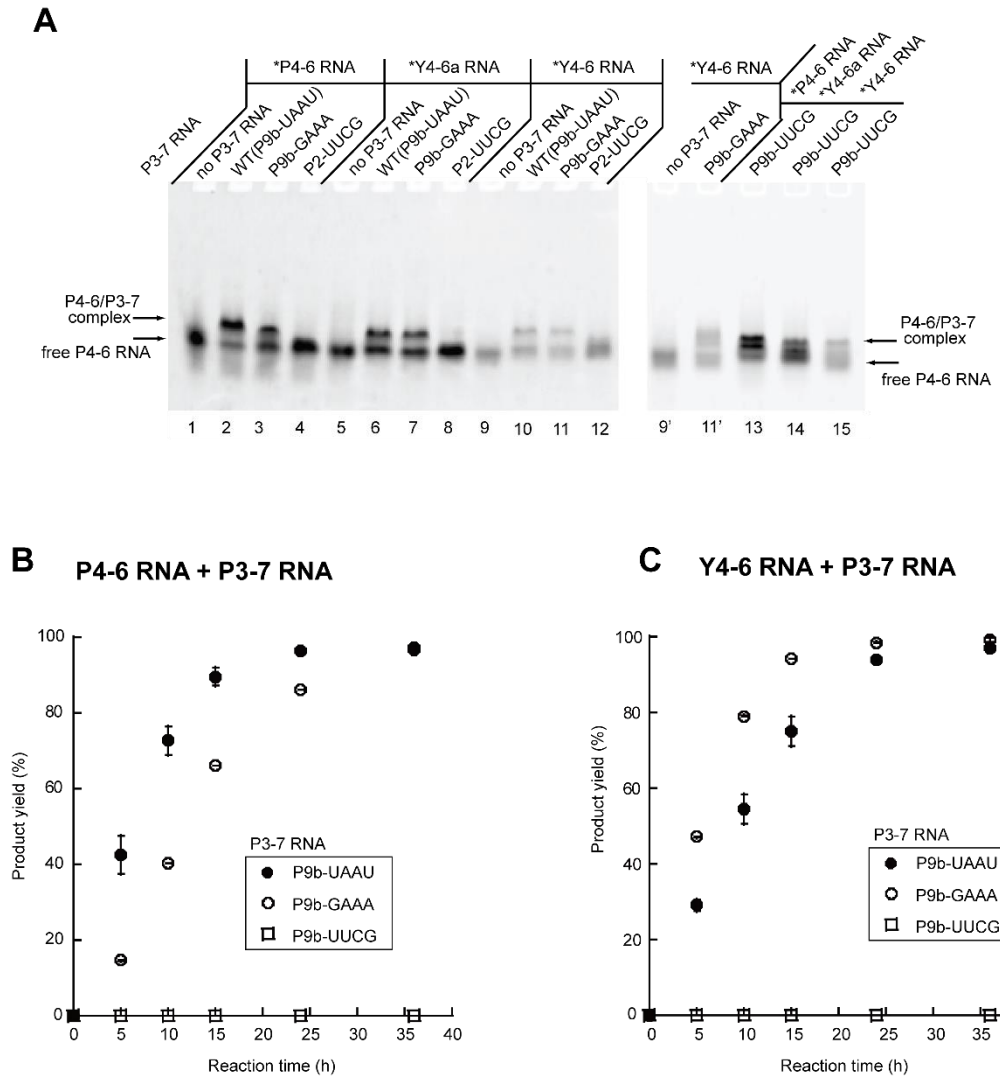

Figure 3-4. Characterization of P4-6/P3-7 bimolecular ribozyme and its Y4-6/P3-7 derivatives. (A) Electrophoretic mobility shift assays of P4-6/P3-7, Y4-6a/P3-7, and Y4-6/P3-7 complexes in the presence of 15 mM Mg^{2+}. The concentrations of RNA components were 0.5 μM. Asterisks indicate RNAs labeled with the BODIPY fluorophore. Electrophoresis was performed at 4°C. (B, C) Time courses of substrate cleavage reactions catalyzed by the P4-6/P3-7 ribozymes (B) and Y4-6/P3-7 ribozymes (**C**) in the presence of 50 mM Mg^{2+}. Reactions were performed at 37°C. The same lot of each P3-7 RNA variant was employed in activity assays shown in B, C.

The author next performed ribozyme activity assay to analyze the functional contribution of the P5–P9b interaction to the catalytic ability of the bimolecular P4-6/P3-7 ribozyme. The substrate cleavage reaction was performed in the presence of equimolar amounts of P4-6 domain RNA (0.5 μM), P3-7 domain RNA (0.5 μM), and 50 mM Mg^{2+}. In the presence of P4-6 RNA, the substrate cleavage reaction proceeded twice as rapidly with P3-7 (P9b-UAAU) RNA (k_{obs} = 0.075 h^{-1}) than P3-7 (P9b-GAAA) RNA (k_{obs} = 0.038 h^{-1}), suggesting that the Tth-type P5 element preferably accepts a UAAU loop over a GAAA loop (**Figure 3-4B**). In the presence of Y4-6 RNA (**Figure 3-4C**), the substrate cleavage reaction proceeded 1.5-fold more rapidly with P3-7 (P9b-GAAA) RNA (k_{obs} = 0.082 h^{-1}) than P3-7 (P9b-UAAU) RNA (k_{obs} = 0.055 h^{-1}). This observation indicated that the Pc-type P5 element preferentially accepts a GAAA loop over a UAAU loop. The catalytic abilities of the bimolecular ribozymes with Y4-6a RNA were almost the same as those with Y4-6 RNA (**Figure 3-3B**). Although bimolecular complex formation was detectable in the presence of P9b-UUCG mutation, three P4-6 domain RNAs showed no activity with P3-7 (P9b-UUCG) RNA (**Figure 3-4B and Figure 3-3B**). This result indicated the functional importance of the P5-P9b interaction in activation of the catalytic ability of the P4-6/P3-7 bimolecular ribozyme rather than its complex formation. It is also noted that two or three distinct bands were observed as retarded bands in lanes 13-15 (**Figure 3-4A**). Identities of these bands have not been elucidated but structural heterogeneity may be formed in the complexes containing P3-P7 (P9b-UUCG). To confirm the adequacy of rational replacement of the parent Tth-type P5-P9b interaction with the Pc-type P5-P9b interaction, the effects of the P9b stem length on the interaction between the GAAA loop and the Pc-type P5 element was experimentally examined (**Figure 3-5A**). In the presence of Y4-6 RNA, two P3-7 (P9b-GAAA) RNA variants with

a single base pair insertion and deletion in the P9b stem showed markedly lower activities (**Figure 3-5B, C**), confirming the adequacy of the original design of the GAAA P9b element in the P3-7 (P9b-GAAA) RNA.

3.3.2. Redesign of P4-6/P3-7 Ribozyme to Form a 1D Ribozyme Assembly

To determine the effects of oligomeric RNA assembly on their biological functions, the oligomerizing ability into the bimolecular P4-6/P3-7 ribozyme was installed. As one of the simplest strategies to generate a 1D ribozyme assembly, a plan was employed to connect the two hairpin stem elements of P4-6 RNA and P3-7 RNA covalently without disruption of their 3D structures and tertiary interactions. As possible candidates for the connector elements, terminal hairpin stems was selected that involved in neither intra-nor interdomain tertiary interactions. Based on the crystal 3D structure of the shortened form of the Tth group I ribozyme as well as the model 3D structure of the full-length Tth group I ribozyme [39, 155], P8 and P9.2 were identified as possible connector elements in the P3-7 domain and P8 was used as a connector element. In the P4-6 domain, two terminal hairpin stems (P5b and P5c) were used for tertiary interactions and the P6b seemed to be structurally unsuitable for 1D assembly design. Therefore, Y4-6 RNA was used with the P5.1 stem as a connector element. By connecting the P5.1 stem in Y4-6 RNA and the P8 stem directly, Oligo-Y RNA was designed as a unit for 1D assembly of the bimolecular ribozyme (**Figure 3-6A**). Oligo-Y RNA possessed both an activator Y4-6 domain and P3-7 domain in a single RNA molecule, but the two modules could be assembled only in an intermolecular manner. The formation of homooligomeric 1D assembly of Oligo-Y RNA directly depends on the formation of bimolecular P4-6/P3-7 ribozyme units (**Figure 3-6B**).

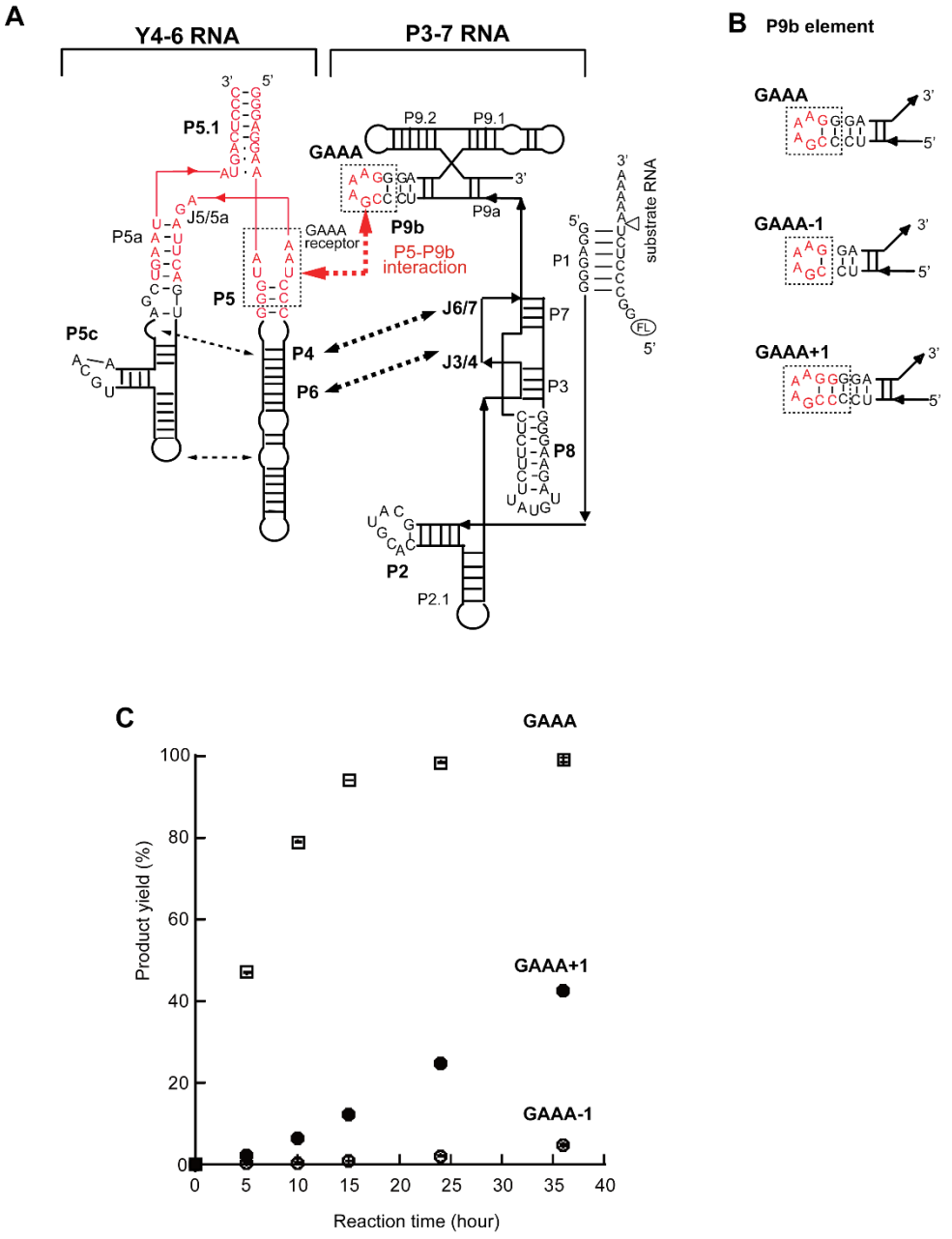

Figure 3-5. Characterization of P9b-GAAA loop as the partner of Pc-type P5a-J5/5a-P5 elements in Y4-6 RNA. A) Secondary structures of the Y4-6/P3-7 bimolecular ribozyme. B) Secondary structures of the P9b-GAAA stem loop in P3-7 RNA. C) Time courses of substrate cleavage reactions catalyzed by the Y4-6/P3-7 ribozymes with distinct P9b stems in the presence of 50 mM Mg^{2+}. Reactions were performed at 37°C.

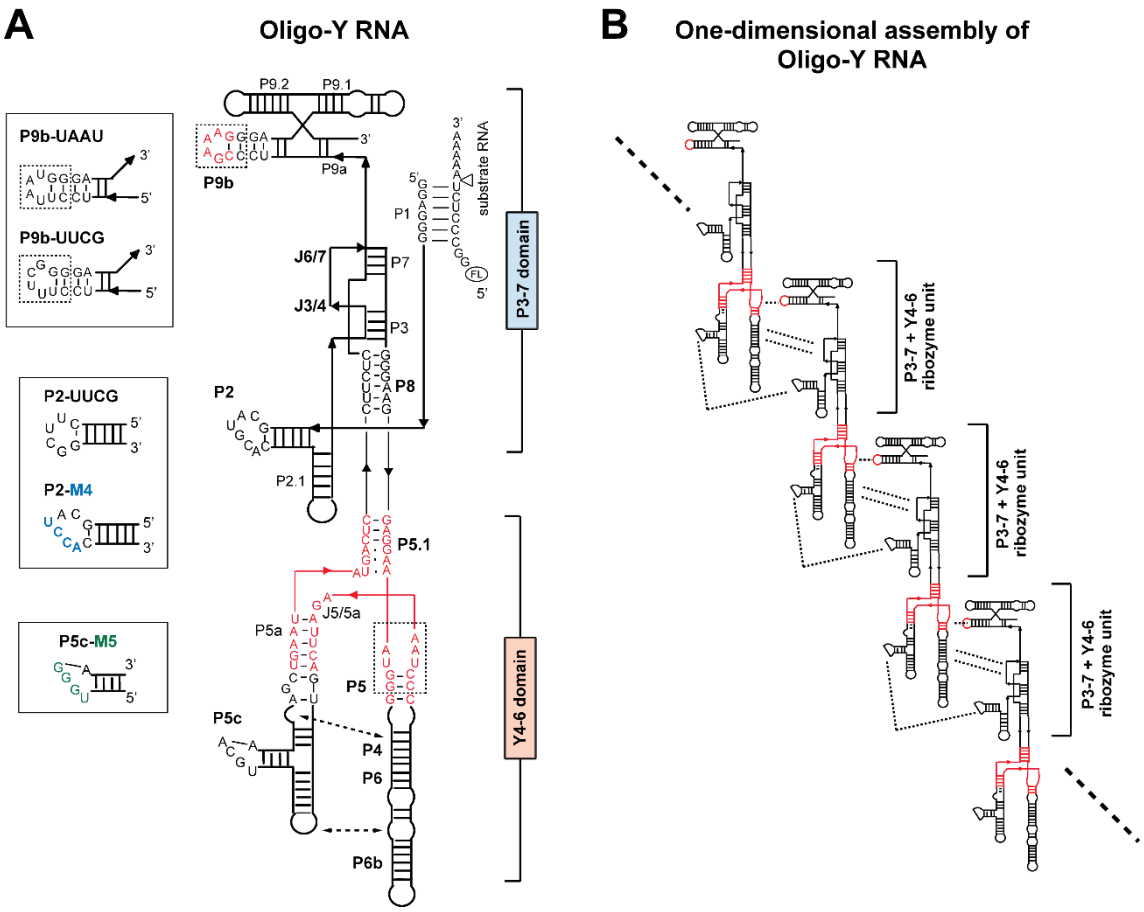

Figure 3-6. Redesign of Y4-6/P3-7 bimolecular ribozyme to form 1D ribozyme assembly. **(A)** Secondary structure of Oligo-Y RNA, which was designed by connecting the P5.1 element of Y4-6 RNA and P8 element of P3-7 RNA. **(B)** Oligomer formation of Oligo-Y RNA through interdomain interactions between the P4-6 domain and P3-7 domain (indicated by thin broken lines)

To determine the effects of redesign for 1D assembly of the bimolecular ribozyme, firstly, the ribozyme activity of Oligo-Y RNA in comparison with the parent bimolecular ribozyme was investigated (**Figure 3-6A, B**). Two Oligo-Y RNAs with either the P9b-GAAA loop or P9b-UAAU loop were tested. Oligo-Y RNA with P9b-GAAA showed nearly the same activity as the parent bimolecular ribozyme (**Figure 3-7A**). Oligo-Y RNA with P9b-UAAU loop, however, showed slightly but distinctly higher activity than the

corresponding bimolecular ribozyme (**Figure 3-7B**). Considering the observation that the P9b-UAAU loop is not the cognate partner of the Pc-type P5 element (**Figure 3-4C**), this result suggested that formation of the 1D assembly may compensate for the mismatched interaction between the P4-6 module and P3-7 module. To confirm the state of 1D assembly of Oligo-Y RNA, EMSA was performed in the presence of 50 mM Mg^{2+} (**Figure 3-7C**), where Oligo-Y RNA formed a high molecular weight oligomer that was incapable of migrating in native polyacrylamide gels. This oligomer was considerably stable in the presence of 0.5-2.0 μM RNAs (**Figure 3-7C**). Two control RNAs were also used to estimate the oligomeric states of Oligo-Y RNA. The two mutant Oligo-Y RNAs had structural defects in the P5c loop or P2 loop, respectively, which disrupted the P5c–P2 interaction. Molecular design of the two mutants eliminated the ability for homooligomer formation. On the other hand, mixing two mutants selectively formed a heterodimer. The electrophoretic mobilities of mutant Oligo-Y RNAs and the heterodimers were comparable to those of monomeric and dimeric states of L1 RNA [73], an engineered Tth ribozyme capable of forming closed trimers, closed tetramers, and higher-order oligomers (**Figure 3-7C**). The closed trimers and closed tetramers of L1 RNA showed triangle and square shapes, respectively, in AFM (atomic force microscopy) analysis [73]. In the presence of 50 mM Mg^{2+}, oligomerization ability of Oligo-Y RNA with GAAA was indistinguishable from Oligo-Y RNA with P9b-UAAU (**Figure 3-7A, B**). Interestingly, residual assembly ability of Oligo-Y RNA was still observed even with disruption of P5c-P2 interaction. The mobility of the P2-UUCG mutant on the gel was close to that of the monomeric variant of Oligo-Y RNA probably due to rapid association/dissociation of the loosely assembled oligomeric state of the P2-UUCG mutant during electrophoresis (**Figure 3-7D**).

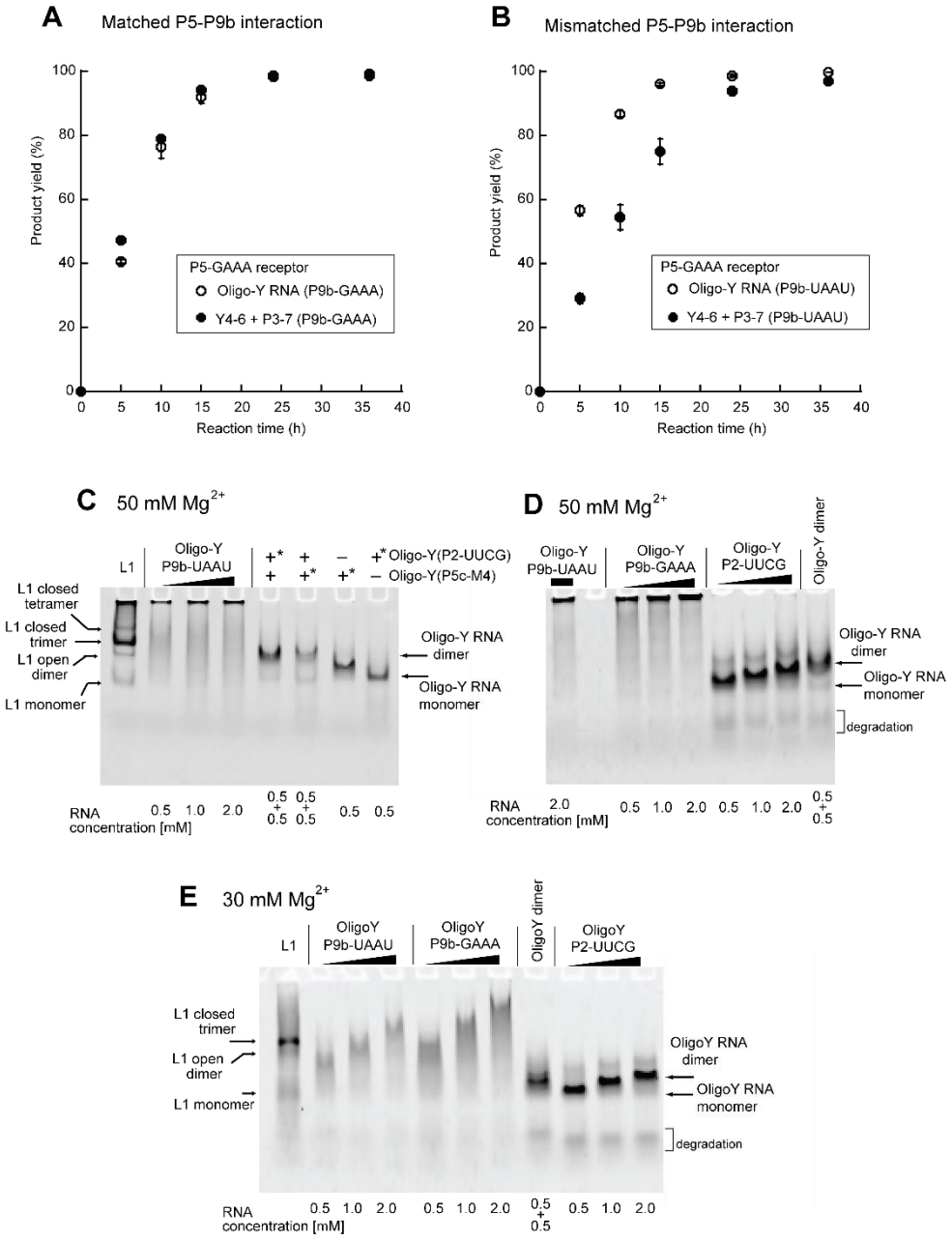

Figure 3-7. Characterization of Oligo-Y RNA. **(A, B)** Time courses of substrate cleavage reactions catalyzed by Oligo-Y (P9b-GAAA) RNA **(A)** and Oligo-Y (P9b-UAAU) RNA **(B)** in the presence of 50 mM Mg^{2+}. For each Oligo-Y RNA, the activity of the corresponding bimolecular ribozyme is also shown as a reference. Reactions were performed at 37°C. **(C)** Electrophoretic mobility shift assay of Oligo-Y RNA with P9b-UAAU loop and its variant in the presence of 50 mM Mg^{2+}. L1 RNA, which forms a closed trimer and a closed tetramer, was used as a size marker. **(D, E)** Electrophoretic mobility shift assays of Oligo-Y RNA (P9b-UAAU), Oligo-Y RNA (P9b-GAAA), and Oligo-Y RNA (P2-UUCG) in the presence of 50 mM Mg^{2+} **(D)** and 30 mM Mg^{2+} **(E).**

To determine the structural differences between P9b-UAAU and P9b-GAAA in contribution to Oligo-Y RNA oligomer formation, EMSA was performed in the presence of 30 mM Mg^{2+}, where tertiary RNA–RNA interactions became weaker than those with 50 mM Mg^{2+}. Under the structurally less stable conditions, Oligo-Y RNAs still formed oligomers although they showed smears and broad bands that migrated slowly (**Figure 3-7E**). This result suggested dynamic association/dissociation of Oligo-Y RNA in the presence of 30 mM Mg^{2+}. With 30 mM Mg^{2+}, Oligo-Y RNA with P9b-GAAA showed lower mobility than that with P9b-UAAU. This observation suggested that the Pc-type P5 element interacts more strongly with the P9b GAAA loop than with the P9b UAAU loop.

3.3.3. Oligomerization of the P4-6/P3-7 Bimolecular Ribozyme Partially Rescues the Structural Defects

The modest improvement of Oligo-Y RNA with P9b-UAAU over the corresponding bimolecular ribozyme (**Figure 3-7B**) prompted us to examine the effects of 1D assembly formation positively supporting the catalytic ability of the P4-6/P3-7 ribozyme. The residual but detectable assembly ability of the P2-UUCG mutant of Oligo-Y RNA (**Figure 3-7C, D**) also prompted us to perform further investigations of Oligo-Y RNA. To expand the comparative assay between Oligo-Y RNA and its parent bimolecular P4-6/P3-7 ribozyme, two sets of P4-6 domain and P3-7 domain were examined. In each set, a tertiary interaction assembling the P4-6 domain and P3-7 domain was modified. One mutation had a partial mismatch (M5-M4 mismatch) between P5c and P2 base pairs, which was expected to cause a relatively modest defect in the P4-6/P3-7 assembly

because this tertiary interaction was stabilized when the G–U pair in M5-M4 mismatch was substituted with a G–C pair or an A–U pair [156]. In the activity assay, the bimolecular ribozyme with partially mismatched P5c–P2 interaction still showed moderate catalytic activity (**Figure 3-8A**) in the presence of 30 mM Mg^{2+}, where the activity of Oligo-Y RNA with M5-M4 mismatch (*k*obs = 0.017 h^{-1}) was 1.5-fold higher than that of the corresponding bimolecular ribozyme (*k*obs = 0.011 h^{-1}). The second mutation had complete disruption of P5c–P2 interaction by the P2-UUCG mutant. This mutation would cause severe defects in P4-6/P3-7 assembly. Defects in RNA–RNA assembly were observed in EMSA of the bimolecular ribozyme (**Figure 3-4A**), while residual but detectable assembly ability was observed in Oligo-Y RNA even with the introduction of this mutation (**Figures 3-7C, D and 3-9**). Mobility of Oligo-Y (P2-UUCG) RNA reduced gradually in a dose-dependent manner, although the extent of the retardation was at most similar to that of the control dimer (**Figures 3-7C, D and 3-9**).

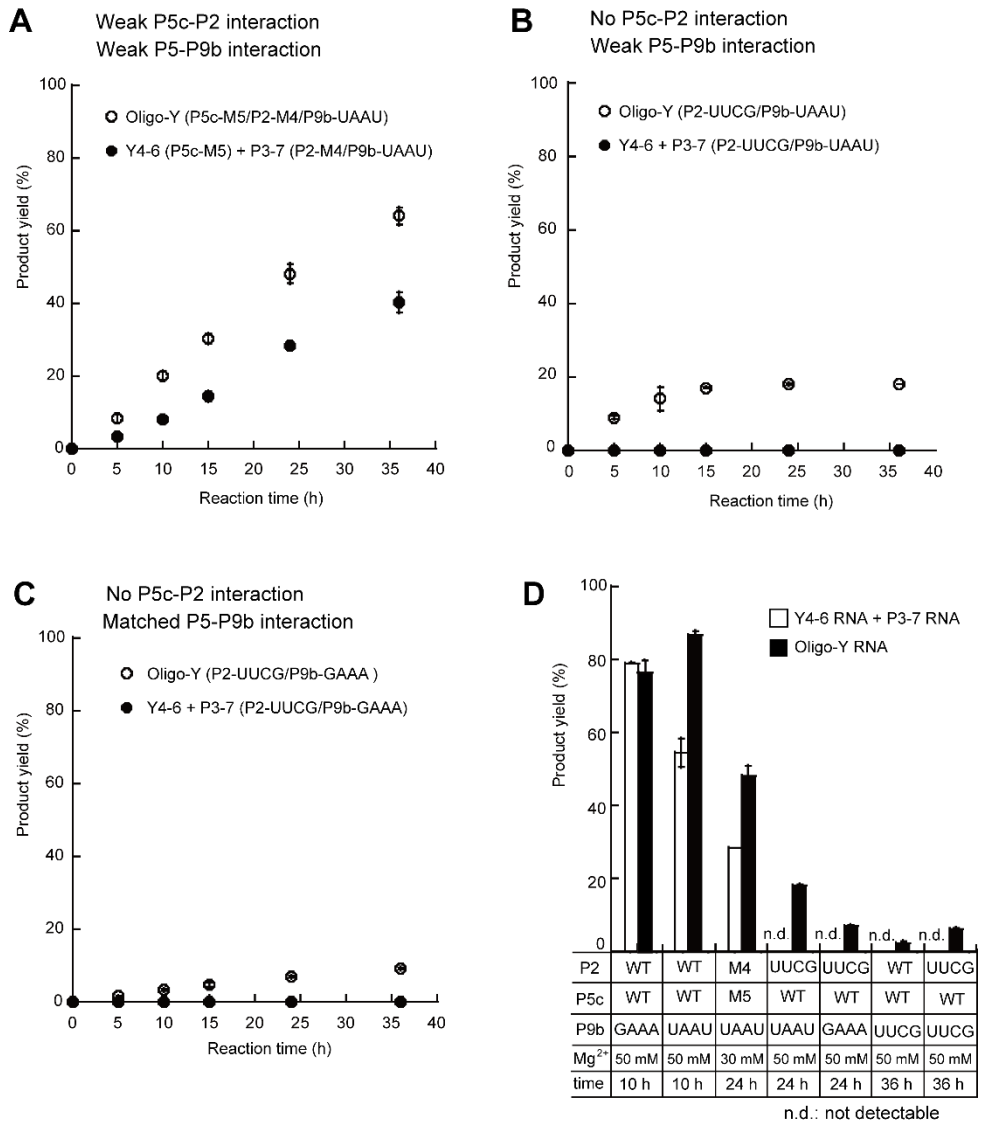

Figure 3-8. Oligomer formation modestly rescued structural defects of the P4-6/P3-7 bimolecular ribozyme. (**A–C**) Time courses of substrate cleavage reactions catalyzed by Oligo-Y RNA with mismatched interdomain interaction. Oligo-Y RNA with two weak P5c–P2 and mismatched P5–P9b interactions (**A**), Oligo-Y RNA with disrupted P5c–P2 and mismatched P5–P9b interactions (**B**), and Oligo-Y RNA with disrupted P5c–P2 and mismatched P5–P9b interactions (**C**). For each Oligo-Y RNA, the activity of the corresponding bimolecular ribozyme is also shown as a reference. Reactions were performed at 37°C in the presence of 30 mM Mg^{2+} (A) or 50 mM Mg^{2+} (**B, C**). The same lot of Y4-6 RNA was employed in activity assays shown in B**, C**, and **figure 3-4C**. (**D**) Summary of the product yields of Oligo-Y RNAs and the corresponding bimolecular RNAs.

With complete disruption of P5c–P2 interaction, P4-6/P3-7 bimolecular ribozymes showed no activity regardless of their P5–P9b interactions (**Figure 3-8B, C**). Interestingly, Oligo-Y RNA exhibited very weak but detectable activity even in the absence of P5c–P2 interaction (**Figure 3-8B, C**). The P2-UUCG/P9b-GAAA construct seemed less active than P2-UUCG/P9b-UAAU construct. A possible reason of this result may be an involvement of the P5–P9b interaction not only in the stability of the correct structure but also in the folding process of Oligo-Y (P2-UUCG) RNA, which may yield misfolding structures. The comparative analysis of seven sets of P4-6/P3-7 ribozyme units were performed that functioned in the bimolecular state and the 1D oligomer state. The results of this analysis suggested that the 1D oligomer formation of the P4-6/P3-7 ribozyme unit may rescue its structural defects to various extents, some of which abolish the catalytic ability in the parent bimolecular format (**Figure 3-8D**).

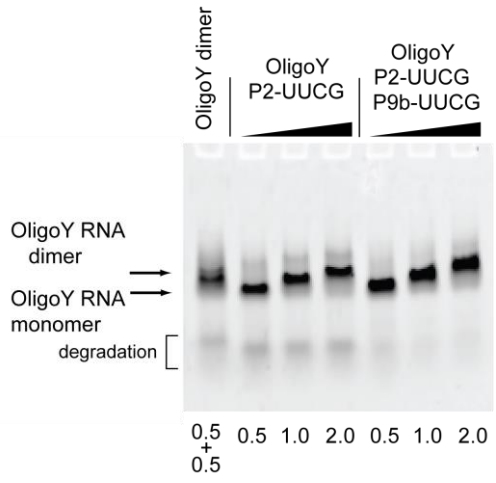

Figure 3-9. EMSA of Oligo-Y RNA (P2-UUCG) and Oligo-Y RNA (P2-UUCG/P9b-UUCG). Electrophoresis was performed at 4°C in the presence of 30 mM Mg^{2+}.

3.4. Discussion

In this study, a 1D ribozyme assembly was designed in which the catalytically active bimolecular ribozymes are organized as repeating units (**Figures 3-1 and 3-6B**). By employing Y4-6 RNA with the P5.1 stem as an extra duplex, the Y4-6/P3-7 bimolecular ribozyme was redesigned to construct a unit RNA (Oligo-Y RNA) for 1D ribozyme assembly (**Figures 3-1 and 3-6).** Our analysis suggested that the 1D assembly structure formation seemed to modestly compensate for the structural defects destabilizing P4-6/P3-7 interdomain assembly. In the 1D assembly (Oligo-Y) form, P2-UUCG mutant and P9b-UUCG mutant, neither of which showed detectable activity in the parent bimolecular (P4-6/P3-7) form, still showed weak but detectable activity. The residual activity of the P2-UUCG mutant of Oligo-Y RNA (**Figure 3-8B, C**) seemed consistent with the behavior of this mutant in EMSA (**Figures 3-7D and 3-9**). In the parent bimolecular ribozyme, P2-UUCG mutant disrupted P5c–P2 interaction, which severely destabilized the P4-6/P3-7 complex, and formed no retarded band in EMSA. In the 1D assembly form of Oligo-Y RNA, however, the mobility of the Oligo-Y RNA mutant bearing P2-UUCG mutation showed slight but detectable retardation of the band (**Figures 3-7D and 3-9**), suggesting that weak P4-6/P3-7 interdomain interactions remained in Oligo-Y RNA to guide the formation of the 1D array.

Weak but detectable compensation of disrupted tertiary interactions may be similar to molecular crowding effects on ribozymes. An example of molecular crowding effects on a ribozyme can be seen in the *Azoarcus* ribozymes, which are a small group I ribozymes with no large peripheral elements [157]. Disruption of tertiary interactions in the *Azoarcus* ribozyme reduced its catalytic activity by either destabilizing its active

structure or by affecting its folding pathways to accumulate misfolded structures. For mutations destabilizing the native structure, molecular crowding effectively rescued the catalytic activity by stabilizing the native structure [158, 159]. On the other hand, molecular crowding had no effect on reduction of catalytic ability caused by mutations altering the folding properties of the ribozyme to accumulate misfolded structures [159]. Molecular crowding effects have not been reported for Tth ribozyme folding and catalysis. No experimental studies have been reported for the folding and assembly process of the P4-6/P3-7 bimolecular ribozyme. Considering the folding properties of the wild-type (unimolecular) Tth group I ribozyme and its modular domains, disruption or destabilization of interdomain interactions (P5–P9b and P5c–P2) is unlikely to markedly affect the folding behavior of respective RNA modules (P4-6 domain RNA and P3-7 domain RNA) in the bimolecular ribozyme. Mutations in these tertiary interactions can therefore be predicted to primarily affect the assembly, maintenance, and/or activation of the catalytically active core structure of the ribozyme. In the wild-type (unimolecular) Tth ribozyme, disruption of P5c–P2 interaction mainly disturbed the docking of P1 substrate helix to the catalytic core [160]. In the bimolecular P4-6/P3-7 ribozyme, P5c–P2 interaction plays a major role in supporting the physical assembly of two RNA domains. In the unimolecular Tth ribozyme, P5–P9b interaction was suggested to contribute to the catalytic mechanism primarily by assisting the formation of the guanosine cofactor binding pocket [160]. The contribution of P5–P9b interaction to catalysis is likely to be preserved in the bimolecular P4-6/P3-7 ribozyme. The proposed functional role of P5–P9b interaction in the wildtype Tth ribozyme seems consistent with the observations in the present study, in which the P9b-UUCG mutant of the bimolecular ribozyme showed no catalytic activity (**Figure 3-4B, C**) despite its ability to form the P4-

6/P3-7 complex (**Figure 3-4A**). The 1D assembly form (Oligo-Y RNA) modestly rescued the two mutants (with disrupted P5c–P2 or P5–P9b interaction). This observation suggests that non-covalent assembly of bimolecular ribozyme can rescue distinct types of structural defects that affect different properties in the parent ribozyme.

Currently, it is unclear whether the connection between molecular crowding effect and self-assembly effect is superficial. Additional experiments are needed to elucidate the self-assembly effect including its connection with molecular crowding effect and also its generality. In the present study, the author examined one type of 1D assembly of the Tth bimolecular ribozyme. Similar 1D assembly structures may be designed using different types of ribozymes with modular structures. These include ribonuclease P (RNase P) RNAs and group II intron RNAs [161-163]. RNase P RNAs are the RNA components of RNase P ribonucleoproteins, a class of nucleolytic enzymes that catalyze site-specific cleavage reactions of 5′ leader sequences of precursor tRNAs using an RNA-based catalytic mechanism. RNase P RNAs have a modular architecture consisting of the substrate recognition domain (S-domain) and the catalytic domain (C-domain) [164, 165]. In bacterial RNase P RNA ribozymes, reconstitution of a bimolecular ribozyme has been reported through non-covalent assembly of separately prepared S-domain RNA and C-domain RNA [164, 165]. Therefore, the modular architecture of RNase P ribozymes is similar to that of group I intron ribozymes. This similarity suggests that RNase P ribozymes may represent a possible platform for 1D assembled ribozyme nanostructures that can be constructed through rational redesign of their parent 3D structures. The 1D assembly of ribozyme modules may not be an optimal form of ribozyme nanostructure to lead to primitive crowding-like or cellular-like effects. Closed 2D oligomers with polygonal shapes may be promising as a possible next step in the evolution toward

spherical (cell-like) or polyhedral (virus capsid-like) 3D shapes, because polygonal 2D oligomers would be more entropically stable than open-form 1D oligomers. The author recently reported this type of ribozyme nanostructure by designing and characterizing closed trimeric ribozymes and closed tetrameric ribozymes, which formed triangular and square shapes, respectively [73]. It would be interesting to examine whether these assemblies would also rescue structural defects of their unit bimolecular ribozymes.

Chapter 4: Effects of molecular crowding on a bimolecular group I ribozyme and its derivative that self-assembles to form ribozyme oligomers

4.1. Abstract

In the RNA world, enrichment of self-replicating RNAs would have been beneficial to their survival, amplification, and evolution. Self-assembly of RNAs may be a strategy by which they enrich themselves. Here, the effects of molecular crowding were examined on the activity of a bimolecular group I ribozyme and its derivative that self-assembles to form ribozyme oligomers. In a comparative activity assay using PEG as a molecular crowder, PEG rescued mutations in the parent bimolecular ribozyme more effectively than those in the oligomeric form.

4.2. Introduction

Ribozymes with self-replication and related abilities have been considered to play central roles in the hypothetical RNA world [117, 137, 166, 167], where concentrations of RNA molecules are a crucial issue for their survival and evolution [117, 127, 137, 167]. If concentrations of essential RNA components for self-replicating systems are too low to maintain their minimal replication speeds, their population would decline and eventually go to extinction through dispersion/diffusion and spontaneous RNA degradation. Enrichment and/or isolation of RNA molecules would represent an effective strategy to overcome these risks [117, 127, 137, 167]. Several environmental conditions involving primitive compartmentalization systems have been investigated experimentally

[122, 127, 139, 168-170]. Self-assembly of ribozymes may be one such strategy, with which ribozymes may enrich themselves and become more tolerant against dispersion/diffusion than the parent ribozymes with dispersed states [169, 170].

As a model system of ribozyme assembly, the author engineered the bimolecular Y4-6/P3-7 group I ribozyme (**Figure 4-1A**), which was derived from the *Tetrahymena* group I ribozyme, to yield a unit RNA (Oligo-Y RNA, **Figure 4-1C**) [169]. Oligo-Y RNA self-assembles to form 1D-ribozyme oligomer (**Figure 4-1D**). This ribozyme oligomer retained the catalytic function (**Figure 4-1B**) because the Y4-6/P3-7 ribozymes were formed as functional units in the oligomer (**Figure 4-1D**). Although the ribozyme unit is the same between the Oligo-Y oligomer and the bimolecular ribozyme, the catalytic activity of Oligo-Y RNA was slightly higher than that of the Y4-6/P3-7 ribozyme [169]. This observation suggested that oligomerization of functional RNAs with modular architecture enhances their activities

While self-assembly of Oligo-Y RNA requires no particular environmental conditions, enzyme functions are often markedly influenced by environmental conditions. Molecular crowding is one such condition that strongly affects folding, assembly, and catalytic properties of protein and RNA enzymes [131, 158, 171-173]. Intracellular conditions are typical molecular crowding conditions but their compositions are highly complex. Biochemical and physicochemical studies of molecular crowding effects on ribozyme folding and catalysis have been performed using *in vitro* systems, in which molecular crowding conditions were generated simply by adding cosolutes, such as polyethylene glycol (PEG), dextran, and Ficoll, to the reaction solutions as molecular crowders [131, 158, 171-173].

Molecular crowding not only influences intracellular enzyme functions but has also been proposed to have facilitated the evolution of functional RNAs in the RNA world [134]. As ribozyme self-assembly and molecular crowding may have facilitated evolution of the RNA world, it is interesting to examine whether self-assembly and molecular crowding improve ribozyme activities cooperatively. To address this issue, the effects of PEG-dependent molecular crowding on the activity of the bimolecular Y4-6/P3-7 ribozyme and its 1D-oligomeric form were compared.

4.3. Results

4.3.1. Effects of PEG on a bimolecular ribozyme and its variants

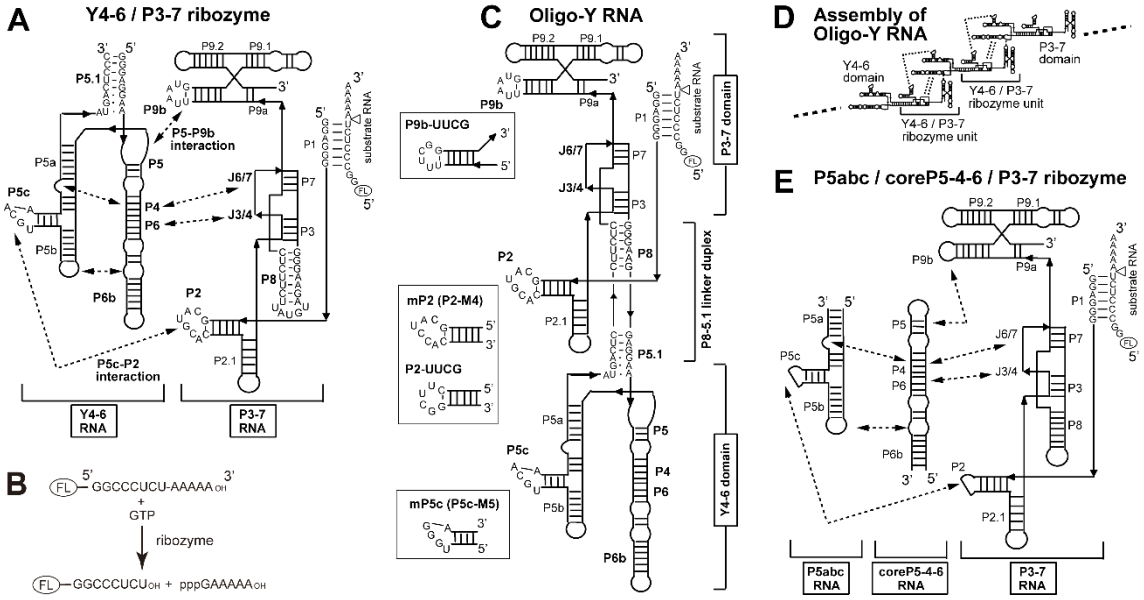

Figure 4-1. Bimolecular Y4-6/P3-7 ribozyme and its derivatives. (**A**) Secondary structure of the Y4-6 and P3-7 bimolecular ribozyme. Broken lines with two arrowheads show tertiary interactions. Mutations introduced in P9b, P2, and P5c elements are shown on the right. (**B**) The substrate cleavage reaction catalyzed by the ribozymes used in this study. FL indicates carboxyfluorescein (FAM) fluorophore covalently attached to the 5′-end of the substrate RNA. (**C**) Secondary structure of Oligo-Y RNA. (D) Oligomeric formation of Oligo-Y RNA. Thin dotted lines indicate the interdomain interaction between two Oligo-Y RNAs. (E) Secondary structure of a trimolecular ribozyme. Broken lines with two arrowheads show tertiary interactions.

To evaluate the effects of molecular crowding conditions on the bimolecular group I ribozyme (Y4-6/P3-7 ribozyme) the catalytic site of which is formed by interdomain assembly (**Figures 4-1A and 4-**2**A**), PEG with distinct molecular weights (PEG8000 and PEG200) were used as molecular crowders. PEG has been used most frequently as a non-

charged molecular crowder [158, 171-173]. The substrate cleavage reaction was performed in the presence of PEG8000 or PEG200.

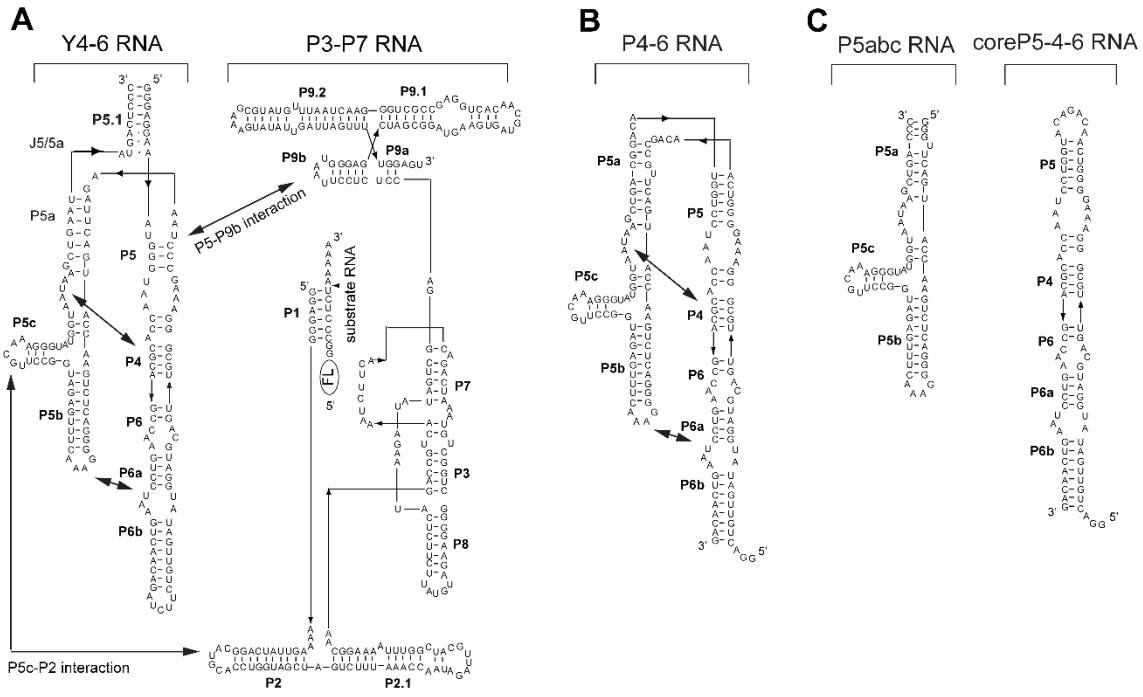

Figure 4-2. Secondary structures of modular RNAs forming the bimolecular and trimolecular ribozymes employed in this study. (**A**) Secondary structure of the Y4-6/P3-7 bimolecular ribozyme. Solid lines with two arrowheads indicate tertiary interactions. (**B**) Secondary structure of the P4-6 RNA that forms a bimolecular ribozyme with P3-7 RNA. Solid lines with two arrowheads indicate tertiary interactions. (**C**) Secondary structures of P5abc RNA and core P4-5-6 RNA. They formed a trimolecular ribozyme with P3-7 RNA.

The optimal concentrations of PEG8000 and PEG200 independently was first screened in the presence of 50 mM Mg^{2+} (**Figures 4**-3**A and 4**-3**B**). The Y4-6/P3-7 ribozyme showed highest substrate cleavage in the presence of 10% PEG8000 and 15% PEG200, respectively (**Figures 4**-3**A and 4**-3**B**), under which conditions the activity of the Y4-6/P3-7 ribozyme was 3.8-fold (k_{obs} = 0.21 h^{-1}) and 9.5-fold (0.53 h^{-1}) higher than

without PEG (0.055 h^{-1}) (**Figure 4-4**). Similar enhancement was also observed for the bimolecular P4-6/P3-7 ribozyme (**Figure 4**-5), in which P4-6 RNA was a prototypical form of Y4-6 RNA and lacked the P5.1 element (**Figure 4**-2) [150, 169].

To determine whether PEG improved a mutant ribozyme with less stable interdomain assembly compared to the Y4-6/P3-7 ribozyme, a mutant with a weaker P5c-P2 interaction under lower Mg^{2+} conditions was examined (**Figure 4-4B**, **4-6A** and **4**-6**B**). In the mY4-6/mP3-7 ribozyme, its P5c-P2 interaction (designated as P5c-M5/P2-M4 mismatch in previous studies) was less strong than that of the parent (**Figure 4-1**) and so the weak P5c-P2 interaction supported the interdomain association between Y4-6 and P3-7 less stably [156]. Under the doubly unfavorable conditions (weaker P5c-P2 interaction and 25 mM Mg^{2+}), mY4-6/mP3-7 with 25 mM Mg^{2+} (0.013 h^{-1}) was 4.2-fold less active than Y4-6/P3-7 with 50 mM Mg^{2+} (0.055 h^{-1}) (**Figure 4-4B**). Whether PEG improved the activity of mY4-6/mP3-7 with 25 mM Mg^{2+} was then examined. At optimal PEG concentration (10% for PEG8000 and 15% for PEG200), k_{obs} values of mY4-6/mP3-7 with 25 mM Mg^{2+} were 0.14 h^{-1} and 0.43 h^{-1}, respectively (**Figure 4-4B**). These values were close to those of the parent Y4-6/P3-7 in the presence of 50 mM Mg^{2+} with the corresponding PEG8000 and PEG200 concentrations (0.23 h^{-1} and 0.42 h^{-1}, respectively, see **Figure 4-4A**).

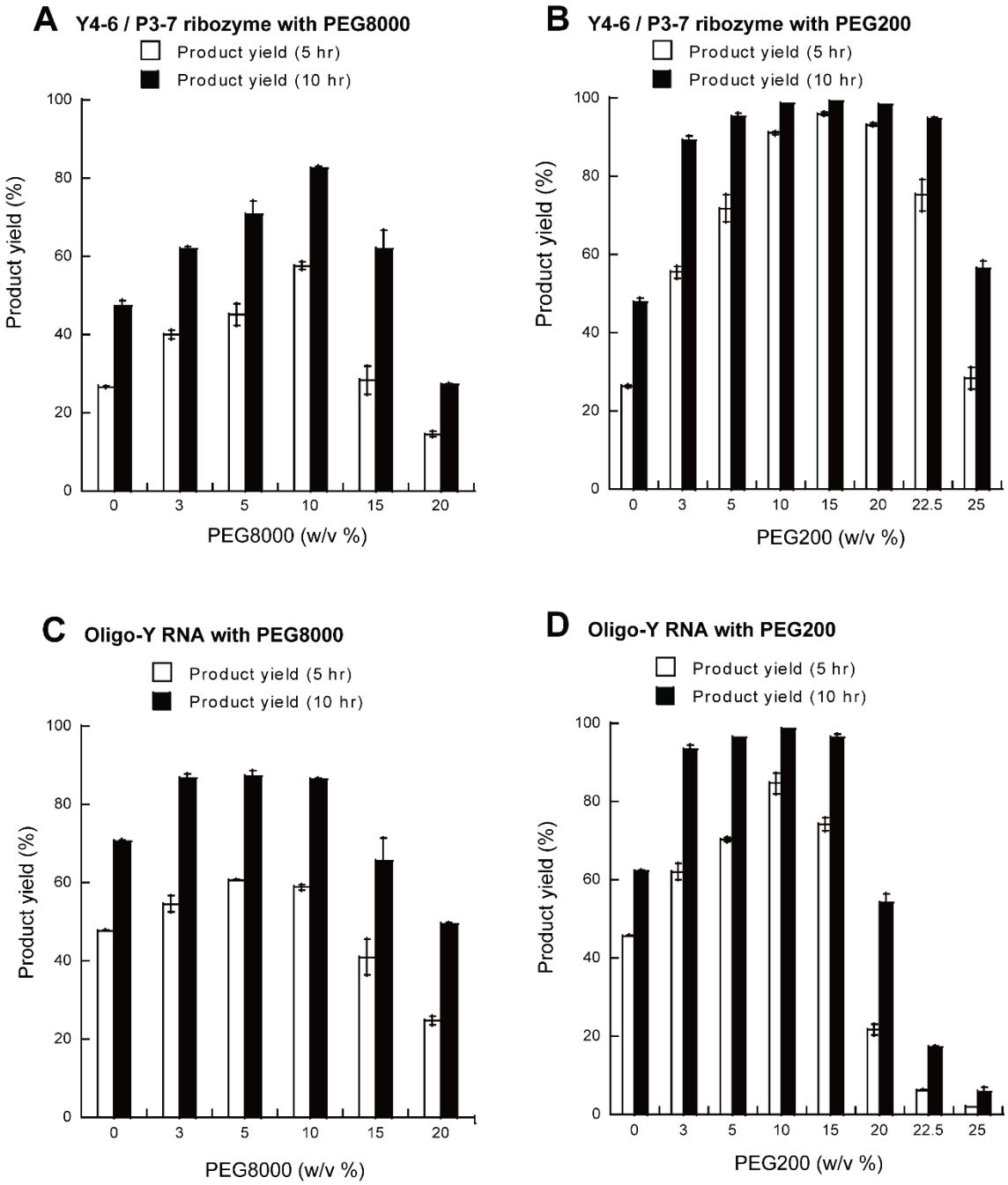

Figure 4-3. Optimization of PEG concentrations for the reaction catalyzed by Y4-6/P3-7 ribozyme and its oligomeric form. (A, B) Substrate cleavage reaction by the Y4-6/P3-7 ribozyme in the presence of 50 mM Mg^{2+} with different concentrations of PEG8000 (A) and PEG200 (B). (C, D) Substrate cleavage reaction by Oligo-Y RNA in the presence of 50 mM Mg^{2+} with different concentrations of PEG8000 (A) and PEG200 (B).

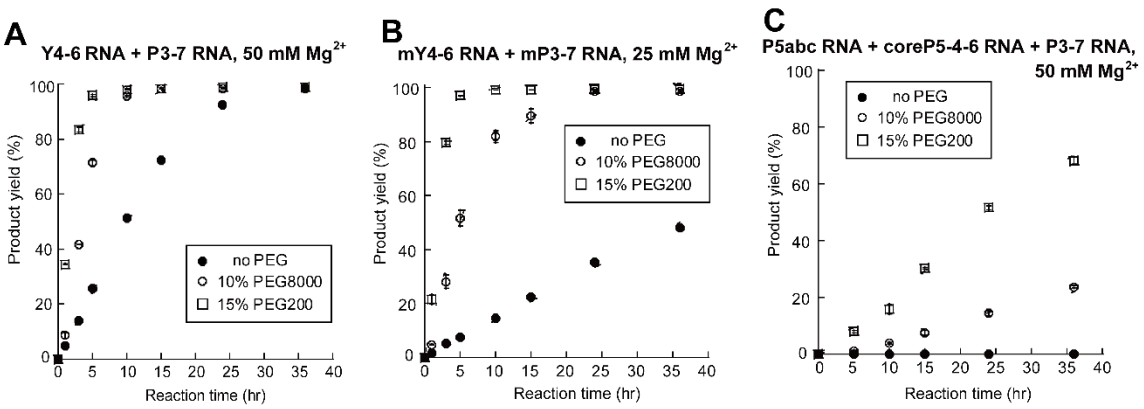

Figure 4-4. Effects of PEG on the activity of the Y4-6/P3-7 ribozyme and its mutant. (**A**) Time courses of the substrate cleavage reaction catalyzed by the Y4-6/P3-7 ribozymes at 50 mM Mg^{2+} with/without optimal concentration of PEG8000 or PEG200. (**B**) Product yield of the substrate cleavage reaction governed by bimolecular mY4-6/mP3-7 ribozymes at 25 mM Mg^{2+} with/without optimal concentration of PEG8000 or PEG200. (**C**) Time courses of substrate cleavage reaction catalyzed by the trimolecular ribozyme at 50 mM Mg^{2+} with/without optimal concentration of PEG8000 or PEG200.

Remarkable effects of PEG800 and PEG200 on improvement of the bimolecular group I ribozymes prompted us to expand our analysis to a trimolecular ribozyme consisting of three modular RNAs (**Figure 4-1E**). The *Tetrahymena* group I ribozyme has been engineered to produce two bimolecular derivatives, P4-6/P3-7 ribozyme [149, 150] and P5abc/ΔP5 ribozyme [156, 174, 175]. The self-folding P4-6 domain RNA is composed of the P5abc subdomain and the core P5-4-6 helical domain. The ΔP5 RNA, which consists of the core P5-4-6 domain and the P3-7 domain, retains the catalytic activity because core elements required for catalysis are located within the core P5-4-6 and P3-7 domains [149, 175]. Therefore, the author designed the physical dissection of the *Tetrahymena* ribozyme into P5abc RNA, core P4-5-6 RNA, and P3-7 RNA. In the absence of PEG, the reaction mixture containing P5abc, core P5-4-6, and P3-7 RNAs (1.0

μM each) yielded no detectable amounts of the reaction product even with 36-hour reaction in the presence of 100 mM Mg^{2+}, suggesting that assembly of three modular RNAs is entropically too unstable to conduct detectable catalytic activity. In the presence of 5% PEG8000 and 15% PEG200, however, the catalytic activity of the trimolecular ribozyme became detectable with 50 mM Mg^{2+} (**Figures 4-5C and 4-7**), with k_{obs} values of 0.0061 h^{-1} and 0.019 h^{-1}, respectively.

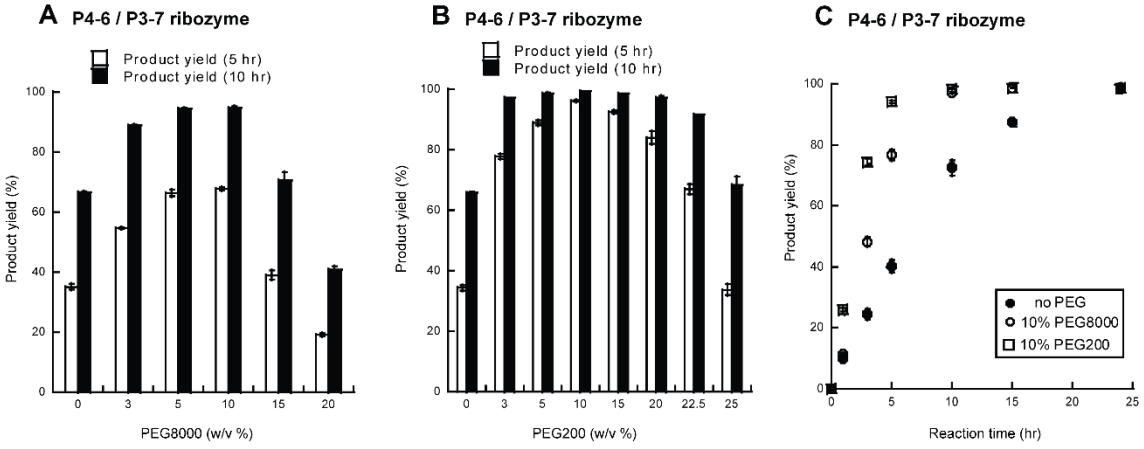

Figure 4-5. Effects of PEG on the substrate cleavage reaction catalyzed by the P4-6/P3-7 bimolecular ribozyme. (**A, B**) Substrate cleavage reaction by the Y4-6/P3-7 ribozyme in the presence of 50 mM Mg^{2+} with different concentrations of PEG8000 (**A**) and PEG200 (**B**). (**C**) Time courses of the substrate cleavage reaction catalyzed by P4-6/P3-7 ribozymes at 50 mM Mg^{2+} with/without the optimal concentration of PEG8000 or PEG200.

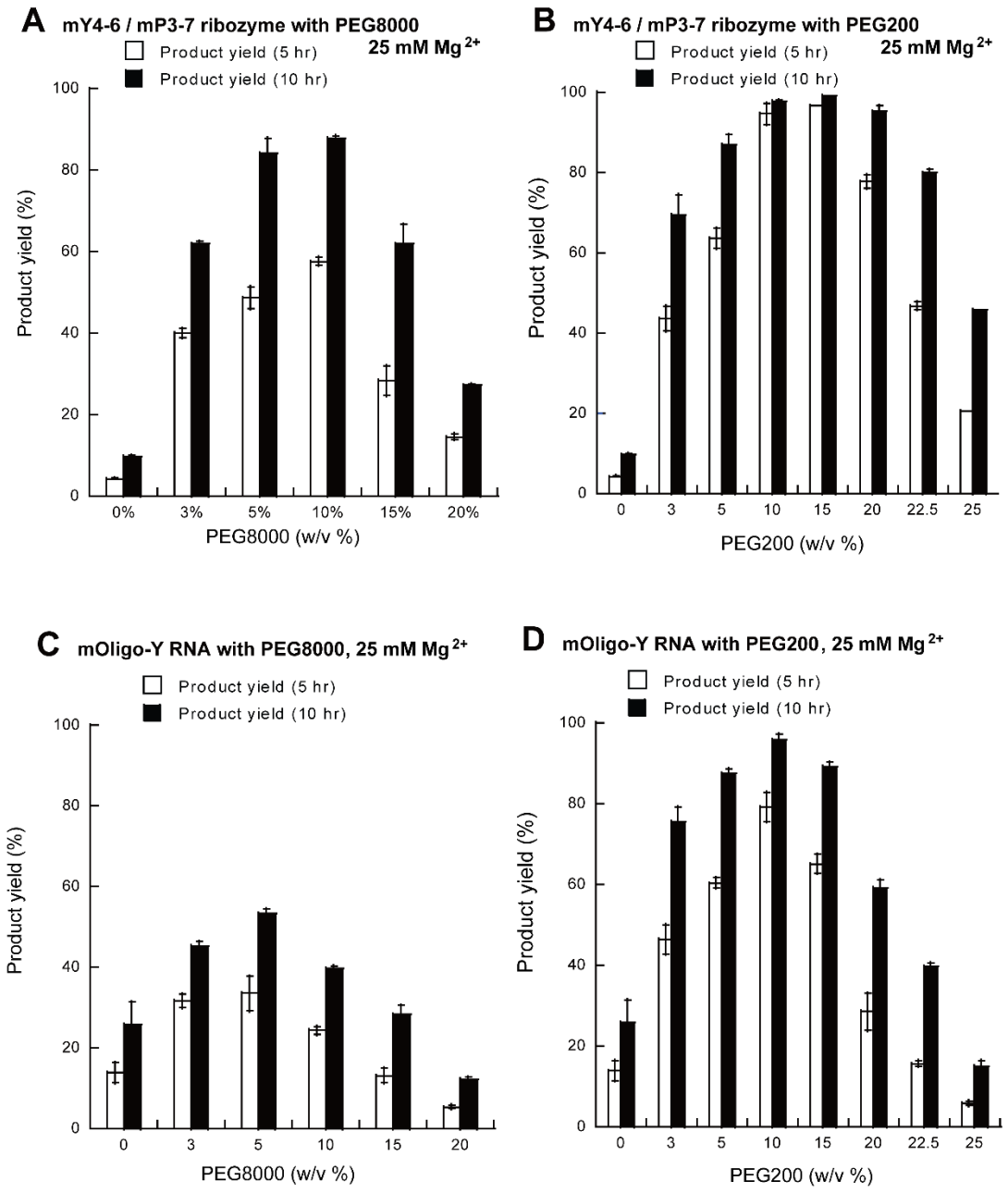

Figure 4-6. Optimization of PEG concentrations for the reaction catalyzed by mY4-6/mP3-7 ribozyme and its oligomeric form. (**A, B**) Substrate cleavage reaction by the mY4-6/mP3-7 ribozyme in the presence of 25 mM Mg^{2+} with different concentrations of PEG8000 (**A**) and PEG200 (**B**). (**C, D**) Substrate cleavage reaction by mOligo-Y RNA in the presence of 25 mM Mg^{2+} with different concentrations of PEG8000 (**A**) and PEG200 (**B**).

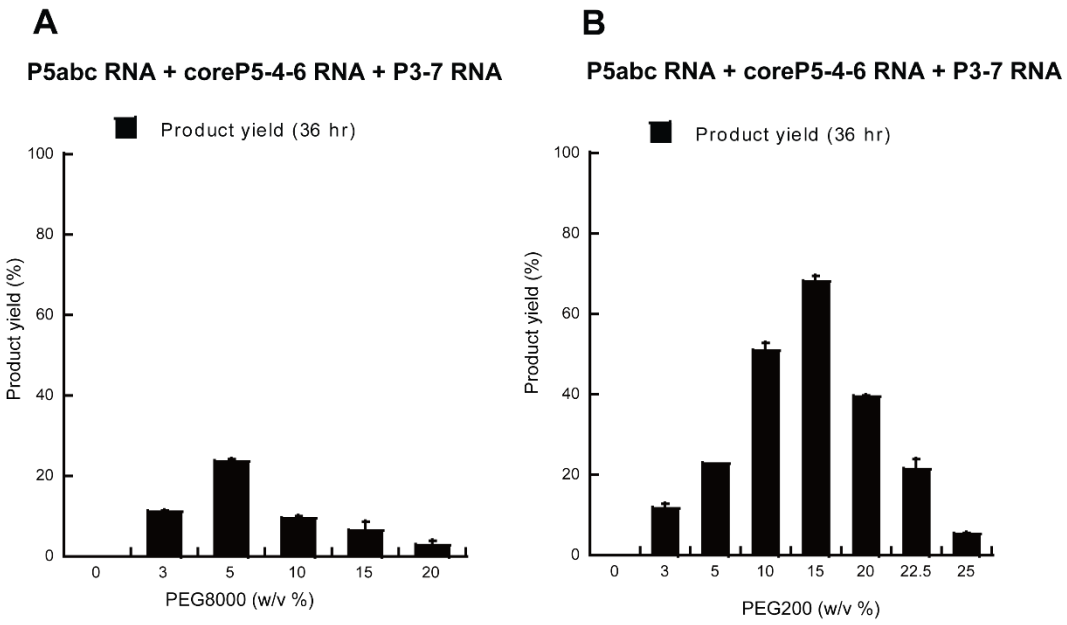

Figure 4-7. Effects of PEG on the substrate cleavage reaction catalyzed by the trimolecular ribozyme. Substrate cleavage reaction by the P5abc/core P5-4-6/P3-7 trimolecular ribozyme in the presence of 50 mM Mg^{2+} with different concentrations of PEG8000 (**A**) and PEG200 (**B**).

4.3.2. Effects of PEG on 1D-assembly of the bimolecular ribozyme

As PEG markedly enhanced the catalytic abilities of the bimolecular and trimolecular ribozymes, the effects of PEG on modulating the oligomeric form of the bimolecular ribozyme were then examined. In the absence of PEG, the ribozyme activity of Oligo-Y RNA (0.13 h^{-1}) was 2.4-fold higher than that of the Y4-6/P3-7 ribozyme (0.055 h^{-1}) (**Figure 4-8C**) [169]. The substrate cleavage reactions of Oligo-Y assembly in the presence of various amounts of PEG8000 or PEG200 were performed with 50 mM Mg^{2+} (**Figures 4-3C and 4-3D**). Oligo-Y RNA showed optimum activity in the presence of 5% PEG8000 and 10% PEG200 (**Figures 4-3C and 4-3D**), under which conditions k_{obs} values were 0.17 h^{-1} and 0.28 h^{-1}, respectively (**Figure 4-8A**). These k_{obs} values were

slightly (less than twofold) smaller than those of the Y4-6/P3-7 ribozyme (0.21 h^{-1} with 10% PEG8000 and 0.55 h^{-1} with 15% PEG200). The 1D-oligomeric form of the mY4-6/mP3-7 mutant was also examined in the presence of 25 mM Mg^{2+} (**Figures 4-8B, 4-6C and 4-6D**). The mY4-6/mP3-7 mutant with 25 mM Mg^{2+} was 4.3-fold less active than the Y4-6/P3-7 ribozyme with 50 mM Mg^{2+} (**Figure 4-8C**). Oligomerization of mY4-6/mP3-7 ribozyme unit (mOligo-Y RNA) resulted in a 1.6-fold increase in its activity to give a k_{obs} value of 0.021 h^{-1} (**Figure 4-8B**), which was 6.1-fold smaller than that of Oligo-Y RNA (0.13 h^{-1}, **Figure 4-4B**), indicating that the doubly unfavorable conditions (weaker P5c-P2 interaction and 25 mM Mg^{2+}) decreased the k_{obs} value similarly in the bimolecular form (4.2-fold reduction) and in the oligomeric form (6.1-fold reduction) (**Figure 4-8C**).

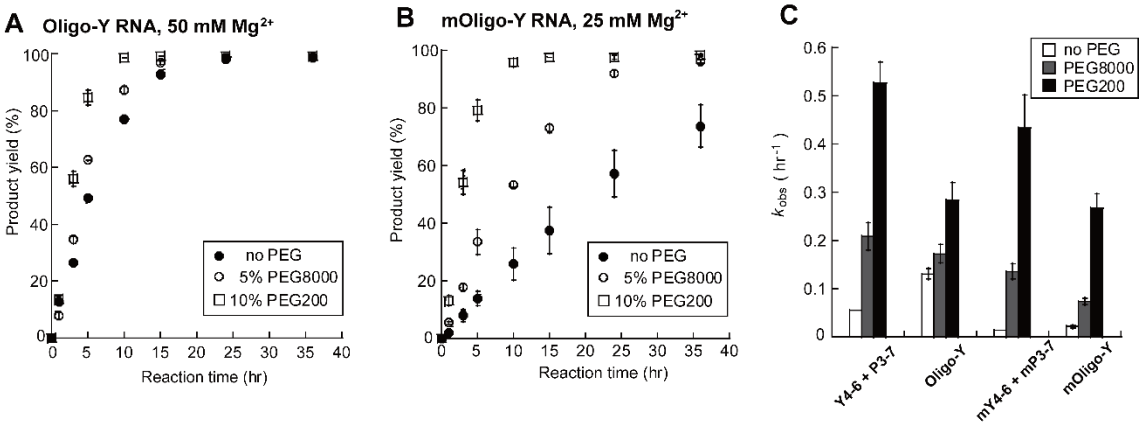

Figure 4-8. Effects of PEG on the activity of the one-dimensional assembly of Oligo-Y RNA and its mutant. (**A**) Time courses of the substrate cleavage reaction catalyzed by Oligo-Y RNA ribozymes at 50 mM Mg^{2+} with/without optimal concentration of PEG8000 or PEG200. (**B**) Time courses of the substrate cleavage reaction catalyzed by mOligo-Y RNA at 25 mM Mg^{2+} with/without optimal concentration of PEG8000 or PEG200. (**C**) Effects of PEG on the activities the bimolecular and oligomeric forms of the Y4-6/P3-7 ribozyme.

The author further investigated the effects of 5% PEG8000 and 10% PEG200 on the mOligo-Y RNA (**Figure 4-8B**). In the presence of 10% PEG200 and 25 mM Mg^{2+}, the k_{obs} value was increased by 13-fold to 0.27 h^{-1}. This value was similar to that of the parent Oligo-Y RNA with 50 mM Mg^{2+} and 10% PEG200 (0.28 h^{-1}) (**Figure 4-8B**), indicating that 10% PEG200 completely compensated for the negative effects of the doubly unfavorable conditions. Negative effects of the doubly unfavorable conditions were partially compensated by 5% PEG8000, under which conditions the k_{obs} of mOligo-Y was increased by 3.5-fold (0.073 h^{-1}) but was 2.3-fold smaller than that of the parent Oligo-Y with 5% PEG8000 (0.17 h^{-1}). These observations showed that PEG compensated for the doubly unfavorable conditions in the bimolecular form (**Figure 4-4**) as well as in the Oligo-Y form (**Figure 4-8**). On the other hand, PEG seem to enhance the Oligo-Y form less effectively than the bimolecular form because in the presence of PEG the Oligo-Y RNA was less active than the Y4-6/P3-7 ribozyme (**Figure 4-8C**).

4.3.3. Different effects of PEG and 1D-assembly on the rescue of severe defects of the bimolecular ribozyme unit

In the bimolecular ribozyme and its oligomeric form, PEG compensated for the negative effects of the doubly unfavorable conditions (**Figure 4-8C**). These observations prompted us to examine the effects of PEG on more severe mutations in the bimolecular Y4-6/P3-7 ribozyme [169]. Complete disruption of P5c-P2 interaction and/or P5-P9b interaction were examined by replacing terminal loop(s) in P2 and/or P9b in the P3-7 domain with the UUCG loop (**Figure 4-1**). In the bimolecular Y4-6/P3-7 form, mutants possessing P2-UUCG, P9b-UUCG and their double mutant showed no detectable

ribozyme activity (**Figure 4-9**) [169]. In the Oligo-Y form, however, all three mutants retained weak but detectable activities (**Figure 4-9**). Therefore, the effects of PEG crowders on the three severe mutations in the bimolecular and oligomeric form were examined.

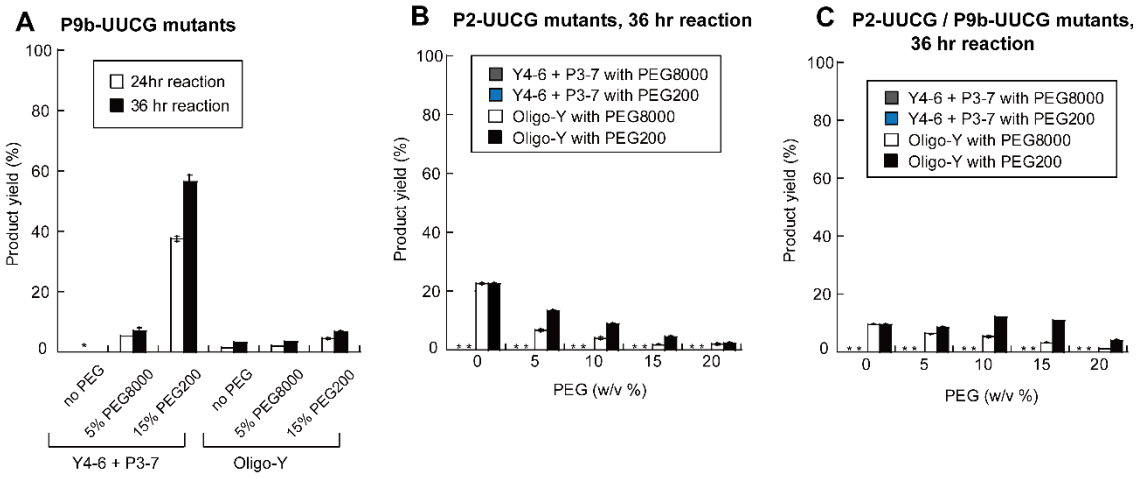

Figure 4-9. Effects of PEG on the bimolecular and oligomeric forms of the Y4-6/P3-7 ribozyme with disrupted interdomain interactions. (**A**) Effects of the P9b-UUCG mutation on the substrate cleavage reactions catalyzed by the bimolecular ribozyme and its oligomeric form. (**B**) Effects of PEG on the substrate cleavage reaction catalyzed by P2-UUCG mutant ribozymes. (**C**) Effects of PEG on the substrate cleavage reaction catalyzed by P2-UUCG/P9b-UUCG double mutant ribozymes.

Firstly, the structural context lacking P5-P9b interaction was examined using RNAs with P9b-UUCG loops (**Figure 4-9A**). In the bimolecular form, fatal effects of P9b-UUCG were rescued modestly by 5% PEG800 and efficiently by 15% PEG200 (**Figures 4-10A and 4-10B**), with which the product yield reached nearly 60% for 36-hour reaction in the presence of 50 mM Mg^{2+} (**Figure 4-9A**). Enhancement of the activity was also observed in the Oligo-Y form affording weak activity to P9b-UUCG mutant (**Figures 4-10C and 4-10D**). However, the effects of PEG200 on the oligomeric form (**Figure 4-9A-right**) were much smaller than those on the bimolecular form (**Figure 4-9A-left**).

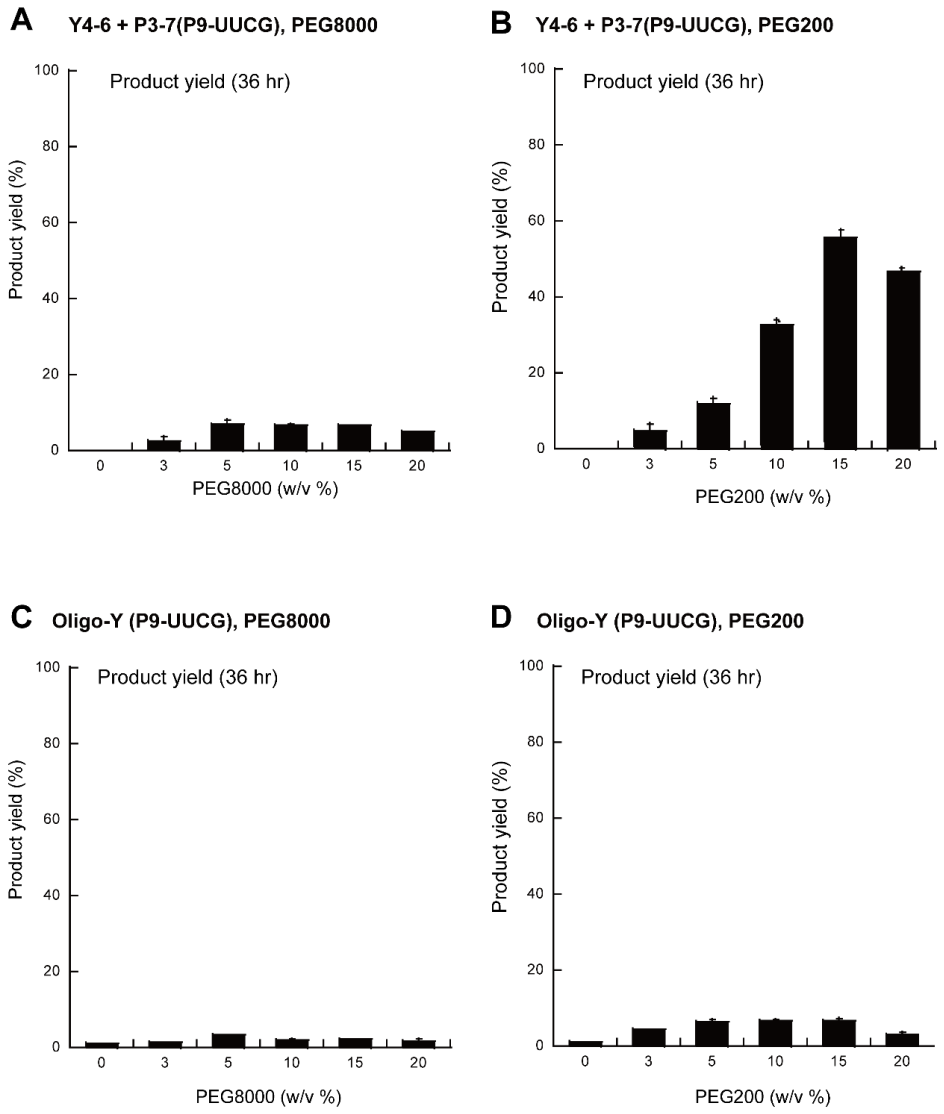

Figure 4-10. Effects of PEG on the substrate cleavage reaction catalyzed by the mutant Y4-6/P3-7 ribozymes and their oligomeric forms possessing P9b-UUCG mutation (**A, B**) Substrate cleavage reaction by the Y4-6/P3-7 ribozyme possessing P9b-UUCG mutation in the presence of 50 mM Mg^{2+} with different concentrations of PEG8000 (**A**) and PEG200 (**B**). (**C, D**) Substrate cleavage reaction by Oligo-Y RNA possessing P9b-UUCG mutation in the presence of 50 mM Mg^{2+} with different concentrations of PEG8000 (**C**) and PEG200 (**D**).

The P2-UUCG mutation that completely disrupts P5c-P2 interaction was then examined (**Figure 4-1**). This mutation has been shown to cause severe defects in the

assembly of Y4-6 and P3-7 RNA and inactivate the bimolecular ribozymes (**Figure 4-9B**). However, the P2-UUCG mutant of Oligo-Y RNA showed weak but detectable activity (**Figure 4-9B**). Neither PEG8000 nor PEG200 activated the P2-UUCG mutant in the bimolecular form (**Figure 4-9B**). In the Oligo-Y form, PEG decreased the catalytic activity in a concentration-dependent manner (**Figure 4-9B**). Finally, the double mutants bearing both P9b-UUCG and P2-UUCG, in which P5-P9b and P5c-P2 interactions were both disrupted was analyzed (**Figure 4-1**). Double disruption inactivated the bimolecular Y4-6/P3-7 ribozyme, the activity of which was not recovered by addition of PEG (**Figure 4-9C**). The mutant bimolecular ribozyme unit with double disruption, however, still exhibited weak but detectable activity in the Oligo-Y form (**Figure 4-9C**). The residual activity of the double mutant in the Oligo-Y form was hardly affected by PEG200 and weakly inhibited by PEG8000 (**Figure 4-9C**).

4.4. Discussion

In this study, the enhancing effects of PEG molecular crowders was investigated on the activity of the bimolecular Y4-6/P3-7 ribozyme and its oligomeric derivative, Oligo-Y RNA. Oligomerization of the Y4-6/P3-7 ribozyme allowed the ribozyme to self-assemble into a 1D-nanostructure, which modestly enhanced the catalytic ability of the parent Y4-6/P3-7 ribozyme. Therefore, the author compared RNA self-assembly and molecular crowding as two possible strategies with which activities of ribozymes may have been improved in the evolution of the RNA-world. A bimolecular group I ribozyme was employed as a model ribozyme because its activity depends on modular assembly of two structural RNAs [149, 150, 169]. Consistent with our prediction that the excluding volume effect under molecular crowding conditions would facilitate the assembly of two

modular RNAs, PEG enhanced the activity of the Y4-6/P3-7 ribozyme. The effect of PEG was so efficient that the bimolecular ribozyme under doubly less-favored conditions (mY4-6/mP3-7 ribozyme with 25 mM Mg^{2+}) became as active as the parent Y4-6/P3-7 ribozyme in the presence of PEG crowders (**Figure 4-8C**). Therefore, the molecular crowding effects of PEG almost completely rescued the structural instability of mY4-6/mP3-7 ribozyme in the presence of 25 mM Mg^{2+}.

In the oligomeric form of the bimolecular ribozyme (Oligo-Y RNA), molecular crowding effects also rescued the structural instability of mY4-6/mP3-7 with 25 mM Mg^{2+} and improved its activity close to that of Y4-6/P3-7 with 50 mM Mg^{2+} (**Figure 4-8C**). Under optimal PEG concentrations, however, the activity of Oligo-Y ribozyme was lower than that of the parent Y4-6/P3-7 ribozyme (**Figure 4-8C**). In the presence of a high concentration (> 20%) of PEG200, the decrease in activity was more severe in the oligomeric form than in the bimolecular form (**Figure 4-3B and 4-3D**). A similar difference was also seen in the comparison between the mutant bimolecular form (mY4-6/mP3-7) and mutant oligomeric form (mOligo-Y) with 25 mM Mg^{2+} (**Figures 4-8C and 4-6**). These observations suggested that PEG may have a stronger negative effect on the activity of Oligo-Y ribozyme than on the bimolecular form. As the ribozyme units in the oligomers share the same secondary structure with the parent Y4-6/P3-7 ribozyme, PEG may negatively affect the structural elements that are present only in Oligo-Y RNA. With regard to the catalytic activity of the oligomeric form, the positive effects of PEG on assembly of the bimolecular catalytic unit may be partially canceled by the negative effects of PEG that are specific to Oligo-Y RNA.

Distinct effects of PEG on the bimolecular form and oligomeric form of the ribozyme were further observed in mutants with severe defects in tertiary interactions involved in assembly of the two module RNAs. Complete disruption of P5-P9b interaction or P5c-P2 interaction in the bimolecular ribozyme led to undetectable ribozyme activity. In the oligomeric form, however, the corresponding mutants (each single mutant and the double mutant) still exhibited residual but detectable activity (**Figure 4-9**). In the oligomeric forms of the three mutants lacking the critical tertiary interactions, PEG showed no significant improvement of the activity. PEG had nearly no effect on the double mutant (**Figure 4-9C**), negative effects on P2-UUCG mutant (**Figure 4-9B**), and a slight positive effect on P9b-UUCG mutant Oligo-Y RNA (**Figure 4-9A**).

In the parent bimolecular Y4-6/P3-7 RNA, these mutants showed no detectable activity. PEG crowders effectively rescued the P9b-UUCG mutant (**Figure 4-9A**), while they failed to restore activity of the P2-UUCG mutant in the bimolecular form (**Figure 4-9B**). Although the molecular basis of the distinct effects of PEG crowders on P9b-UUCG mutant and P2-UUCG mutant remains to be determined, the two tertiary interactions play different roles in assembly and catalysis of the bimolecular ribozyme. The P5–P9b interaction mainly plays roles in fine-tuning of the active tertiary structure to organize the binding pocket of the guanosine cofactor [160]. On the other hand, the P5c–P2 interaction is a dominant player in the assembly of Y4-6 and P3-7 RNAs [169]. PEGs may be able to rescue disruptions of local RNA tertiary structures supported by non-Watson–Crick interactions, such as P5–P9b. On the other hand, PEG may be unable to compensate for disruptions of the global assembly of large RNA domains supported by consecutive Watson–Crick base pair interactions, such as P5c-P2.

Although further studies are needed to elucidate the molecular basis of the distinct effects of PEG on the bimolecular Y4-6/P3-7 ribozyme and its oligomeric form, the differences may be related to the opposite effects of PEG on Watson–Crick base pairs and non-Watson–Crick tertiary interactions. PEG was reported to stabilize non-Watson–Crick tertiary interactions [159, 176-178] but destabilize Watson–Crick duplexes [179]. In the oligomeric form of the ribozyme, the two modular units (Y4-6 and P3-7) are connected covalently through nine consecutive base pairs (**Figure 4-1C**), with which the 1D-ribozyme oligomer is established (**Figure 4-1D**). This linker duplex may be destabilized by PEG [179]. Under conditions of PEG-dependent molecular crowding, the bimolecular ribozyme unit in the oligomeric form may become less stable than that in the bimolecular form.

Experimental Sections

In my research, there were some unique procedures and reaction conditions. However, each of these procedures and reaction conditions were modified in every chapter depending on the purpose and study plan. So that, the author demonstrated the experimental sections of each chapter separately.

Chapter 2

Plasmid Construction and RNA Preparation

Plasmids encoding mutants of ΔP5 RNA and P5abc RNA were generated by PCR-based mutagenesis of pTZ-ΔP5 and pP5abc [107], respectively. Plasmids encoding Lα RNA, Lβ RNA, F RNA, and their mutants were also derived from ΔP5 RNA by PCR-based mutagenesis. These plasmids were then used as templates for PCR to produce DNA fragments for in vitro transcription. The T7 promoter sequence was attached by PCR to a T7 promoter-containing sense primer. Transcription reactions were performed for 4.5 h at 37°C in the presence of nucleotide triphosphates (1 mM each) and Mg^{2+} (15 mM). The DNA template in the reaction mixture was removed by DNase treatment. The transcribed RNA was purified in a 6% or 9% denaturing polyacrylamide gel. A published protocol was used for 3′-end labeling of RNAs with the BODIPY-fluorophore synthesized in our laboratory [180].

Electrophoretic Mobility Shift Assay (EMSA)

Electrophoretic mobility shift assays (EMSA) for bimolecular P5abc/ΔP5 complexes were performed according to the procedure reported by Tanaka et al. [101].

EMSAs were carried out to analyze the assembly of Lα RNA, Lβ RNA, and F RNA according to the procedure reported by Oi et al. [73].

Ribozyme Activity Assay

Aqueous solutions containing DP5 RNA (final concentration: 0.5 μM) and P5abc RNA (final concentration: 0.75 μM) were heated separately at 80°C for 5 min and then cooled to 37°C. The 10-fold concentrated reaction buffer (final concentrations: 30 mM Tris-HCl, pH 7.5, and given concentration of $MgCl_2$) containing 2 mM guanosine triphosphate (final concentration: 0.2 mM) was added to the RNA solutions, which were further incubated at 37°C for 30 min. Ribozyme reactions were initiated by adding 5′-FAM-labeled substrates (final concentration: 0.5 μM) and allowed to proceed at 37°C. Aliquots were taken at given time points and treated with 1.5 volumes of stop solution containing 75% formamide, 0.1% xylene cyanol, and 100 mM EDTA. The mixtures were electrophoresed in 15% denaturing polyacrylamide gels. The gels were then analyzed with a Pharos FX fluoroimager (BioRad, Hercules, CA, USA). All assays were repeated at least twice. The mean values are plotted in the figures, with the minimum and maximum values indicated by error bars.

Chapter 3

Plasmid Construction and RNA Synthesis

Preparation of plasmids encoding P3-7 RNA (designated as pTZ-P3-7 in this study) and P4-6 RNA (designated as pTZ-P4-6 in this study) has been reported [150]. Plasmids encoding mutants of P3-7 RNA and P4-6 RNA were prepared by PCR-based mutagenesis. Plasmids encoding Y4-6 RNA (pTZ-Y4-6) and Y4-6a RNA were also synthesized by PCR-based mutagenesis of pTZ-IVS. Plasmids encoding Oligo-Y RNA were obtained by recombination of pTZ-P3-7 and pTZ-Y4-6. Using these plasmids as PCR templates, DNA fragments were amplified by PCR with suitable primer sets. Relatively high concentration of template plasmids (10 ng per 100 μM PCR reaction) was employed to minimize PCR errors. These DNA fragments were then used as templates for in vitro transcription with T7 RNA polymerase at 37°C for 4.5 h. After enzymatic RNA synthesis, DNase I treatment was performed to remove the template DNA. The synthesized RNAs were purified in 6% or 9% denaturing polyacrylamide gels. To visualize RNA molecules, the 3′ ends of the RNAs of interest were labeled with the BODIPY fluorophore [180]. It should be noted that the efficiency of BODIPY labeling was somewhat fluctuated presumably due to its multi-step chemical reactions. The labeling efficiency was lower in Y4-6 RNA than P4-6 RNA and Y4-6a RNA probably due to different locations of their 3′ ends. Experiments were preformed based on the concentrations of RNAs that were determined from intensities of UV absorption at 260 nm.

Ribozyme Activity Assays

RNA solutions (final concentration: 0.5 μM each) were heated at 80°C for 5 min and then cooled to 37°C. A tenfold concentrated reaction buffer (final concentration: 30 mM Tris-HCl, 50 mM $MgCl_2$, and pH 7.5) containing guanosine triphosphate (final concentration: 0.5 mM) and spermidine (final concentration: 5 mM) was added to the RNA solution, and incubated for 30 min at 37°C. Reactions were initiated by the addition of 5′-FAM-labeled substrate RNAs (final concentration: 0.5 μM) and proceeded at 37°C. Aliquots were removed at specific time points and mixed with 1.5 volumes of stop solution containing 150 mM EDTA, 75% formamide, and 0.1% xylene cyanol. The reaction products were separated on 15% denaturing polyacrylamide gels containing 8 M urea. The substrates and reaction products were analyzed using a Pharos FX fluoroimager (BioRad, Hercules, CA). All activity assays were performed at least twice. Because some of time course curves were deviated from single-exponential behavior, linear fitting in the early phase of the reactions was used to estimate their observed rate constants. The mean values were used for graphical data analysis, in which maximum and minimum values of each point were shown with error bars.

Electrophoretic Mobility Shift Assay (EMSA)

Electrophoretic mobility shift assays (EMSAs) for P4-6/P3-7, Y4-6/P3-7, and Y4-6a/P3-7 bimolecular complexes were carried out according to the procedure reported previously by Tanaka et al. [181]. The BODIPY fluorophore labeled P4-6 (or Y4-6) RNA and unlabeled P3-7 RNA were incubated separately at 80°C for 5 min. Each RNA was then mixed at 37°C. Folding buffer (10×, final concentrations: 71.2 mM Tris–borate, pH

8.3, and given concentration of $Mg(OAc)_2$) was added to the RNA solution and incubated at 37°C for 30 min. The mixture was subsequently incubated at 4°C for 30 min. After addition of 6× loading buffer containing 50% glycerol and 0.1% xylene cyanol, the samples were loaded onto a 5% non-denaturing polyacrylamide gel (29:1 acrylamide:bisacrylamide) containing 71.2 mM Tris–borate (pH 8.3) and given concentration of Mg(OAc)2. Electrophoresis was performed at 4°C, 200 V for the initial 5 min, followed by 75 V. A Pharos FX fluoroimager was used to visualize and analyze the resulting gels. EMSAs to analyze the oligomer formation of Oligo-Y RNA were also performed in a similar manner, in which BODIPY-labeled Oligo-Y RNA was employed in place of P4-6 RNA and P3-7 RNA [73].

Chapter 4

RNA synthesis

Template DNAs for Y4-6 RNA, P3-7 RNA, Oligo-Y RNA and their mutants were prepared as described previously [169]. The plasmid encoding the core P4-5-6 RNA was constructed from pTZΔP5 [174] by PCR-based mutagenesis. Template DNAs for the P5abc RNA and coreP5-4-6 RNA were prepared by PCR using plasmids containing the *Tetrahymena* ribozyme (pTZIVSU [174]) and the core P4-5-6 RNA as templates respectively and suitable primer sets. *In vitro* transcription reactions were pre-formed with T7 RNA polymerase and the products were purified by electrophoresis on 6% or 9% polyacrylamide gels containing 8 M urea. The concentrations of purified RNAs were calculated from intensities of UV absorption at 260 nm.

Substrate cleavage reactions

Substrate cleavage reactions used in this study was shown in **Figure 4-1B**. RNAs dissolved in H_2O were warmed for 5 minutes at 80°C and then cooled to 37°C. Aqueous solutions of PEG8000 or PEG200 were then added to the RNA solution before reaction buffer. Concentrations of PEG8000 and PEG200 were shown in percent (w/v). A tenfold concentrated reaction buffer (final concentration: 30 mM Tris-Cl (pH 7.5), 25 mM or or 50 mM MgCl2) containing spermidine (final concentration: 5 mM), and GTP (final concentration: 0.5 mM) was then added to the solution. The reaction mixture was further incubated at 37°C for 30 minutes. Substrate cleavage reactions were started by the addition of 5′-FAM labeled substrate (final concentration 0.5 μM) and proceeded at 37°C. Aliquots were taken at given time points and treated with 1.5-volumes of the stop solution containing 150 mM EDTA and 75% formamide. Reaction mixtures were separated by

electrophoresis on 15% polyacrylamide gels containing 8 M urea. The substrate and reaction products were analyzed using a Pharos FX fluoroimager (BioRad, Hercules, CA, USA). All reactions were repeated at least twice and the mean values were employed for data analysis, in which maximum and minimum values for each time point were shown with error bars in graphs.

Plasmids and primers used in this thesis:

Chapter-2

(1) Construction of plasmids encoding the *Tetrahymena* group I ribozyme with various loop/receptor interactions

A. Insertion of LR(C-Loop) and R(C loop) into plasmids encoding full-length group I ribozyme and ΔP5 ribozyme, respectively

Desired plasmid: pTZ-LR(C-loop)

Template plasmid: pTZ-IVS

TIL-250: GAGCAGCAAGGATGCAGTTCACAGACTAAATGT

TIL-251: GCATCGCCACGGACTTGGCTGCGTGGTTAGG

TIL-252: CGCCAGCTTTTGAGATGGCCTTGCAAA

TIL-253: AACCAGTGCTCCTGAGACTTGGTACTG

Desired plasmid: pTZ-ΔP5 R(C-loop)

Template plasmid: pTZ-ΔP5

TIL-250: GAGCAGCAAGGATGCAGTTCACAGACTAAATGT

TIL-251: GCATCGCCACGGACTTGGCTGCGTGGTTAGG

B. Insertion of R(GAAC) into plasmid encoding the *Tetrahymena* ΔP5 ribozyme

Desired plasmid: pTZ- ΔP5 R(GAAC)

Template plasmid: pTZ-ΔP5

Kyi-565: CCCGACGGGTCTCCTTCGGGCGCCAATTCATTGCAGTTCACAGACTAAATGTC-GGT

Kyi-566: CCCGACGGGTCTCCCGAAGGCGTTGCTTTCTTGGCTGCGTGGTTAGGACCAT

(2) Construction of plasmids encoding unit RNA that involved in the formation of 1D array based on ΔP5 and P5abc bimolecular ribozyme

Desired plasmid: pTZ-F

Template plasmid: pTZ-LR C-loop and pTZ-ΔP5 R-C-loop

Til-327: ACAGCCCGGTCTCGCCAGCTTTTGAGATGGCCTTGCAAAG

Til-328: ACAGCCCGGTCTCCCAAGCCAGTGCTCCTGAGACTTGGTACTG

Til-329: ACAGCCCGGTCTCTCGGGGTTCAGTACCAAGTCTCAGG

Til-330: ACAGCCCGGTCTCACCCGAAGGGTCAGCTTATTACCATACCCTTTGC

Til-331: ACAGCCCGGTCTCGCTTGGTTCGGTCCTAACCACGCAG

Til-332: ACAGCCCGGTCTCCCTGGCCCGGTTCGACCCCTTTCCCG

Desired plasmid: pTZ-Fy

Template plasmid: pTZ-LR C-loop and pTZ-ΔP5 R-C-loop

Til-398: ACAGCCCGGTCTCGCCAGCTTTTGAGATGGCCTTGGGAAGGG

Til-328: ACAGCCCGGTCTCCCAAGCCAGTGCTCCTGAGACTTGGTACTG

Til-329: ACAGCCCGGTCTCTCGGGGTTCAGTACCAAGTCTCAGG

Til-330: ACAGCCCGGTCTCACCCGAAGGGTCAGCTTATTACCATACCCTTTGC

Til-331: ACAGCCCGGTCTCGCTTGGTTCGGTCCTAACCACGCAG

Til-332: ACAGCCCGGTCTCCCTGGCCCGGTTCGACCCCTTTCCCG

(3) Construction of plasmids encoding RNA for the construction of closed triangle and square based on ΔP5 and P5abc bimolecular ribozyme

A. Construction of plasmids encoding RNAs for the formation of closed triangle

Desired plasmid: pTZ-Lx

Template plasmid: pTZ-IVS and pTZ-ΔP5 R(1)

Kyi-888: ACAGCCCGGTCTCCCGTACTCTTCTCATAAGATATAGTCG

Kyi-889: ACAGCCCGGTCTCTCGGACGTACTCTTCCCCGACCGACAT

Kyi-768: ACAGCCCGGTCTCGTCCGTCAGTACCAAGTCTCAGGG

TIL-396: ACAGCCCGGTCTCCTACGTCCGTCAGCTTATTACCATACCCTTCTC-AAGGCC

Desired plasmid: pTZ-Ly

Template plasmid: pTZ-GGAA and pTZ-ΔP5 R(GAAC)

Kyi-888: ACAGCCCGGTCTCCCGTACTCTTCTCATAAGATATAGTCG

Kyi-889: ACAGCCCGGTCTCTCGGACGTACTCTTCCCCGACCGACAT

Kyi-768: ACAGCCCGGTCTCGTCCGTCAGTACCAAGTCTCAGGG

TIL-395: ACAGCCCGGTCTCCTACGTCCGTCAGCTTATTACCATACCCTTCCC-AAGGCC

Desired plasmid: pTZ-Lz

Template plasmid: pTZ-GAAC and pTZ-ΔP5

Kyi-888: ACAGCCCGGTCTCCCGTACTCTTCTCATAAGATATAGTCG

Kyi-889: ACAGCCCGGTCTCTCGGACGTACTCTTCCCCGACCGACAT

TIL-400: ACAGCCCGGTCTCGTCCGTCAGTACCAAGTCTCTCC

Kyi-767: ACAGCCCGGTCTCCTACGTCCGTCAGCTTATTACCATACCCT

B. Construction of plasmids encoding RNAs for the formation of square

Desired plasmid: pTZ-Lα plasmid

Template plasmid: pTZ-IVS and pTZ-ΔP5 R(GAAC)

Kyi-888: ACAGCCCGGTCTCCCGTACTCTTCTCATAAGATATAGTCG

Kyi-889: ACAGCCCGGTCTCTCGGACGTACTCTTCCCCGACCGACAT

Kyi-768: ACAGCCCGGTCTCGTCCGTCAGTACCAAGTCTCAGGG
TIL-395: ACAGCCCGGTCTCCTACGTCCGTCAGCTTATTACCATACCCTTCCC-AAGGCC

Desired plasmid: pTZ-Lβ

Template plasmid: pTZ-GAAC and pTZ-ΔP5
Kyi-888: ACAGCCCGGTCTCCCGTACTCTTCTCATAAGATATAGTCG
Kyi-889: ACAGCCCGGTCTCTCGGACGTACTCTTCCCCGACCGACAT
TIL-400: ACAGCCCGGTCTCGTCCGTCAGTACCAAGTCTCTCC
Kyi-767: ACAGCCCGGTCTCCTACGTCCGTCAGCTTATTACCATACCCT

Chapter-3 and 4

(4) Construction of plasmids encoding P4-6 RNA, Y4-6 RNA, Y4-6a RNA and P3-7 RNA

Desired plasmid: pTZ-P4-6

Template plasmid: pTZ-IVS
TIL-430: ACAGCCCGAATTCGGACTGTTGATATGGATGCAGTTGCGGGAAAG-GGGTCAACAGCC
TIL-431: ACAGCCCAAGCTTCTGTTGACTTAGGACTTGGCTGCG

Desired plasmid: pTZ-Y4-6a

Template plasmid: pTZ-P4-6
TIL-471: GCAAAGGGTATGGTAATAAGCTTGAATATGACTCTTCGGAGGAAA-TGGGTAACCACGCAGCCA
TIL-472: AAGGCCATCTCAAAGTTTCCCCTGAGACTTGGTACTTGAATCTTTA-GGGCTTTCCCGCAACTG

Desired plasmid: pTZ-Y4-6

Template plasmid: pTZ-Y4-6a
TIL-473: ACAGCCCGAATTCGGGAGGAAATGGGTAACCACGCAGC
TIL-474: ACAGCCCAAGCTTGGGAGTCATATTCAAGCTTATTACC
TIL-475: ACAGCCCGGTCTCGAGATTCAAGTACCAAGTCTC
TIL-476: ACAGCCCGGTCTCCATCTTTAGGGCTTTCCCGCAACTGCATCCATA-TC

Desired plasmid: pTZ-Y4-6 (P5c-M5)

Template plasmid: pTZ-Y4-6
Kyi-584: TGGGAAGGGTATGGTAATAAGCT
TIL-552: AGGCCATCTCAAAGTTTCC

Desired plasmid: pTZ-P3-7 (P9b-UAAU)

Template plasmid: pTZ-IVS

TIL-428: TTCACAGACTAAATGTCGGTCGG

TIL-429: GATTTGACGGTCTTGCCTT

Desired plasmid: pTZ-P3-7 (P9b-GAAA)

Template plasmid: Oligo-Y (P9b-UAAU)

TIL-595: CGAAAGGGAGCTAGCGGATGAAGTGA

TIL-593: GGAGAGGTCCGACTATATCTT

Desired plasmid: pTZ-P3-7 (P9b-UUCG)

Template plasmid: Oligo-Y (P9b-UUCG)

TIL-526: CGGGGAGCTAGCGGATGAAG

TIL-527: AAAGGAGAGGTCCGACTATA

(5) Construction of plasmid encoding Oligo-Y RNA involved in 1D array formation based on Y4-6/P3-7 bimolecular ribozyme

Desired plasmid: pTZ-Oligo-Y (P9b-UAAU)

Template plasmid: pTZ-P3-7 + pTZ-Y4-6

TIL-511: ACAGCCCGGTCTCGGAGGAAATGGGTAACCACGCAGCCAAG

TIL-512: ACAGCCCGGTCTCCCCTCCTTCCCCGACCGACATTTAGTC

TIL-513: ACAGCCCGGTCTCGCTTCTCATAAGATATAGTCGG

TIL-514: ACAGCCCGGTCTCCGAAGGAGTCATATTCAAGCTTATTACCATACC-C

Desired plasmid: pTZ-Oligo-Y (P9b-GAAA)

Template plasmid: Oligo-Y (P9b-UAAU)

TIL-595: CGAAAGGGAGCTAGCGGATGAAGTGA

TIL-593: GGAGAGGTCCGACTATATCTT

Desired plasmid: pTZ-Oligo-Y (P9b-UUCG)

Template plasmid: Oligo-Y (P9b-UUCG)

TIL-526: CGGGGAGCTAGCGGATGAAG

TIL-527: AAAGGAGAGGTCCGACTATA

Desired plasmid: pTZ-Oligo-Y (P5C-M5-P2-M4)

Template plasmid: Oligo-Y (P9b-UAAU)

Kyi-584: TGGGAAGGGTATGGTAATAAGCT

TIL-552: AGGCCATCTCAAAGTTTCC

Primers used for *in vitro* RNA synthesis:

Chapter-2

(1) Primers involved for the synthesis of P5abc RNA and ΔP5 RNA that used for characterization of loop-receptor interactions

A. Synthesis of P5abc RNA possessing various loop motifs

P5abc L(C-loop) RNA

Template plasmid: pTZ-LR(C-loop)

TIL-276: CTAATACGACTCACTATAGGGTTCAGTACCAAGTCTCAGGAGCA

Kyi-726: GGGTCAGCTTATTACCATACCCTTTGCA

P5abc L(GAAC) RNA

Template plasmid: pTZ-LR(GAAC)

TIL-275: CTAATACGACTCACTATAGGGTTCAGTACCAAGTCTCTCCG

Kyi-726: GGGTCAGCTTATTACCATACCCTTTGCA

P5abc L(GGAA) RNA

Template plasmid: pTZ-LR(GGAA)

TIL-730: CTAATACGACTCACTATAGGGTTCAGTACCAAGTCTCAGGGGGAA

Kyi-726: GGGTCAGCTTATTACCATACCCTTTGCA

B. Synthesis of ΔP5 RNA possessing various receptor motifs

ΔP5-R (1) RNA

Template: pTZ-LR(1)

TIL-403: CTAATACGACTCACTATAGGAGGGAAAAGTTATCAGGCATGCACC-TGGTAGCTAGTCTTTAAACC

Anti-ScaI: ACTCCAAAACTAATCAATAT

ΔP5-R (GAAC) RNA

Template: pTZ-LR(GAAC)

TIL-403: CTAATACGACTCACTATAGGAGGGAAAAGTTATCAGGCATGCACC-TGGTAGCTAGTCTTTAAACC

Anti-ScaI: ACTCCAAAACTAATCAATAT

ΔP5-R (GGAA) RNA

Template: pTZ-LR(GGAA)

TIL-403: CTAATACGACTCACTATAGGAGGGAAAAGTTATCAGGCATGCACC-TGGTAGCTAGTCTTTAAACC

Anti-ScaI: ACTCCAAAACTAATCAATAT

(2) Primers involved for the synthesis of P5abc RNA and ΔP5 RNA that used for the characterization of loop-loop (P14) interactions

A. Synthesis of P5abc RNA possessing various L5c loop motifs

P5abc L5c-Wt RNA

Template plasmid: pTZ-IVS

Kyi-729: CTAATACGACTCACTATAGGGTTCAGTACCAAGTCTCAGGGGAAA

Kyi-726: GGGTCAGCTTATTACCATACCCTTTGCA

P5abc L5c-M3 RNA

Template plasmid: pTZ-IVS

Kyi-729: CTAATACGACTCACTATAGGGTTCAGTACCAAGTCTCAGGGGAAA

Kyi-732: GGGTCAGCTTATTACCATACCCTTCTCAAGGCCATCTCAA

P5abc L5c-M4 RNA

Template plasmid: pTZ-IVS

Kyi-729: CTAATACGACTCACTATAGGGTTCAGTACCAAGTCTCAGGGGAAA

TIL-318: GGGTCAGCTTATTACCATACCCTTTCCAAGGCCATCTCAA

P5abc L5c-M5 RNA

Template plasmid: pTZ-IVS

Kyi-729: CTAATACGACTCACTATAGGGTTCAGTACCAAGTCTCAGGGGAAA

TIL-319: GGGTCCAGCTTATTACCATACCCTTCCCAAGGCCATCTCAA

B. Synthesis of ΔP5 RNA possessing various L2 loop motifs

ΔP5 P2-Wt RNA

Template plasmid: pTZ-ΔP5

TIL-403: CTAATACGACTCACTATAGGAGGGAAAAGTTATCAGGCATGCACC-TGGTAGCTAGTCTTTAAACC

Anti-ScaI: ACTCCAAAACTAATCAATAT

ΔP5 P2-M3 RNA

Template plasmid: pTZ-ΔP5

Kyi-807: AGTAATACGACTCACTATAGGAGGGAAAAGTTATCAGGCACTCAC-CTGGTAGCTAGTCTTTAAACCA

Anti-ScaI: ACTCCAAAACTAATCAATAT

ΔP5 P2-M4 RNA

Template plasmid: pTZ-ΔP5

TIL-320: CTAATACGACTCACTATAGGAGGGAAAAGTTATCAGGCATCCACC-TGGTAGCTAGT

Anti-ScaI: ACTCCAAAACTAATCAATAT

ΔP5 P2-M5 RNA

Template plasmid: pTZ-ΔP5

TIL-321: CTAATACGACTCACTATAGGAGGGAAAAGTTATCAGGCACCCACC-TGGTAGCTAGT

Anti-ScaI: ACTCCAAAACTAATCAATAT

(3) Primers used for the synthesis of F RNAs involved in the formation of 1D array

F RNA

Template plasmid: pTZ-F

TIL-403: CTAATACGACTCACTATAGGAGGGAAAAGTTATCAGGCATGCACC-TGGTAGCTAGTCTTTAAACC

Anti-ScaI: ACTCCAAAACTAATCAATAT

Fx RNA

Template plasmid: pTZ-F

TIL-41: CTAATACGACTCACTATAGGAGGGAAAAGTTATCAGCTTCGGCTGG-TAGCTAGTCTTTAAACCA

Anti-ScaI: ACTCCAAAACTAATCAATAT

Fy RNA

Template plasmid: pTZ-Fy

TIL-403: CTAATACGACTCACTATAGGAGGGAAAAGTTATCAGGCATGCACC-TGGTAGCTAGTCTTTAAACC

Anti-ScaI: ACTCCAAAACTAATCAATAT

(4) Primers used for the synthesis of RNAs involve in formation of triangle

Lx RNA

Template plasmid: pTZ-Lx

TIL-321: CTAATACGACTCACTATAGGAGGGAAAAGTTATCAGGCACCCACC-TGGTAGCTAGT

Anti-ScaI: ACTCCAAAACTAATCAATAT

Ly RNA

TIL-403: CTAATACGACTCACTATAGGAGGGAAAAGTTATCAGGCATGCACC-TGGTAGCTAGTCTTTAAACC

Anti-ScaI: ACTCCAAAACTAATCAATAT

Lz RNA

Kyi-807: AGTAATACGACTCACTATAGGAGGGAAAAGTTATCAGGCACTCAC-CTGGTAGCTAGTCTTTAAACCA

Anti-ScaI: ACTCCAAAACTAATCAATAT

(5) Primers used for the synthesis of RNAs involve in formation of square

Lα PNA

Template plasmid: pTZ-Lα

TIL-403: CTAATACGACTCACTATAGGAGGGAAAAGTTATCAGGCATGCACC-TGGTAGCTAGTCTTTAAACC

Anti-ScaI: ACTCCAAAACTAATCAATAT

Lβ PNA

Template plasmid: pTZ-Lβ

TIL-321: CTAATACGACTCACTATAGGAGGGAAAAGTTATCAGGCACCCACC-TGGTAGCTAGT

Anti-ScaI: ACTCCAAAACTAATCAATAT

Chapter-3 and 4

(1) Primers used for the synthesis of P4-6 RNA, Y4-6 RNA and Y4-6a RNA

P4-6 RNA

Template plasmid: pTZ-P4-6

TIL-464: CTAATACGACTCACTATAGGACTGTTGATATGGATGCAGTTGCGG

TIL-465: CTGTTGACTTAGGACTTGGCTGCG

Y4-6a RNA

Template plasmid: pTZ-Y4-6a

TIL-464: CTAATACGACTCACTATAGGACTGTTGATATGGATGCAGTTGCGG

TIL-465: CTGTTGACTTAGGACTTGGCTGCG

Y4-6 RNA

Template plasmid: pTZ-Y4-6

TIL-481: CTAATACGACTCACTATAGGGAGGAAATGGGTAACCACGC

TIL-482: GGGAGTCATATTCAAGCTTATTACC

Y4-6 (P5c-M5) RNA

Template plasmid: pTZ-Y4-6 (P5c-M5)

TIL-481: CTAATACGACTCACTATAGGGAGGAAATGGGTAACCACGC

TIL-482: GGGAGTCATATTCAAGCTTATTACC

(2) Primers used for the synthesis of P3-7 (P9b-UAAU), P3-7 (P9b-GAAA), P3-7 (P9b-UUCG) and P3-7 (P2-UUCG)

P3-7 (P9b-UAAU) RNA

Template plasmid: pTZ-P3-7 (P9b-UAAU)

TIL-403: CTAATACGACTCACTATAGGAGGGAAAAGTTATCAGGCATGCACC-TGGTAGCTAGTCTTTAAACC

Anti-ScaI: ACTCCAAAACTAATCAATAT

P3-7 (P9b-GAAA) RNA

Template plasmid: pTZ-P3-7 (P9b-GAAA)

TIL-403: CTAATACGACTCACTATAGGAGGGAAAAGTTATCAGGCATGCACC-TGGTAGCTAGTCTTTAAACC

Anti-ScaI: ACTCCAAAACTAATCAATAT

P3-7 (P9b-UUCG) RNA

Template plasmid: pTZ-P3-7 (P9b-UUCG)

TIL-403: CTAATACGACTCACTATAGGAGGGAAAAGTTATCAGGCATGCACC-TGGTAGCTAGTCTTTAAACC

Anti-ScaI: ACTCCAAAACTAATCAATAT

P3-7 (P2-UUCG) RNA

Template plasmid: pTZ-P3-7 (P9b-UAAU)

TIL-41: CTAATACGACTCACTATAGGAGGGAAAAGTTATCAGCTTCGGCTGG-TAGCTAGTCTTTAAACCA

Anti-ScaI: ACTCCAAAACTAATCAATAT

(3) Primers used for the synthesis of Oligo-Y RNA

Oligo-Y (P9b-UAAU) RNA

Template plasmid: pTZ-Oligo-Y (UAAU)

TIL-403: CTAATACGACTCACTATAGGAGGGAAAAGTTATCAGGCATGCACC-TGGTAGCTAGTCTTTAAACC

Anti-ScaI: ACTCCAAAACTAATCAATAT

Oligo-Y (P9b-GAAA) RNA

Template plasmid: pTZ-Oligo-Y (GAAA)

TIL-403: CTAATACGACTCACTATAGGAGGGAAAAGTTATCAGGCATGCACC-TGGTAGCTAGTCTTTAAACC

Anti-ScaI: ACTCCAAAACTAATCAATAT

Oligo-Y (P9b-UUCG) RNA

Template plasmid: pTZ-Oligo-Y (UUCG)

TIL-403: CTAATACGACTCACTATAGGAGGGAAAAGTTATCAGGCATGCACC-TGGTAGCTAGTCTTTAAACC

Anti-ScaI: ACTCCAAAACTAATCAATAT

Oligo-Y (P2-UUCG) RNA

Template plasmid: pTZ-Oligo-Y (UAAU)

TIL-41: CTAATACGACTCACTATAGGAGGGAAAAGTTATCAGCTTCGGCTGG-TAGCTAGTCTTTAAACCA

Anti-ScaI: ACTCCAAAACTAATCAATAT

Oligo-Y (P5C-M5-P2-M4) RNA

Template plasmid: pTZ-Oligo-Y (P5C-M5-P2-M4)

TIL-320: CTAATACGACTCACTATAGGAGGGAAAAGTTATCAGGCATCCACC-TGGTAGCTAGT

Anti-ScaI: ACTCCAAAACTAATCAATAT

References

[1] A. Haller, M.F. Souliere, R. Micura, The dynamic nature of RNA as key to understanding riboswitch mechanisms, Accounts of Chemical Research, 44 (2011) 1339-1348.

[2] A. Serganov, L. Huang, D.J. Patel, Coenzyme recognition and gene regulation by a flavin mononucleotide riboswitch, Nature, 458 (2009) 233.

[3] G. Talini, S. Branciamore, E. Gallori, Ribozymes: Flexible molecular devices at work, Biochimie, 93 (2011) 1998-2005.

[4] C.G. Hoogstraten, M. Sumita, Structure–function relationships in RNA and RNP enzymes: recent advances, Biopolymers: Original Research on Biomolecules, 87 (2007) 317-328.

[5] Y. Ikawa, K. Tsuda, S. Matsumura, T. Inoue, De novo synthesis and development of an RNA enzyme, Proceedings of the National Academy of Sciences of the United States of America, 101 (2004) 13750-13755.

[6] E. Dausse, S.D.R. Gomes, J.J. Toulme, Aptamers: a new class of oligonucleotides in the drug discovery pipeline?, Current Opinion in Pharmacology, 9 (2009) 602-607.

[7] R.R. Breaker, Prospects for riboswitch discovery and analysis, Molecular Cell, 43 (2011) 867-879.

[8] P. Munoz-Tello, L. Rajappa, S. Coquille, S. Thore, Polyuridylation in eukaryotes: a 3′-end modification regulating RNA life, BioMed Research International, 2015 (2015) 12.

[9] S.C. Li, K.W. Tsai, H.W. Pan, Y.M. Jeng, M.R. Ho, W.H. Li, MicroRNA 3'end nucleotide modification patterns and arm selection preference in liver tissues, BMC Systems Biology, BioMed Central, 6 (2012) pp. S14.

[10] D.L. Nelson, A.L. Lehninger, M.M. Cox, Lehninger principles of biochemistry, Macmillan 2008.

[11] D.S. Anson, The use of retroviral vectors for gene therapy-what are the risks? A review of retroviral pathogenesis and its relevance to retroviral vector-mediated gene delivery, Genetic Vaccines and Therapy, 2 (2004) 9.

[12] M. Salazar, O.Y. Fedoroff, J.M. Miller, N.S. Ribeiro, B.R. Reid, The DNA strand in DNA.cntdot.RNA hybrid duplexes is neither B-form nor A-form in solution, Biochemistry, 32 (1993) 4207-4215.

[13] J.M. Berg, J.L. Tymoczko, G. Gatto Jr, Stryer: Biochemistry, WH Freeman and Company, 5 (2002) 306-307.

[14] S.E. Butcher, A.M. Pyle, The molecular interactions that stabilize RNA tertiary structure: RNA motifs, patterns, and networks, Accounts of Chemical Research, 44 (2011) 1302-1311.

[15] G. Zemora, C. Waldsich, RNA folding in living cells, RNA Biology, 7 (2010) 634-641.
[16] P.G. Higgs, RNA secondary structure: physical and computational aspects, Quarterly Reviews of Biophysics, 33 (2000) 199-253.
[17] J.C. Lee, R.R. Gutell, Diversity of Base-pair Conformations and their Occurrence in rRNA Structure and RNA Structural Motifs, Journal of Molecular Biology, 344 (2004) 1225-1249.
[18] J. Ishikawa, H. Furuta, Y. Ikawa, RNA tectonics (tectoRNA) for RNA nanostructure design and its application in synthetic biology, Wiley Interdisciplinary Reviews: RNA, 4 (2013) 651-664.
[19] A. Pyle, Metal ions in the structure and function of RNA, JBIC Journal of Biological Inorganic Chemistry, 7 (2002) 679-690.
[20] C.S. Koh, L.P. Sarin, Transfer RNA modification and infection – Implications for pathogenicity and host responses, Biochimica et Biophysica Acta (BBA) - Gene Regulatory Mechanisms, 1861 (2018) 419-432.
[21] D.K. Hendrix, S.E. Brenner, S.R. Holbrook, RNA structural motifs: building blocks of a modular biomolecule, Quarterly Reviews of Biophysics, 38 (2005) 221-243.
[22] P.B. Moore, Structural Motifs in RNA, Annual Review of Biochemistry, 68 (1999) 287-300.
[23] D.J. SenGupta, B. Zhang, B. Kraemer, P. Pochart, S. Fields, M. Wickens, A three-hybrid system to detect RNA-protein interactions in vivo, Proceedings of the national Academy of Sciences, 93 (1996) 8496-8501.
[24] T. Hermann, D.J. Patel, Adaptive recognition by nucleic acid aptamers, Science, 287 (2000) 820-825.
[25] N.A. Denesyuk, D. Thirumalai, How do metal ions direct ribozyme folding?, Nature Chemistry, 7 (2015) 793.
[26] J.H. Cate, J.A. Doudna, Metal-binding sites in the major groove of a large ribozyme domain, Structure, 4 (1996) 1221-1229.
[27] R.T. Batey, R.P. Rambo, J.A. Doudna, Tertiary motifs in RNA structure and folding, Angewandte Chemie International Edition, 38 (1999) 2326-2343.
[28] J.H. Cate, A.R. Gooding, E. Podell, K. Zhou, B.L. Golden, C.E. Kundrot, T.R. Cech, J.A. Doudna, Crystal Structure of a Group I Ribozyme Domain: Principles of RNA Packing, Science, 273 (1996) 1678-1685.
[29] M.R. Stahley, S.A. Strobel, Structural Evidence for a Two-Metal-Ion Mechanism of Group I Intron Splicing, Science, 309 (2005) 1587-1590.
[30] K. Lang, R. Rieder, R. Micura, Ligand-induced folding of the thiM TPP riboswitch

investigated by a structure-based fluorescence spectroscopic approach, Nucleic acids Research, 35 (2007) 5370-5378.
[31] J. Ishikawa, Y. Fujita, Y. Maeda, H. Furuta, Y. Ikawa, GNRA/receptor interacting modules: versatile modular units for natural and artificial RNA architectures, Methods, 54 (2011) 226-238.
[32] A. Lescoute, E. Westhof, The A-minor motifs in the decoding recognition process, Biochimie, 88 (2006) 993-999.
[33] P. Nissen, J.A. Ippolito, N. Ban, P.B. Moore, T.A. Steitz, RNA tertiary interactions in the large ribosomal subunit: the A-minor motif, Proceedings of the National Academy of Sciences, 98 (2001) 4899-4903.
[34] C. Geary, S. Baudrey, L. Jaeger, Comprehensive features of natural and in vitro selected GNRA tetraloop-binding receptors, Nucleic Acids Research, 36 (2007) 1138-1152.
[35] Y. Xin, C. Laing, N.B. Leontis, T. Schlick, Annotation of tertiary interactions in RNA structures reveals variations and correlations, RNA, 14 (2008) 2465-2477.
[36] C. Laing, D. Wen, J.T. Wang, T. Schlick, Predicting coaxial helical stacking in RNA junctions, Nucleic Acids Research, 40 (2011) 487-498.
[37] R. Tyagi, D.H. Mathews, Predicting helical coaxial stacking in RNA multibranch loops, RNA, 13 (2007) 939-951.
[38] E. Ennifar, P. Walter, B. Ehresmann, C. Ehresmann, P. Dumas, Crystal structures of coaxially stacked kissing complexes of the HIV-1 RNA dimerization initiation site, Nature Structural Biology, 8 (2001) 1064-1068.
[39] V. Lehnert, L. Jaeger, F. Michele, E. Westhof, New loop-loop tertiary interactions in self-splicing introns of subgroup IC and ID: a complete 3D model of the Tetrahymena thermophila ribozyme, Chemistry & Biology, 3 (1996) 993-1009.
[40] N.-K. Kim, Q. Zhang, J. Zhou, C.A. Theimer, R.D. Peterson, J. Feigon, Solution Structure and Dynamics of the Wild-type Pseudoknot of Human Telomerase RNA, Journal of Molecular Biology, 384 (2008) 1249-1261.
[41] H. Kawasaki, K. Taira, R. Wadhwa, World of small RNAs: from ribozymes to siRNA and miRNA, Differentiation, 72 (2004) 58-64.
[42] N.K. Tanner, Ribozymes: the characteristics and properties of catalytic RNAs, FEMS Microbiology Reviews, 23 (1999) 257-275.
[43] M.P. Robertson, G.F. Joyce, The origins of the RNA world, Cold Spring Harbor Perspectives in Biology, 4 (2012) pii: a003608.
[44] G. Abera, G. Berhanu, A. Tekewe, Ribozymes: nucleic acid enzymes with potential pharmaceutical applications: a review, Pharmacophore, 3 (2012) 164-178.

[45] D.J. Gaughan, A.S. Whitehead, Function and biological applications of catalytic nucleic acids, Biochimica et Biophysica Acta, 1445 (1999) 1-20.
[46] K. Kruger, P.J. Grabowski, A.J. Zaug, J. Sands, D.E. Gottschling, T.R. Cech, Self-splicing RNA: autoexcision and autocyclization of the ribosomal RNA intervening sequence of Tetrahymena, Cell, 31 (1982) 147-157.
[47] K.-Y. Lee, B.-J. Lee, Structural and biochemical properties of novel self-cleaving ribozymes, Molecules, 22 (2017) 678.
[48] N. Fong, M. Öhman, D.L. Bentley, Fast ribozyme cleavage releases transcripts from RNA polymerase II and aborts co-transcriptional pre-mRNA processing, Nature Structural and Molecular Biology, 16 (2009) 916-922.
[49] D.M. Chadalavada, E.A. Gratton, P.C. Bevilacqua, The human HDV-like CPEB3 ribozyme is intrinsically fast-reacting, Biochemistry, 49 (2010) 5321-5330.
[50] J.d.l. Cruz, K. Karbstein, J.L.W. Jr., Functions of Ribosomal Proteins in Assembly of Eukaryotic Ribosomes In Vivo, Annual Review of Biochemistry, 84 (2015) 93-129.
[51] S. M. Marquez, J. L. Chen, D. Evans, and N. R. Pace, Structure and Function of Eukaryotic Ribonuclease P RNA, 24 (2006) 445-456.
[52] B.L. Golden, A.R. Gooding, E.R. Podell, T.R. Cech, A Preorganized Active Site in the Crystal Structure of the Tetrahymena Ribozyme, Science, 282 (1998) 259-264.
[53] P. Guo, F. Haque, B. Hallahan, R. Reif, H. Li, Uniqueness, advantages, challenges, solutions, and perspectives in therapeutics applying RNA nanotechnology, Nucleic Acid Therapeutics, 22 (2012) 226-245.
[54] E. Winfree, F. Liu, L.A. Wenzler, N.C. Seeman, Design and self-assembly of two-dimensional DNA crystals, Nature, 394 (1998) 539-544.
[55] P.W. Rothemund, Folding DNA to create nanoscale shapes and patterns, Nature, 440 (2006) 297-302.
[56] P. Chidchob, H.F. Sleiman, Recent advances in DNA nanotechnology, Current Opinion in Chemical Biology, 46 (2018) 63-70.
[57] S.S. Simmel, P.C. Nickels, T. Liedl, Wireframe and tensegrity DNA nanostructures, Accounts of Chemical Research, 47 (2014) 1691-1699.
[58] D. Moll, C. Huber, B. Schlegel, D. Pum, U.B. Sleytr, M. Sára, S-layer-streptavidin fusion proteins as template for nanopatterned molecular arrays, Proceedings of the National Academy of Sciences, 99 (2002) 14646-14651.
[59] K. Rajagopal, J.P. Schneider, Self-assembling peptides and proteins for nanotechnological applications, Current opinion in structural biology, 14 (2004) 480-486.
[60] N. Isola, D. Stokes, T. Vo-Dinh, Protein Nanotechnology: The New Frontier in Biosciences, Analytical Chemistry, 70 (1998) 1352-1356.

[61] C.-J. Tsai, J. Zheng, C. Alemán, R. Nussinov, Structure by design: from single proteins and their building blocks to nanostructures, TRENDS in Biotechnology, 24 (2006) 449-454.
[62] S. Banta, Z. Megeed, M. Casali, K. Rege, M.L. Yarmush, Engineering protein and peptide building blocks for nanotechnology, Journal of Nanoscience and Nanotechnology, 7 (2007) 387-401.
[63] I. Severcan, C. Geary, A. Chworos, N. Voss, E. Jacovetty, L. Jaeger, A polyhedron made of tRNAs, Nature Chemistry, 2 (2010) 772-779.
[64] I. Severcan, C. Geary, E. Verzemnieks, A. Chworos, L. Jaeger, Square-Shaped RNA Particles from Different RNA Folds, Nano Letters, 9 (2009) 1270-1277.
[65] C. Geary, P.W.K. Rothemund, E.S. Andersen, A single-stranded architecture for cotranscriptional folding of RNA nanostructures, Science, 345 (2014) 799-804.
[66] C. Geary, A. Chworos, E. Verzemnieks, N.R. Voss, L. Jaeger, Composing RNA Nanostructures from a Syntax of RNA Structural Modules, Nano Letters, 17 (2017) 7095-7101.
[67] M.B. Johnson, J.R. Halman, E. Satterwhite, A.V. Zakharov, M.N. Bui, K. Benkato, V. Goldsworthy, T. Kim, E. Hong, M.A. Dobrovolskaia, E.F. Khisamutdinov, I. Marriott, K.A. Afonin, Programmable Nucleic Acid Based Polygons with Controlled Neuroimmunomodulatory Properties for Predictive QSAR Modeling, Small, 13 (2017) 1701255.
[68] A. Chworos, I. Severcan, A.Y. Koyfman, P. Weinkam, E. Oroudjev, H.G. Hansma, L. Jaeger, Building Programmable Jigsaw Puzzles with RNA, Science, 306 (2004) 2068-2072.
[69] M.A. Boerneke, S.M. Dibrov, T. Hermann, Crystal−Structure-Guided Design of Self−Assembling RNA Nanotriangles, Angewandte Chemie International Edition, 55 (2016) 4097-4100.
[70] C. Chen, C. Zhang, P. Guo, Sequence requirement for hand-in-hand interaction in formation of RNA dimers and hexamers to gear φ29 DNA translocation motor, RNA, 5 (1999) 805-818.
[71] P. Guo, C. Zhang, C. Chen, K. Garver, M. Trottier, Inter-RNA interaction of phage φ29 pRNA to form a hexameric complex for viral DNA transportation, Molecular Cell, 2 (1998) 149-155.
[72] D. Shu, W.-D. Moll, Z. Deng, C. Mao, P. Guo, Bottom-up assembly of RNA arrays and superstructures as potential parts in nanotechnology, Nano Letters, 4 (2004) 1717-1723.
[73] H. Oi, D. Fujita, Y. Suzuki, H. Sugiyama, M. Endo, S. Matsumura, Y. Ikawa,

Programmable formation of catalytic RNA triangles and squares by assembling modular RNA enzymes, The Journal of Biochemistry, 161 (2017) 451-462.
[74] T. Tanaka, Y. Ikawa, S. Matsumura, Rational Engineering of a Modular Group I Ribozyme to Control Its Activity by Self-Dimerization, Methods in Molecular Biology, 1632 (2017) 325-340.
[75] E. Westhof, B. Masquida, L. Jaeger, RNA tectonics: towards RNA design, Folding and Design, 1 (1996) R78-R88.
[76] Y. Takeuchi, M. Endo, Y. Suzuki, K. Hidak, G. Durand, E. Dausse, J. J. Toulmé and H. Sugiyama, Single-molecule observations of RNA–RNA kissing interactions in a DNA nanostructure, Biomaterials Science, 4 (2016) 130-135.
[77] L.P. Villarreal, G. Witzany, The DNA Habitat and its RNA Inhabitants: At the Dawn of RNA Sociology, Genomics Insights, 6 (2013) 1-12.
[78] K.E. McGinness, G.F. Joyce, In Search of an RNA Replicase Ribozyme, Chemistry & Biology, 10 (2003) 5-14.
[79] J.T. Sczepanski, G.F. Joyce, A cross-chiral RNA polymerase ribozyme, Nature, 515 (2014) 440-442.
[80] A.D. Ellington, J.W. Szostak, In vitro selection of RNA molecules that bind specific ligands, Nature, 346 (1990) 818-822.
[81] C. Tuerk, L. Gold, Systematic evolution of ligands by exponential enrichment: RNA ligands to bacteriophage T4 DNA polymerase, Science, 249 (1990) 505-510.
[82] D.L. Robertson, G.F. Joyce, Selection in vitro of an RNA enzyme that specifically cleaves single-stranded DNA, Nature, 344 (1990) 467-468.
[83] D. Bartel, J. Szostak, Isolation of new ribozymes from a large pool of random sequences [see comment], Science, 261 (1993) 1411-1418.
[84] Y. G. Yingling and B. A. Shapiro, Computational Design of an RNA Hexagonal Nanoring and an RNA Nanotube, Nano Letters, 7 (2007) 2328-2334.
[85] W.W. Grabow, P. Zakrevsky, K.A. Afonin, A. Chworos, B.A. Shapiro, L. Jaeger, Self-assembling RNA nanorings based on RNAI/II inverse kissing complexes, Nano Letters, 11 (2011) 878-887.
[86] B. Zhu, L. Wang, J. Li, C. Fan, Precisely tailored DNA nanostructures and their theranostic applications, The Chemical Record, 17 (2017) 1213-1230.
[87] W.W. Grabow, L. Jaeger, RNA self-assembly and RNA nanotechnology, Accounts of Chemical Research, 47 (2014) 1871-1880.
[88] D. Jasinski, F. Haque, D.W. Binzel, P. Guo, Advancement of the emerging field of RNA nanotechnology, ACS Nano, 11 (2017) 1142-1164.
[89] P. Guo, The emerging field of RNA nanotechnology, Nature Nanotechnology, 5

(2010) 833-842.
[90] F. Hong, F. Zhang, Y. Liu, H. Yan, DNA origami: scaffolds for creating higher order structures, Chemical Reviews, 117 (2017) 12584-12640.
[91] M. Endo, Y. Takeuchi, T. Emura, K. Hidaka, H. Sugiyama, Preparation of chemically modified RNA origami nanostructures, Chemistry–A European Journal, 20 (2014) 15330-15333.
[92] N. B. Leontis, E. Westhof, Self-assembled RNA nanostructures, Science, 345 (2014) 732-733.
[93] S.L. Sparvath, C.W. Geary, E.S. Andersen, Computer-aided design of RNA origami structures, Methods in Molecular Biology, 1500 (2017) 51-80.
[94] J. Kozyra, A. Ceccarelli, E. Torelli, A. Lopiccolo, J.-Y. Gu, H. Fellermann, U. Stimming, N. Krasnogor, Designing uniquely addressable bio-orthogonal synthetic scaffolds for DNA and RNA origami, ACS Synthetic Biology, 6 (2017) 1140-1149.
[95] K.A. Afonin, E. Bindewald, A.J. Yaghoubian, N. Voss, E. Jacovetty, B.A. Shapiro, L. Jaeger, In vitro assembly of cubic RNA-based scaffolds designed in silico, Nature Nanotechnology, 5 (2010) 676-682.
[96] M.N. Bui, M.B. Johnson, M. Viard, E. Satterwhite, A.N. Martins, Z. Li, I. Marriott, K.A. Afonin, E.F. Khisamutdinov, Versatile RNA tetra-U helix linking motif as a toolkit for nucleic acid nanotechnology, Nanomedicine: Nanotechnology, Biology and Medicine, 13 (2017) 1137-1146.
[97] M. Li, M. Zheng, S. Wu, C. Tian, D. Liu, Y. Weizmann, W. Jiang, G. Wang & C. Mao, In vivo production of RNA nanostructures via programmed folding of single-stranded RNAs, Nature Communications, 9 (2018) 2196.
[98] C.J. Delebecque, A.B. Lindner, P.A. Silver, F.A. Aldaye, Organization of intracellular reactions with rationally designed RNA assemblies, Science, 333 (2011) 470-474.
[99] G. van der Horst, A. Christian, T. Inoue, Reconstitution of a group I intron self-splicing reaction with an activator RNA, Proceedings of the National Academy of Sciences, 88 (1991) 184-188.
[100] E.A. Doherty, D. Herschlag, J.A. Doudna, Assembly of an exceptionally stable RNA tertiary interface in a group I ribozyme, Biochemistry, 38 (1999) 2982-2990.
[101] T. Tanaka, H. Furuta, Y. Ikawa, Installation of orthogonality to the interface that assembles two modular domains in the Tetrahymena group I ribozyme, Journal of Bioscience and Bioengineering, 117 (2014) 407-412.
[102] M.A. Engelhardt, E.A. Doherty, D.S. Knitt, J.A. Doudna, D. Herschlag, The P5abc peripheral element facilitates preorganization of the Tetrahymena group I ribozyme for

catalysis, Biochemistry, 39 (2000) 2639-2651.
[103] S.P. Ohuchi, Y. Ikawa, Y. Nakamura, Selection of a novel class of RNA–RNA interaction motifs based on the ligase ribozyme with defined modular architecture, Nucleic Acids Research, 36 (2008) 3600-3607.
[104] J. Ishikawa, S. Matsumura, L. Jaeger, T. Inoue, H. Furuta, Y. Ikawa, Rational optimization of the DSL ligase ribozyme with GNRA/receptor interacting modules, Archives of Biochemistry and Biophysics, 490 (2009) 163-170.
[105] M.J. Serra, J.D. Baird, T. Dale, B.L. Fey, K. Retatagos, E. Westhof, Effects of magnesium ions on the stabilization of RNA oligomers of defined structures, RNA, 8 (2002) 307-323.
[106] Z.-J. Tan, S.-J. Chen, Importance of diffuse metal ion binding to RNA, Metal Ions in Life Sciences, 9 (2011) 101-124.
[107] Y. Naito, H. Shiraishi, T. Inoue, P5abc of the Tetrahymena ribozyme consists of three functionally independent elements, RNA, 4 (1998) 837-846.
[108] I.V. Novikova, B.H. Hassan, M.G. Mirzoyan, N.B. Leontis, Engineering cooperative tecto–RNA complexes having programmable stoichiometries, Nucleic Acids Research, 39 (2010) 2903-2917.
[109] L. Jaeger, E. Westhof, N.B. Leontis, TectoRNA: modular assembly units for the construction of RNA nano-objects, Nucleic Acids Research, 29 (2001) 455-463.
[110] G.F. Joyce, Evolution in an RNA world, Cold Spring Harbor symposia on quantitative biology, Cold Spring Harbor Laboratory Press, 74 (2009) 17-23.
[111] L.K. Cheng, P.J. Unrau, Closing the circle: replicating RNA with RNA, Cold Spring Harbor Perspectives in Biology, 2 (2010) a002204.
[112] T.A. Lincoln, G.F. Joyce, Self-sustained replication of an RNA enzyme, Science, 323 (2009) 1229-1232.
[113] A. Wochner, J. Attwater, A. Coulson, P. Holliger, Ribozyme-catalyzed transcription of an active ribozyme, Science, 332 (2011) 209-212.
[114] N. Vaidya, M.L. Manapat, I.A. Chen, R. Xulvi-Brunet, E.J. Hayden, N. Lehman, Spontaneous network formation among cooperative RNA replicators, Nature, 491 (2012) 72-77.
[115] H. S. Zaher and P. J. Unrau, Selection of an improved RNA polymerase ribozyme with superior extension and fidelity, RNA, 13 (2007) 1017-1026.
[116] P.G. Higgs, N. Lehman, The RNA World: molecular cooperation at the origins of life, Nature Reviews Genetics, 16 (2015) 7-17.
[117] J.W. Szostak, D.P. Bartel, P.L. Luisi, Synthesizing life, Nature, 409 (2001) 387-390.
[118] S. Mansy, J. Szostak, Reconstructing the emergence of cellular life through the

synthesis of model protocells, Cold Spring Harbor symposia on quantitative biology, Cold Spring Harbor Laboratory Press, 74 (2009) 47-54.
[119] A. Szilágyi, I. Zachar, I. Scheuring, Á. Kun, B. Könnyű, T. Czárán, Ecology and Evolution in the RNA World Dynamics and Stability of Prebiotic Replicator Systems, Life, 7 (2017) 48.
[120] G. Ertem, J.P. Ferris, Synthesis of RNA oligomers on heterogeneous templates, Nature, 379 (1996) 238-240.
[121] P.C. Joshi, M.F. Aldersley, J.W. Delano, J.P. Ferris, Mechanism of montmorillonite catalysis in the formation of RNA oligomers, Journal of the American Chemical Society, 131 (2009) 13369-13374.
[122] E. Biondi, S. Branciamore, L. Fusi, S. Gago, E. Gallori, Catalytic activity of hammerhead ribozymes in a clay mineral environment: implications for the RNA world, Gene, 389 (2007) 10-18.
[123] E. Biondi, S. Branciamore, M.-C. Maurel, E. Gallori, Montmorillonite protection of an UV-irradiated hairpin ribozyme: evolution of the RNA world in a mineral environment, BMC Evolutionary Biology, 7 (2007) S2.
[124] S. Jheeta, P.C. Joshi, Prebiotic RNA synthesis by montmorillonite catalysis, Life, 4 (2014) 318-330.
[125] J.D. Stephenson, M. Popović, T.F. Bristow, M.A. Ditzler, Evolution of ribozymes in the presence of a mineral surface, RNA, 22 (2016) 1893-1901.
[126] P.A. Monnard, H. Ziock, Eutectic phase in water−ice: a self−assembled environment conducive to metal−catalyzed non−enzymatic RNA polymerization, Chemistry & Biodiversity, 5 (2008) 1521-1539.
[127] J. Attwater, A. Wochner, V.B. Pinheiro, A. Coulson, P. Holliger, Ice as a protocellular medium for RNA replication, Nature Communications, 1 (2010) 76.
[128] J. Attwater, A. Wochner, P. Holliger, In-ice evolution of RNA polymerase ribozyme activity, Nature Chemistry, 5 (2013) 1011-1118.
[129] H. Mutschler, A. Wochner, P. Holliger, Freeze–thaw cycles as drivers of complex ribozyme assembly, Nature Chemistry, 7 (2015) 502-508.
[130] A.P. Minton, Influence of macromolecular crowding upon the stability and state of association of proteins: predictions and observations, Journal of Pharmaceutical Sciences, 94 (2005) 1668-1675.
[131] S. Mittal, R.K. Chowhan, L.R. Singh, Macromolecular crowding: Macromolecules friend or foe, Biochimica et Biophysica Acta (BBA)-General Subjects, 1850 (2015) 1822-1831.
[132] K.A. Leamy, S.M. Assmann, D.H. Mathews, P.C. Bevilacqua, Bridging the gap

between in vitro and in vivo RNA folding, Quarterly Reviews of Biophysics, 49 (2016) e10.
[133] S.-i. Nakano, N. Sugimoto, Model studies of the effects of intracellular crowding on nucleic acid interactions, Molecular BioSystems, 13 (2017) 32-41.
[134] R. Saha, A. Pohorille, I.A. Chen, Molecular crowding and early evolution, Origins of Life and Evolution of Biospheres, 44 (2014) 319-324.
[135] R. Saha, S. Verbanic, I.A. Chen, Lipid vesicles chaperone an encapsulated RNA aptamer, Nature Communications, 9 (2018) 2313.
[136] R.J. Gillams, T.Z. Jia, Mineral Surface-Templated Self-Assembling Systems: Case Studies from Nanoscience and Surface Science towards Origins of Life Research, Life, 8 (2018) pii: E10.
[137] A. Pressman, C. Blanco, I.A. Chen, The RNA world as a model system to study the origin of life, Current Biology, 25 (2015) R953-R963.
[138] M.M. Hanczyc, S.M. Fujikawa, J.W. Szostak, Experimental models of primitive cellular compartments: encapsulation, growth, and division, Science, 302 (2003) 618-622.
[139] I.A. Chen, K. Salehi-Ashtiani, J.W. Szostak, RNA catalysis in model protocell vesicles, Journal of the American Chemical Society, 127 (2005) 13213-13219.
[140] F. Anella, C. Danelon, Prebiotic Factors Influencing the Activity of a Ligase Ribozyme, Life, 7 (2017) 17.
[141] T.F. Zhu, J.W. Szostak, Coupled growth and division of model protocell membranes, Journal of the American Chemical Society, 131 (2009) 5705-5713.
[142] K.P. Adamala, A.E. Engelhart, J.W. Szostak, Collaboration between primitive cell membranes and soluble catalysts, Nature Communications, 7 (2016) 11041.
[143] R. Fiammengo, M. Crego-Calama, D.N. Reinhoudt, Synthetic self-assembled models with biomimetic functions, Current Opinion in Chemical Biology, 5 (2001) 660-673.
[144] K. Kurihara, M. Matsuo, T. Yamaguchi, S. Sato, Approach to biomolecular science by cyborg Supramolecular chemistry, Biochimica et Biophysica Acta (BBA)-General Subjects, 1862 (2018) 358-364.
[145] Z. Liu, J. Qiao, Z. Niu, Q. Wang, Natural supramolecular building blocks: from virus coat proteins to viral nanoparticles, Chemical Society Reviews, 41 (2012) 6178-6194.
[146] J. Glasgow, D. Tullman-Ercek, Production and applications of engineered viral capsids, Applied Microbiology and Biotechnology, 98 (2014) 5847-5858.
[147] D. Shu, L.P. Huang, S. Hoeprich, P. Guo, Construction of phi29 DNA-packaging RNA monomers, dimers, and trimers with variable sizes and shapes as potential parts for

nanodevices, Journal of Nanoscience and Nanotechnology, 3 (2003) 295-302.
[148] Y. Shu, M. Cinier, D. Shu, P. Guo, Assembly of multifunctional phi29 pRNA nanoparticles for specific delivery of siRNA and other therapeutics to targeted cells, Methods, 54 (2011) 204-214.
[149] J.A. Doudna, T.R. Cech, Self-assembly of a group I intron active site from its component tertiary structural domains, RNA, 1 (1995) 36-45.
[150] Y. Ikawa, T. Inoue, Designed structural-rearrangement of an active group I ribozyme, Journal of Biochemistry, 133 (2003) 189-195.
[151] Y. Ikawa, H. Shiraishi, T. Inoue, A small structural element, Pc-J5/5a, plays dual roles in a group IC1 intron RNA, Biochemical and Biophysical Research Communications, 274 (2000) 259-265.
[152] F.L. Murphy, Y.-H. Wang, J.D. Griffith, T.R. Cech, Coaxially stacked RNA helices in the catalytic center of the Tetrahymena ribozyme, Science, 265 (1994) 1709-1712.
[153] Y. Ikawa, T. Yoshimura, H. Hara, H. Shiraishi, T. Inoue, Two conserved structural components, A−rich bulge and P4 XJ6/7 base ‐ triples, in activating the group I ribozymes, Genes to Cells, 7 (2002) 1205-1215.
[154] M. Costa, F.o. Michel, Frequent use of the same tertiary motif by self ‐ folding RNAs, The EMBO Journal, 14 (1995) 1276-1285.
[155] F. Guo, A.R. Gooding, T.R. Cech, Structure of the Tetrahymena ribozyme: base triple sandwich and metal ion at the active site, Molecular Cell, 16 (2004) 351-362.
[156] M.M. Rahman, S. Matsumura, Y. Ikawa, Artificial RNA Motifs Expand the Programmable Assembly between RNA Modules of a Bimolecular Ribozyme Leading to Application to RNA Nanostructure Design, Biology, 6 (2017) 37.
[157] M. Tanner, T. Cech, Activity and thermostability of the small self-splicing group I intron in the pre-tRNA (lle) of the purple bacterium Azoarcus, RNA, 2 (1996) 74-83.
[158] R. Desai, D. Kilburn, H.-T. Lee, S.A. Woodson, Increased ribozyme activity in crowded solutions, Journal of Biological Chemistry, 289 (2014) 2972-2977.
[159] H.-T. Lee, D. Kilburn, R. Behrouzi, R.M. Briber, S.A. Woodson, Molecular crowding overcomes the destabilizing effects of mutations in a bacterial ribozyme, Nucleic Acids Research, 43 (2014) 1170-1176.
[160] T.L. Benz-Moy, D. Herschlag, Structure–function analysis from the outside in: long-range tertiary contacts in RNA exhibit distinct catalytic roles, Biochemistry, 50 (2011) 8733-8755.
[161] Q. Wu, L. Huang, Y. Zhang, The structure and function of catalytic RNAs, Science in China Series C: Life Sciences, 52 (2009) 232-244.
[162] A. Mondragón, Structural studies of RNase P, Annual Review of Biophysics, 42

(2013) 537-557.
[163] A.M. Pyle, Group II intron self-splicing, Annual Review of Biophysics, 45 (2016) 183-205.
[164] T. Pan, Higher order folding and domain analysis of the ribozyme from Bacillus subtilis ribonuclease P, Biochemistry, 34 (1995) 902-909.
[165] A. Loria, T. Pan, Domain structure of the ribozyme from eubacterial ribonuclease P, RNA, 2 (1996) 551-563.
[166] L.L. Martin, P.J. Unrau, U.F. Müller, RNA synthesis by in vitro selected ribozymes for recreating an RNA world, Life, 5 (2015) 247-268.
[167] G.F. Joyce, J.W. Szostak, Protocells and RNA Self-Replication, Cold Spring Harbor Perspectives in Biology, 10 (2018) a034801.
[168] U.F. Müller, D.P. Bartel, Improved polymerase ribozyme efficiency on hydrophobic assemblies, RNA, 14 (2008) 552-562.
[169] M.M. Rahman, S. Matsumura, Y. Ikawa, Oligomerization of a Bimolecular Ribozyme Modestly Rescues its Structural Defects that Disturb Interdomain Assembly to Form the Catalytic Site, Journal of Molecular Evolution, 86 (2018) 431-442.
[170] B. Drobot, J.M. Iglesias-Artola, K. Le Vay, V. Mayr, M. Kar, M. Kresying, H. Mutschler, T.D. Tang, Compartmentalized RNA catalysis in membrane-free coacervate protocells, bioRxiv, (2018) 273417.
[171] G. Hervé, S. Tobé, T. Heams, J. Vergne, M.-C. Maurel, Hydrostatic and osmotic pressure study of the hairpin ribozyme, Biochimica et Biophysica Acta (BBA)-Proteins and Proteomics, 1764 (2006) 573-577.
[172] S.-i. Nakano, H.T. Karimata, Y. Kitagawa, N. Sugimoto, Facilitation of RNA enzyme activity in the molecular crowding media of cosolutes, Journal of the American Chemical Society, 131 (2009) 16881-16888.
[173] C.A. Strulson, N.H. Yennawar, R.P. Rambo, P.C. Bevilacqua, Molecular crowding favors reactivity of a human ribozyme under physiological ionic conditions, Biochemistry, 52 (2013) 8187-8197.
[174] K.P. Williams, D.N. Fujimoto, T. Inoue, A region of group I introns that contains universally conserved residues but is not essential for self-splicing, Proceedings of the National Academy of Sciences, 89 (1992) 10400-10404.
[175] M.A. Gulshan, M.M. Rahman, S. Matsumura, T. Higuchi, N. Umezawa, Y. Ikawa, Biogenic triamine and tetraamine activate core catalytic ability of Tetrahymena group I ribozyme in the absence of its large activator module, Biochemical and Biophysical Research Communications, 496 (2018) 594-600.
[176] D. Miyoshi, H. Karimata, N. Sugimoto, Hydration regulates thermodynamics of G-

quadruplex formation under molecular crowding conditions, Journal of the American Chemical Society, 128 (2006) 7957-7963.
[177] D. Miyoshi, K. Nakamura, H. Tateishi-Karimata, T. Ohmichi, N. Sugimoto, Hydration of Watson−Crick base pairs and dehydration of Hoogsteen base pairs inducing structural polymorphism under molecular crowding conditions, Journal of the American Chemical Society, 131 (2009) 3522-3531.
[178] N.F. Dupuis, E.D. Holmstrom, D.J. Nesbitt, Molecular-crowding effects on single-molecule RNA folding/unfolding thermodynamics and kinetics, Proceedings of the National Academy of Sciences, 111 (2014) 8464-8469.
[179] S. Pramanik, S. Nagatoishi, S. Saxena, J. Bhattacharyya, N. Sugimoto, Conformational flexibility influences degree of hydration of nucleic acid hybrids, The Journal of Physical Chemistry B, 115 (2011) 13862-13872.
[180] Y. Ikawa, S. Moriyama, H. Furuta, Facile syntheses of BODIPY derivatives for fluorescent labeling of the 3′ and 5′ ends of RNAs, Analytical biochemistry, 378 (2008) 166-170.
[181] T. Tanaka, S. Matsumura, H. Furuta, Y. Ikawa, Tecto‐GIRz: Engineered Group I Ribozyme the Catalytic Ability of Which Can Be Controlled by Self‐Dimerization, ChemBioChem, 17 (2016) 1448-1455.
[182] Luc Jaeger, The New World of ribozymes, Current opinion in structural biology, 7 (1997) 324-335.
[183] C.A. Trujillo, A.A. Nery, J.M. Alves, A.H. Martins, H. Ulrich, Development of the anti-VEGF aptamer to a therapeutic agent for clinical ophthalmology, Clinical ophthalmology (Auckland, N.Z.), 1 (2007) 393-402.
[184] C. Olea, Jr., J. Weidmann, P.E. Dawson, G.F. Joyce, An L-RNA Aptamer that Binds and Inhibits RNase, Chemistry & biology, 22 (2015) 1437-1441.
[185] L. Jaeger, M.C. Wright, G.F. Joyce, A complex ligase ribozyme evolved in vitro from a group I ribozyme domain, 96 (1999) 14712-14717.
[186] W. Yoshioka, Y. Ikawa, L. Jaeger, H. Shiraishi, T. Inoue, Generation of a catalytic module on a self-folding RNA, RNA (New York, N.Y.), 10 (2004) 1900-1906.
[187] Y. Ikawa, K. Fukada, S.-i. Watanabe, H. Shiraishi, T. Inoue, Design, Construction, and Analysis of a Novel Class of Self-Folding RNA, Structure, 10 (2002) 527-534.
[188] Y. Fujita, H. Furuta, Y. Ikawa, Tailoring RNA modular units on a common scaffold: a modular ribozyme with a catalytic unit for beta-nicotinamide mononucleotide-activated RNA ligation, RNA (New York, N.Y.), 15 (2009) 877-888.
[189] A.B. Chadee, The roles of CYT-18 in folding, misfolding and structural specificity of the Tetrahymena group I ribozyme, (2009).

[190] Y. Nozawa, M. Hagihara, S. Matsumura, Y. Ikawa, Modular Architecture of Bacterial RNase P Ribozymes as a Structural Platform for RNA Nanostructure Design, 72 (2018) 882-887.

Publications list

1. **Md. Motiar Rahman**, Shigeyoshi Matsumura and Yoshiya Ikawa, Artificial RNA Motifs Expand the Programmable Assembly between RNA Modules of a Bimolecular Ribozyme Leading to Application to RNA Nanostructure Design, *Biology,* **2017**, *6*(4), 37.

2. Mst Ara Gulshan, **Md Motiar Rahman**, Shigeyoshi Matsumura, Tsunehiko Higuchi, Naoki Umezawa, Yoshiya Ikawa, Biogenic triamine and tetraamine activate core catalytic ability of Tetrahymena group I ribozyme in the absence of its large activator module, Biochemical and biophysical research communications, **2018**, 496(2), 594-600.

3. Md. Motiar Rahman, Shigeyoshi Matsumura and Yoshiya Ikawa, Oligomerization of a Bimolecular Ribozyme Modestly Rescues its Structural Defects that Disturb Interdomain Assembly to Form the Catalytic Site, Journal of Molecular Evolution, **2018**, 86 (7), 431-442.

4. Md. Motiar Rahman, Shigeyoshi Matsumura and Yoshiya Ikawa, Effects of molecular crowding on a bimolecular group I ribozyme and its derivative that self-assembles to form ribozyme oligomers, Biochemical and Biophysical Research Communications, **2018,** 507, 136-141.

Acknowledgement

The studies described in this literature were carried out under the supervision of Professor Dr. Yoshiya Ikawa at the Graduate School of Innovative Life Science, University of Toyama. The author would like to thank Professor Yoshiya Ikawa for providing the opportunity to study RNA biochemistry in his well-equipped lab and for his recommendation to get the MEXT scholarship. The author also likes to express the deepest gratitude to Professor Ikawa for his excellent instructions, guidance, support and scientific discussion during research activities. Therefore, the author likes to thank him for his outstanding support to adapt me to the environment in Toyama.

The author like to thank Dr. Shigeyoshi Matsumura, Instructor at the Department of Chemistry, Graduate School of Science and Engineering, University of Toyama, for his scientific cooperation, helpful discussion, and advice during the time of Ph.D. thesis. I also like to thank to my examination committee members for their insightful discussions and suggestions to develop my dissertation.

I am very grateful to Mst Gulshan Ara, my wife, for her continuous overall support in my life. I would like to express my love to Adiat Rahman Talha, my son, for giving me the entertainment after every day's hard work. The author would like to thank all my family members who guide me throughout my life.

The author would like to thank Dr. Takahiro Tanaka, former Ph.D. student in the Ikawa group, for his outstanding support during the initial period of my Ph.D. studies. I am grateful to all of my former and present lab members and collaborators in the Ikawa laboratory at the University of Toyama including, Md Sohanur Rahman, Md Dobirul

Islam, Ms. Inuzuka Saki, Mr. Ryuji Kiyooka, Mr. Maejima Takaya, Ms. Hagihara Megumi, Ms. Airi Furukawa, Mr. Takuto Naito, Mr. Hiroki Oi, Ms. Ayaka Matsuyama, Ms. Yuri Nozawa, Mr. Kentaro Wakui, Mr. Kazuma Tazawa, Mr. Koutaro Ishihara, Ms. Aoyama Risako, Mr. Junya Akagi, Mr. Takashi Usui, Mr. Motochika Ehara, Mr. Katsushi Miyazaki, Mr. Kai Yu, Mr. Takaki Koyama, Mr. Kazuki Tsuchida, Mr. Ryusei Tsuruga, Ms. Yuka Nishiyama, Mr. Yuuki Mori.

The author wishes to thank MEXT (Ministry of Education, Culture, Sports, Science, and Technology) for their support during my Ph.D. life by providing the scholarship.